SOLUBLE PHOSPHATE AMENDMENTS FOR METAL AND RADIONUCLIDE IMMOBILIZATION

by

FRANTISEK MAJS

(Under the Direction of William P. Miller)

ABSTRACT

Intensive mining and processing of metals and radionuclides have resulted in significant soil and sediment contamination. Phosphate-based in-situ immobilization of the metals and radionuclides has been proposed as an alternative to disruptive and expensive cleanup strategies. This dissertation summarizes results of two experiments, which tested potential of four phosphate amendments [trisodium trimetaphosphate, dodecasodium phytate (Na-IP6), calcium phytate (Ca-IP6) and hydroxyapatite] to immobilize Cu, Zn, and Pb in soil and Ni and U in sediment. Stability of immobilized contaminants was tested by selective leaching and solid phase speciation techniques.

Hydroxyapatite lowered trace metal and U solubility with increasing treatment level and Ca-IP6 behaved in general similarly, except for a slight increase in Ni and Cu solubilities at higher amendment levels, presumably due to the chelation potential of phytate. Application of metaphosphate and Na-IP6 were proven unsuitable due to dispersion of soil organic matter and colloidal particles, which had a negative impact on contaminant solubility. Leaching techniques revealed amendment-derived changes in element fractionation and indicated that HA was suitable for Cu, Zn, and Pb

immobilization, whereas Ca-IP6 only for Pb and U immobilization, and brought into question the efficacy of applying phosphates for immobilization of Ni. Qualitative spectroscopy disclosed Pb speciation in solid phase in the untreated soil and mechanisms of its transformation upon phosphate addition, but failed to identify any crystalline form of U in the sediment. Unamended Pb-contaminated soil showed strong diffraction patterns for anglesite, cerussite, and plumbojarosite. Hydroxyapatite and Ca-IP6 amendments facilitated precipitation of corkite and to a lesser extent drugmanite and pyromorphite. This is significant because pyromorphite is usually proposed as the main sink of Pb in the amended soils.

INDEX WORDS: μ-XRD, μ-XRF, apatite, copper, corkite, drugmanite, lead, nickel, phytate, plumbojarosite, pyromorphite, trimetaphosphate, uranium, zinc

SOLUBLE PHOSPHATE AMENDMENTS FOR METAL AND RADIONUCLIDE IMMOBILIZATION

by

FRANTISEK MAJS

B.S., Mendel Agriculture and Forestry University, Czech Republic, 1996

M.S., Mendel Agriculture and Forestry University, Czech Republic, 1999

M.S., University of Minnesota, 2003

A Dissertation Submitted to the Graduate Faculty of The University of Georgia in Partial Fulfillment of the Requirements for the Degree

DOCTOR OF PHILOSOPHY

ATHENS, GEORGIA

2009

SOLUBLE PHOSPHATE AMENDMENTS FOR METAL AND RADIONUCLIDE IMMOBILIZATION

by

FRANTISEK MAJS

Major Professor: William P. Miller

Committee: Miguel L. Cabrera
Brian P. Jackson
David E. Radcliffe
Aaron Thompson

Electronic Version Approved:

Maureen Grasso
Dean of the Graduate School
The University of Georgia
December 2009

DEDICATION

I would like to dedicate this work to my wife and to my parents. I would not be here without you.

ACKNOWLEDGEMENTS

I would like to thank my advisor Dr. Bill Miller, who joined my doctoral advisory committee after it was well under way and eventually took over its leadership. I certainly would not be where I am today without his support, guidance, and encouragement. His help and critical evaluation made it possible for me to navigate the final stages of my dissertation writing. I would also like to extend my thanks to all my committee members – Dr. Miguel Cabrera, Dr. Brian Jackson, Dr. David Radcliffe, and Dr. Aaron Thompson – for their support throughout my years at University of Georgia.

Financial assistance was provided through Financial Assistance Award number DE-FC09-07SR22506 from the U.S. Department of Energy to the University of Georgia Research Foundation and by the Department of Crop and Soil Sciences at the University of Georgia. Research was performed in part at Beamline X26A, National Synchrotron Light Source (NSLS), Brookhaven National Laboratory. Beamline X26A is supported by the Department of Energy (DOE) – Geosciences (DE-FG02-92ER14244 to the University of Chicago – CARS) and DOE – Office of Biological and Environmental Research, Environmental Remediation Sciences Division (DE-FC09-96-SR18546 to the University of Georgia). Use of the NSLS was supported by DOE under Contract No. DE-AC02-98CH10886.

TABLE OF CONTENTS

Page

LIST OF TABLES

Page

LIST OF FIGURES

Page

1. INTRODUCTION

Life on Earth has evolved as a function of a relatively small number of natural chemical elements out of the finite number in the periodic table, in addition to solar and geothermal energy inputs and liquid water. While many of the elements are required in large quantities in order to sustain life (e.g., N, K, Ca), others are required only in trace amounts and only by certain life forms (e.g. Ni, Cu, Zn), and many have no known biological function in any terrestrial life form whatsoever and are toxic, e.g., Hg, Pb, U (Adriano, 2001). Trace elements are rarely supplied to the organisms by their environment in the ideal proportions and unneeded or toxic elements are frequently present as well. This imbalance on the outside, however, does not automatically constitute a problem for the organism as each element can be absorbed by biota only in specific chemical forms. Actual biological uptake and expression of essentiality or toxicity of the element (not all chemical forms can participate in biological processes or exhibit toxicity, i.e., inhibition of or damage to organism's functionality) complete the path from the source to the consummation. Smaller bioavailable fractions of a trace or toxic element can be related to its much larger total content in the environment through a two-step process (Pettersen and Hertwich, 2008). Firstly, solid phase speciation of a trace or toxic element reveals its susceptibility to dissolution and secondly, liquid phase speciation determines its mobility and suitability for an uptake by the target organism. This dissertation predominately deals with Pb and U whose mobility and bioavailability can be altered through changes in solid phase speciation (Lindsay, 1979; Nriagu, 1984).

Problem Definition

Chemical composition of the inanimate environment was historically a function of natural inputs (i.e., parent rock, biological activity, atmospheric deposition), but is becoming more and more function of anthropogenic inputs, e.g., fertilizer and pesticide applications, landfills, wastewater, biosolids and manures, combustion residues, mining, and atmospheric deposition (Adriano, 2001). Whether it was the introduction of small quantities of foreign chemicals (pesticides) or disproportionate quantities of ubiquitous compounds (manures) in order to enhance agriculture production, or redistribution of elements during ore mining and smelting, e.g., Al, Fe, Pb, or energy generation, i.e., crude oil, coal, nuclear fuel, for industrial production and household consumption, damage to ecosystem ensued.

Lead: The US has seen a huge increase in Pb demand with the advent of the electrification and communication age in the early 1900s that was, together with automobile mass production, accelerated by the First World War (Wright and Meyer, 1933). Traditional Pb consumption for ammunition, brass and pewter alloys, ceramic glazes, leaded glass, paint and waterworks has been increased by Pb used in cable casings, solder, bearing metal and battery production to approximately 880,000 Mg by the late 1920s (Wright and Meyer, 1933) of which 33% was from recycled metal. Recycling steadily increased to the current level of 75% (Smith, 2004) out of the 1,600,000 Mg annual use (Guberman, 2009; Wright and Meyer, 1933). Compliance with environmental regulations in the 1990s has reduced or eliminated non-battery Pb use in products such as gasoline, paints, solders, and water systems, but total demand remained at the same level as Pb use for batteries steadily increased; while battery manufacturing

represented only 23% and 35% in the late 1920s and early 1930s (Wright and Meyer, 1933), it was 88% in 2008 (Guberman, 2009) and further increase is inevitable with implementation of hybrid electric car technology. Increase in Pb recycling together with release of Pb from the strategic stockpiles has led to a decline in primary production in the US (ore mining and smelting), but long abandoned ore mines, smelters and recycling operations continue to represent a significant, highly localized environmental burden (Holmgren et al., 1993; Ryan et al., 2004). Many decades of flaking paint, industrial and waste incineration emissions, leaded gasoline use, and application of pesticides have contributed to accumulation of Pb, especially in urban soils, to harmful levels in a more diffuse manner.

Uranium: Most of the known commercial U deposits in the world are found in low-temperature, low redox sedimentary environments (Langmuir, 1997a). Leaching had removed the soluble uranyl ion (UO_2^{2+}) and its complexes from siliceous rocks, and U precipitated upon encountering a low redox potential due to the very low solubility of U^{4+} in minerals such as UO_2. Natural deposits have been studied extensively to determine optimum characteristics of depository for spend nuclear fuel, which is largely uranous dioxide (UO_2). The first U-bearing deposits mined in the United States, located on the Colorado Plateau, actually contain carnotite [$K_2(UO_2)_2(VO_4)_2 \cdot 3H_2O$] and were exploited between 1912 and 1945 as a source of radium and later vanadium (Finch, 1998). Tailings from those mines were reprocessed starting in 1942 and eventually contributed 1,225 Mg of U_3O_8 or 14% of the U needed for the three nuclear bombs. At the onset of the Cold War, U was mined specifically for nuclear armament production, and primary U production increased from 35,000 Mg in 1947 to 4,700,000 Mg over eleven years, and by

1960 there was already a registered surplus (USDOE, 1996). The early 1960s saw a rapid investment in U mining for nuclear power production, but the interest was relatively short-lived due to the Three Mile Island accident in 1979 (Finch, 1998). Mined quantities oscillated over the years from 17,000 Mg in 1960 to 9,000 Mg only five years later, and 20,000 Mg by the time of the accident. Annual production of U_3O_8 further dropped by 1990s due to the Chernobyl disaster (1986) and since then has ranged between 1,000 and 2,200 Mg (EIA, 2009a; EIA, 2009b). Economic pressure of constantly dropping U prices in the early 1990s has brought about changes in mining strategy in the US, when traditional underground or open-pit mining of rich U-ores was nearly completely replaced (95%) by in-situ leaching (ISL) of permeable sandstones with basic solutions of bicarbonate (HCO_3^-) as lixiviate mixed with oxygen gas (O_2) as an oxidant (Szymanski, 1994). Acidic ISL techniques using H_2SO_4 were also developed and tested in the US, but never dominated domestic uranium production (Mudd, 2001a; Mudd, 2001b). Decades of mining, milling and chemical extraction of U-bearing ores have left stockpiles of fissile materials and extensive environmental contamination of soils and sediments.

2. LITERATURE REVIEW

Risk Assessment of Metal and Radionuclide Contaminated Soil and Sediment

Accumulation of metals and radionuclides in soils and sediments (i.e., natural polymineralic substrates) presents a serious problem for individual organisms and for ecosystems as whole due to their negative impacts on tissues, organs, biological processes, and bioaccumulation in food chains (Adriano, 2001). Yet, risk assessment can be quite challenging, as bulk substrate concentration of contaminants does not necessarily correlate with toxicity. In order to accurately correlate substrate content with toxicity it is necessary to correctly identify the most susceptible organism and an uptake pathway for that organism. Uptake pathways can be direct by ingestion of contaminated polymineralic substrates by the target organism, in the case of less mobile metals and radionuclides, or more or less indirect, e.g., soil-plant-animal-human, soil-water-human, in the case of more mobile contaminants (Ryan and Chaney, 1992). The assessment is further complicated by the complexity of metal and radionuclide behavior in soils and sediments as related to weathering, adsorption, precipitation, oxidation-reduction, aqueous complexation, and chemical kinetics (Langmuir, 1997b). This dissertation predominately deals with Pb and U, which are considered to belong to the group of the less mobile environmental contaminants.

Ingestion of Pb has been linked to learning disabilities and behavioral problems in children, whereas U intake is linked mainly to kidney chemotoxicity and bone accumulation (ATSDR, 2008; McClain et al., 2005; NCEH, 2009). Children are

especially susceptible to Pb and U exposure because they are the most likely group to directly ingest contaminated soil or sediment. In addition to direct ingestion, U can also enter human or animal bodies via the soil-plant-animal pathway (Linsalata, 1994). In either case, solid phase speciation in the soil or sediment provides a better understanding of metal or radionuclide partitioning, which is vital for assessment of solubility in the child's stomach after direct ingestion or availability for plant uptake in soil.

One way to assess the stability of substrate contaminants is leaching of the polymineralic substrate by application of a single, more or less selective, extractant or predefined series of extractants of an increasing harshness for a specific length of time and under specific environmental conditions, i.e., solid to solution ratio, type and length of agitation, temperature, lack of visible light, or pressure (Shang and Zelazny, 2008). The assumption at the core of selective leachability is that a targeted phase in polymineralic substrate has a unique solubility under specific experimental conditions. However, this unambiguous requirement is frequently not satisfied in such substrates. Leaching techniques cannot be thus viewed as a proxy for a specific process (e.g., weatherability, mobility, bioavailability) or a specific chemical phase (e.g., carbonate vs. phosphate) in soil or sediment, but rather as extractant- and condition-specific 'fractions' (Bacon and Davidson, 2008; Quevauviller, 2002).

Another, more mechanistic stability assessment is based on qualitative description and quantitative inventory of the contaminants through direct mineralogical speciation. Knowledge of mineralogical speciation permits an 'out-of-the-black-box' approach to risk assessment through application of chemical speciation models for more accurate solubility prediction in polymineralic substrates. Despite the apparent upside of the direct

mineralogical speciation approach, there are some serious drawbacks that prevent broader application of these physical methods. Most serious is a need for expensive equipment (i.e., X-ray diffractometer, electron microscope with a variety of detectors) and accessibility and availability of synchrotron-based techniques. Application of physical methods to direct speciation of solid phases can also suffer from poor detection limits, interferences and interpretive difficulties (Shang and Zelazny, 2008). It is for those reasons the leaching techniques remain part of the environmental soil chemistry arsenal even though the direct mineralogical speciation methods gain in popularity (Bacon and Davidson, 2008).

Leaching Procedures

Sequential chemical extraction (SE) techniques fractionate the total metal or radionuclide content of soil or sediment by application of a series of increasingly harsh extractants that can be completed by total digestion of the residuum after the last step of the procedure. Conceptually, the SE fractionation of trace metal or radionuclides in polymineralic substrates borrows from earlier work on nonmetallic elements (Jackson, 1958). There has been a constant increase of interest in trace metal fractionation methods ever since the pivotal work by Tessier et al. (1979), who designed a method to derive five, operationally-defined fractions (Bacon and Davidson, 2008). This extraction procedure was further altered, simplified or expanded by many workers in the field. An example of a simplified SE procedure is the Community Bureau of Reference of the Commission of the European Communities (BCR) procedure conducted by a group of researchers centered around Quevauviller and Ure (Quevauviller et al., 1994; Rauret et

al., 1999; Ure et al., 1993), whereas an example of an expanded SE procedure is the nine-step sequence conducted by Miller et al. (1986). Sequential extraction procedures have been used, in many instances uncritically, to operationally evaluate shifts in metal and radionuclide partitioning (Arey et al., 1999; Kaplan and Knox, 2004; Knox et al., 2003; Ma et al., 1993; Ma et al., 1994a; Ma et al., 1994b; Seaman et al., 2001a; Seaman et al., 2001b; Seaman et al., 2003; Xu and Schwartz, 1994; Xu et al., 1994).

A single extraction Toxicity Characteristic Leaching Procedure (TCLP) was devised by the US Environmental Protection Agency (EPA) under the Resource Conservation and Recovery Act (RCRA) to determine the mobility of both organic and inorganic analytes present in solid wastes that were categorized as 'hazardous waste' (USEPA, 1992). The TCLP reagent applicable in acidic soil and sediment is dilute (0.1 *M*) acetic acid (CH_3COOH) with pH adjusted to 4.93 with sodium hydroxide (NaOH). This method has been used widely to assess metal leachability from many environmental materials (Berti and Cunningham, 1997; Chen et al., 2003; Hettiarachchi et al., 2000; Melamed et al., 2003; Seaman et al., 2003; Yoon et al., 2007) even if its use for specific material has not been extensively tested.

An excellent review of philosophical and technical issues related to applications of SE procedures by Bacon and Davidson (2008) addresses its four major problems, which are "redistribution of analytes among fractions during extraction, non-selectivity of reagents for target phase, incomplete extraction, and precipitation of 'new' mineral phases during extraction". Redistribution and re-adsorption of analytes (i.e., Cu, Pb) was illustrated in extraction studies of spiked natural and synthetic model substrates (Guy et al., 1978; Shan and Bin, 1993). For example, distribution of Pb in spiked, synthetic,

polymineralic substrate fractionated either according to the Tessier (Tessier et al., 1979) or the BCR (Quevauviller et al., 1994) procedure was found to be procedure-specific and remarkably similar in all samples extracted according to the same SE procedure despite the distinct forms of the Pb-enriched spike phase, i.e., calcite ($CaCO_3$), goethite (α-FeOOH), hausmannite (Mn_3O_4), halloysite [$Al_2Si_2O_5(OH)_4$] or humic acid (Raksasataya et al., 1996). They found hausmannite and humic acid were the adsorbing phases in the synthetic substrates. In order to further test the importance of Mn oxides and soil organic matter (SOM) as adsorbing phases in Pb redistribution, Raksasataya et al. (1996) added Pb enriched calcite to two natural soils, a peat soil with 25% of SOM by weight and a mineral soil with 4% SOM, 3% Fe and 0.1% Mn. The study indicated that SE fractionation of Pb in both spiked soils was mostly a function of the distinct soil properties, high SOM and Mn content, rather than the nature of the contamination.

The validity of such spiked evidence in extrapolation to natural and 'naturally contaminated' polymineralic substrates has been questioned on the basis of natural redistribution in 'real' substrates and unrealistically high spiking levels (Belzile et al., 1989; Tessier and Campbell, 1988; Tessier and Campbell, 1991). Nevertheless, concerns related to non-specificity of extractants and redistribution of Pb in natural substrates were supported with spectroscopic evidence by Ostergren et al. (1999) when a high ionic strength extractant (1 *M* $MgCl_2$) aimed at removal of the 'exchangeable' fraction instead dissolved the Pb-bearing mineral jarosite [$Pb(Fe)_6(SO_4)_4(OH)_{12}$]. Liberated Pb was subsequently scavenged from solution by soil Fe hydroxides (i.e., adsorbed Pb as a new phase) and nearly none was removed with the supernatant at the end of the equilibration period. A number of other studies provide similar evidence for non-specificity and

redistribution (Dermatas et al., 2006; Gomez-Ariza et al., 1999; Gomez-Ariza et al., 2000).

An additional point recognized by both sides of the non-specificity of extractants and redistribution argument is proportionality of the mineral phases in the synthetic polymineralic substrates. It omits an important fact that bearers of the active surfaces in natural substrates (e.g., goethite, kaolinite, gibbsite, organic matter) frequently do not co-exist one next to another, but rather form mixed phases on grains of detrital (e.g., quartz) or secondary (e.g., kaolinite) origin (Reilly et al., 2009; Schroeder et al., 2000), frequently coating (i.e., occluding) each other (Shang and Zelazny, 2008). The obvious solution to this problem is through sample preparation (e.g., drying) and homogenization (e.g., grinding, mixing), which greatly improves the extraction procedure, its repeatability and between-batch comparability. On the other hand, the same preparation procedure exposes new active surfaces and may cause a shift of the metal or radionuclide distribution to different fractions, thus creating an artifact that might have significant implications in interpretation of the results.

Solid Phase Speciation

Application of electron or X-ray beams in elemental or structural analyses (i.e., spectroscopic and diffraction techniques) can provide direct evidence for risk assessment of contaminated soils. Both beam sources can be used for either chemical or structural analyses, since either beam has a potential to ‘excite’ atoms by dislocation of core level electrons to the continuum (core electrons are those electrons in an electron cloud located closest to the nucleus) and to be diffracted due to repeating structural arrangement of

crystals. However, X-ray beam application has a major advantage over the electron beam because it does not require a vacuum; while the path of free electrons in the presence of gaseous molecules is at maximum only a few centimeters, X-rays propagate under the same conditions over much larger distance. This allows for application of X-ray beams in analysis of soil or sediment sample at or close to their field conditions, and changes in metal and radionuclide speciation caused by drying of the sample can be avoided.

Energy dispersive (EDS) and wavelength dispersive (WDS) spectrometries detect excess energy given off in the form of X-rays by the excited atom in a process called fluorescence. Fluorescence X-rays are given off by the excited atom while the 'electron hole' is being filled by an electron via translocation from one of the nearest, higher energy levels in the electron cloud. Fluorescence X-ray gains its energy from a difference between the higher energy state and that of the electron hole. Because each electron level in the electron cloud of each element is well-defined in terms of energy, we can detect the element of interest by measuring the intensity of the specific fluorescence X-ray, which is also called a 'characteristic line'. Characteristic lines are marked with a combination of capital letters K, L, and M, lower case Greek letters α, β, and γ and Arabic numbers. Throughout the measurement we have to be aware of potential for overlap between lines of different elements at the same energy level. Multiple elements can be recorded within a predefined energy window instantaneously by EDS detectors, whereas WDS detectors are calibrated to measure one characteristic line at a time. The elemental composition of the analyzed sample can be estimated from the intensity of the lines in the EDS spectrum and quantified by the WDS measurement. In either case, elemental composition represents the whole excited sample volume, whose cross sectional area depends on a

beam size, whereas the depth of excitation depends on beam energy and elemental composition of the sample due to a negative correlation between atomic number and beam penetration.

Spectroscopic results can be further refined by obtaining structural data and quantification of individual chemical or mineralogical phases. This can be achieved by means of synchrotron-based X-ray absorption spectroscopy, which is beyond the scope of this work, and X-ray micro-diffraction. X-ray diffraction techniques derive from the capacity of crystals to diffract radiation due to their repeating structural arrangement. Actual crystal structure is then determined in reverse from the known wavelength of the monochromatic X-rays and known diffraction angles through the use of Bragg's law. Crystalline phases are then identified from the obtained diffraction pattern, which can greatly aid in decisive identification of the mineralogy of the studied chemical element.

Powder X-ray diffraction analyses have been used previously to determine supposed metal or radionuclide speciation in contaminated soils. This method usually includes some form of sample pretreatment to separate only the very fine soil or sediment grains where contaminants generally accumulate in association with clays, sesquioxides and other chemically active surfaces. Very high metal or radionuclide levels are required for identification because larger quantities of pure chemical phases are necessary to diffract the monochromatic X-ray beam. Relatively pure, macrocrystalline mineral assemblages also minimize diffraction from neighboring mineral phases in the case of polymineralic substrates. This avoids creation of overly complex diffraction patterns where some lines of the associated phase might overlap with the diffraction lines of the target phase. Even if we disregard potential alteration of elemental speciation through

redox changes and metal redistribution during sieving and drying, there is still a question of representativeness of the powder diffraction analysis.

In addition, there are no assurances in the published literature that the lists of the identified species are complete. There may be scores of other species in contaminated soil samples whose identification is hampered by overlap between its diffraction lines and those of common soil constituents. What if there were other metal- or radionuclide-bearing microcrystalline minerals in the contaminated soil or sediment that constituted a significant quantity of the metal or radionuclide, but repeatability of diffraction planes was insufficient to produce detectable diffraction signals? The presence of an unidentified species might alter the entire risk assessment outcome due to an unknown solubility product or different solubility trend with regard to pH shifts. Application of synchrotron-based micro-focused X-ray beam in micro-X-ray fluorescence (μ-XRF) mapping and micro-X-ray diffraction (μ-XRD) can be used to identify even smaller crystalline phases in heterogeneous media in its native state (Bertsch et al., 1994; Duff et al., 2001; Lanson et al., 2008; Manceau et al., 2002). In combination these experimental techniques can substantially increase our understanding of metal and radionuclide status in contaminated soils.

Lead in Soil

Lead use for lead-acid batteries, hereafter referred as batteries, constitutes currently approximately 88% of the reported annual U.S. Pb consumption, most of which (up to 80%) is supplied by recycling of spent batteries (Guberman, 2009). Scrap lead-acid battery recycling can result, in some instances, in heavy soil contamination (Cao et al.,

2003c). Battery plates are manufactured from either elemental lead (Pb^0) or lead dioxide (PbO_2) and submerged in 4.5 to 6 *M* sulfuric acid electrolyte. Discharging of batteries leads to an accumulation of lead sulfate ($PbSO_4$) on the surface of either plate (Eqs. 1 and 2).

$$\text{Anode } Pb^0 + HSO_4^- \leftrightarrow Pb^{2+}SO_4(s) + H^+ + 2e^- \qquad \textbf{Equation 1.}$$

$$\text{Cathode } Pb^{4+}O_2 + HSO_4^- + 3H^+ + 2e^- \leftrightarrow Pb^{2+}SO_4(s) + 2H_2O \qquad \textbf{Equation 2.}$$

These three Pb forms (Pb^0, PbO_2, and $PbSO_4$) represent possible inputs to soil during the recycling process. Under conditions common in well-drained aerobic soils tetravalent Pb readily dissolves and undergoes reduction to the divalent form, and elemental Pb oxidizes to a Pb^{2+}. Concentration of Pb^{2+} in solution is controlled by soil pH, availability of cation exchange sites, dissolved and exchangeable cations and availability of ligands such as carbonate, sulfate, phosphate (Lindsay, 1979; Nriagu, 1984). The solubility of Pb in the absence of other ligands was found to be controlled by precipitation of hydrocerussite [$Pb_3(CO_3)_2(OH)_2$] and/or cerussite ($PbCO_3$) (Cao et al., 2003c; Vantelon et al., 2005). Cerussite and hydrocerussite together with massicot (orthorhombic PbO), anglesite ($PbSO_4$) and pyromorphite [$Pb_5(PO_4)_3$(OH, Cl, or F)] were also identified as weathering products of elemental Pb in soils (Cao et al., 2003a; Lin et al., 1995; Vantelon et al., 2005). Solubility of several important Pb-bearing minerals is summarized in Figure 1, which was adapted from Lindsay (1979) for the situation where Ca^{2+} and Cl^- are supplied by 0.01 *M* $CaCl_2$ as background electrolyte. Hydroxycerussite is not included in the Figure 1 because its solubility under normal atmospheric conditions

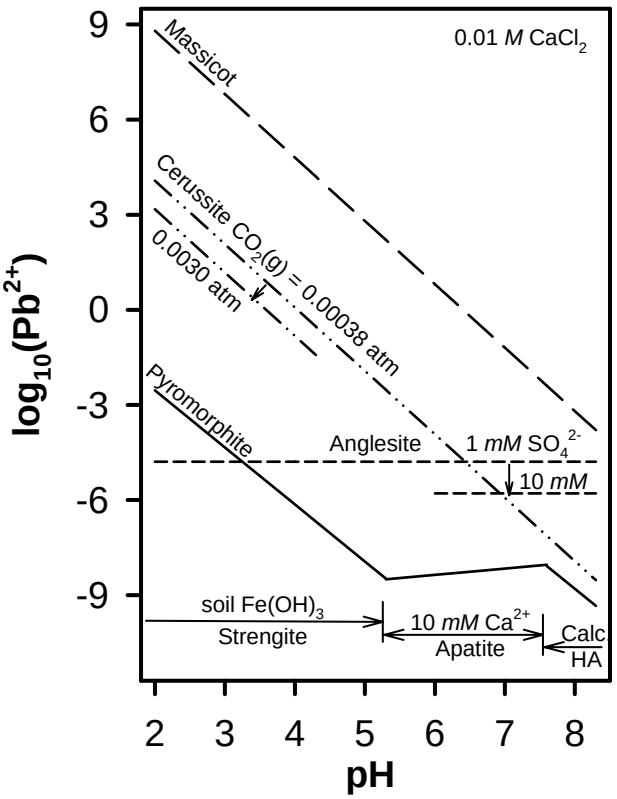

Figure 1. Solubility of common lead minerals plotted as a function of soil pH. Included minerals are massicot (PbO), cerussite ($PbCO_3$), anglesite ($PbSO_4$) and chloropyromorphite [$Pb_5(PO_4)_3Cl$]. Parallel lines represent two different molarities of sulfate (SO_4^{2-}) in dissolution of anglesite or two different pressures of gaseous carbon dioxide [$CO_2(g)$] in pH dependent dissolution of cerussite. Figure was adapted from (Lindsay, 1979) assuming 0.01 *M* $CaCl_2$. Phosphate levels are controlled by dissolution of strengite ($FePO_4 \cdot 2H_2O$) at pH<5.3 or hydroxyapatite [HA, $Ca_5(PO_4)_3OH$] above that pH. Detail calculations and all applicable equilibrium constants can be found in appendix.

is nearly identical with that of cerussite, but cerussite becomes more stable under elevated CO_2 pressures that are common in soils (Lindsay, 1979).

In the absence of phosphate Pb solubility is controlled by anglesite at acid pH and by cerussite above near-neutral pH. It is obvious that Pb solubility can be altered by pH manipulations and/or ligand introduction to the system (Fig. 1). Alkalization, through liming for example, to or above a near neutral pH clearly lowers Pb solubility due to cerussite formation, but acidification requires more detailed knowledge of the system as anglesite still controls Pb solubility in the presence of substantial sulfate concentration, a fact that is not always recognized (Cao et al., 2002; Cao et al., 2003b). Pyromorphite controls Pb solubility in the presence of the phosphate in soil systems, and the stability boundary is controlled by solubility of cations that bind strongly to phosphate (Fe or Al at low pH and divalent Ca at higher pH). As Fe or Al hydroxides become less and less soluble with increasing crystallinity and pH (Fig. 1), $FePO_4 \bullet 2H_2O$ and $AlPO_4 \bullet 2H_2O$ are replaced in controlling of the phosphate solubility by Ca-bearing phosphates such as apatite [$Ca_5(PO_4)_3$(OH, F, or Cl)]. Influence of Ca^{2+} becomes even more pronounced as pH increases further and calcite ($CaCO_3$) precipitates, lowering Ca^{2+} solubility further.

Because sulfate concentration in soil solution is commonly far too low and the solubilities of Pb carbonates and oxides exceed that of Pb-bearing phosphates by several orders of magnitude, in-situ Pb immobilization through the formation of Pb-bearing phosphates can potentially provide a long-term reduction in bioavailability and stabilize Pb over a wide range of geochemical conditions (Berti and Cunningham, 1997; Lindsay, 1979). However, caution is needed since full Pb speciation in the contaminated substrate

needs to be known (Cao et al., 2002; Cao et al., 2003b) and many published solubility products must be evaluated critically (Martinez et al., 2004).

Uranium in Sediment

Uranium has been historically used for colored glass and ceramic glaze production and only relatively recently for a nuclear fuel production. Nuclear material for either reactor fuel rods or nuclear armament requires enrichment of the fissile isotope ^{235}U, which constitutes only 0.719% by mass in most mineral deposits, the other isotopes being ^{234}U and ^{238}U with 0.006% and 99.275%, respectively (Langmuir, 1997a; McClain et al., 2005). The most abundant isotope ^{238}U has found its major use recently in the defense industry in high-density kinetic energy penetrators and as a stock for weapon-grade plutonium (^{239}Pu) manufacturing. Uranium is a radioactive element which means that its nucleus is unstable and disintegrates through emission of α or β particles or γ radiation in a decay series of actinide daughters. Each actinide daughter disintegrates for specific half-life, some in a matter of minutes and others over thousand years, until a stable end-member in that series is reached, i.e., ^{206}Pb, ^{207}Pb or ^{208}Pb (Langmuir, 1997a). Nuclear fission, on the other hand, splits the nucleus of ^{235}U into two fission fragments of approximately the same size. Fission products are unstable and also disintegrate.

The onset and especially the first two decades of the Cold War saw tremendous effort to mass-produce nuclear armaments on both sides of the Iron Curtain. Lack of environmental laws and regulations and limited concern for mining and processing waste disposal together with contemporary technology and know-how have led to localized heavy contamination of soils and sediment with U and associated contaminants, e.g.,

actinide daughters, fission products, metals, and solvents (Antunes et al., 2007; Clark et al., 2006). Since then additional environmental burdens have been added by testing and discharge of nuclear weapons, reactor failures, and more recently by discharges of armor-piercing tank ammunition (McClain et al., 2005). The fervor of the nuclear arms race as well as tactical and political decisions have sidetracked environmental concerns until the last few decades of the 20th century, and in some instances sidetrack those concerns even today (McClain et al., 2005).

The main oxidation states of U are uranous (4+) and uranyl (6+) ions; intermediary 5+ state is mostly unstable relative to the other two. Uranous minerals such as coffinite ($USiO_4$) and uraninite (UO_2) are only sparingly soluble, whereas the solubility of uranyl minerals is in general higher. Least soluble uranyl minerals are vanadates [$(VO_4)^{3-}$] such as carnotite [$K_2(UO_2)_2(VO_4)_2$] and tyuyamunite [$Ca(UO_2)_2(VO_4)_2$]; only slightly more soluble is autunite [$Ca(UO_2)_2(PO_4)_2$] and the most soluble uranyl mineral is schoepite (β-$UO_3 \bullet 2H_2O$) (Langmuir, 1997a). Increasing bicarbonate (HCO_3^-) content of the solution under oxidized conditions greatly increases U^{6+} solubility above pH 5, especially in equilibrium with schoepite, through formation of carbonate complexes (Langmuir, 1997a). This has been used as a mining strategy in in-situ leaching of permeable sandstones (Szymanski, 1994) and heap-leaching of U ore and contaminated soils (Mason et al., 1997).

Solid phase speciation of U in contaminated polymineralic substrates such as soils and sediments is to a large extent a function of redox conditions. Oxidized soils and exposed sediments are generally dominated by the hexavalent oxidation state in the form of schoepite, uranyl complexes with organic ligands or mixed oxides and hydroxides

(Bertsch et al., 1994; Duff et al., 2000; Hunter and Bertsch, 1998; Lind et al., 2009; Morris et al., 1996). Under reducing conditions U speciation shifts toward the tetravalent uranous forms (Duff et al., 2000; Tokunaga et al., 2008; Tokunaga et al., 2005). Risk assessment is thus greatly dependent on the redox conditions of U contaminated polymineralic substrates. Uranium solubility in oxidized polymineralic substrates can be altered by manipulation of redox conditions (flooding) with support of obligatory anaerobic microbial population or by ligand addition (orthophosphate) to lower U solubility through formation of autunite-like solid phases (Arey et al., 1999; Seaman et al., 2001a; Seaman et al., 2001b; Seaman et al., 2003).

Phosphate Additions to Soil and Sediment

Unfortunately, the phosphate content in most soils is insufficient to facilitate natural precipitation of Pb- or U- phosphates. Phosphate addition obviously shifts equilibria in favor of Pb-bearing phosphate mineral and mixed mineral formation (Ma et al., 1993) even if iron and aluminum phosphates control P solubility at acid soil pH (Fig. 1). In recent years, phosphate applications from various chemical sources have received considerable attention as a practical remediation strategy for soils contaminated with both metals (Pb, Ni) and radionuclides (Th, U) (Arey et al., 1999; Basta et al., 2001; Kaplan and Knox, 2004; Knox et al., 2003; Seaman et al., 2003). Such an approach to soil remediation was proven to be more cost effective and less disruptive when compared to soil excavation and off-site treatment or disposal (Hettiarachchi and Pierzynski, 2004).

Of all phosphate minerals, apatites are by far the most abundant and widely studied (Hughes and Rakovan, 2002). Pyromorphite was identified and suggested as a

common product of Pb precipitation after apatite or rock phosphate addition to Pb-contaminated soils (Basta et al., 2001; Ma et al., 1993; Xu and Schwartz, 1994). Even though most apatite amendment studies have focused on Pb-contaminated soils, several other studies demonstrated the effectiveness of such strategy in addressing a range of common metal and radionuclide contaminants such as Cd, Cu, Zn, Ni, and U (Arey et al., 1999; Xu et al., 1994). The suggested molar P : Pb application ratio ranges from 3:1 to 3:5, depending on the presence of additional contaminants that may compete with Pb for phosphate in solution (Basta et al., 2001; Hettiarachchi et al., 2001; Ma et al., 1994a; Ma et al., 1994b).

The low solubility of natural hydroxyapatite [HA: $Ca_5(PO_4)_3OH$] rather than mineral surface area was identified as a major factor limiting its effectiveness in metal immobilization (Ma et al., 1993). The limited solubility of HA restricts application to surficial materials where the amendments can be thoroughly mixed with contaminated materials of interest. To overcome this limitation, several studies evaluated the potential use of more soluble forms of phosphate (De Stefano et al., 2006; Jensen et al., 1996; Nash et al., 1998; Seaman et al., 2003; Tsao et al., 1997). Several recent studies focused on myo-inositol hexakisphosphate, also known as phytic acid (IP6: $C_6H_{18}O_{24}P_6$, Fig. 2) (Jensen et al., 1996; Nash et al., 1998; Seaman et al., 2003).

Phytate is commonly found as a phosphorus storage compound in plants and is produced as a byproduct of the fermentation industry (Turner et al., 2002). Accumulation of IP6 in the manure of monogastric animals results from the low levels of the appropriate enzyme in their digestive tracts, and for the same reason IP6 also accumulates in appreciable quantities in sewage sludge biosolids from residential areas (Golovan et

al., 2001; Sharpley and Moyer, 2000; Shober et al., 2006). Phytate, with six phosphate groups, has a high charge density and strongly interacts with the soil, either being adsorbed to clays and iron oxides (Celi et al., 2003; Celi et al., 1999) or precipitated as insoluble salts of Fe, Al, Ca, and Mg (Jensen et al., 1996). Phytate salts of trivalent ions (Fe^{3+} and Al^{3+}) are comparatively less soluble than the salts of divalent ions (Ca^{2+} and Mg^{2+}) and those are still less soluble than comparable ortho-phosphates (Crea et al., 2004; Jackman and Black, 1951a). The strength of these reactions effectively stabilizes IP6 in soils, prevents enzymatic hydrolysis, and causes IP6 accumulation especially in waste amended soils (Jackman and Black, 1951b; Turner et al., 2002). Therefore, significant research has been conducted to evaluate the role of IP6 in eutrophication associated with soil erosion (Turner et al., 2002).

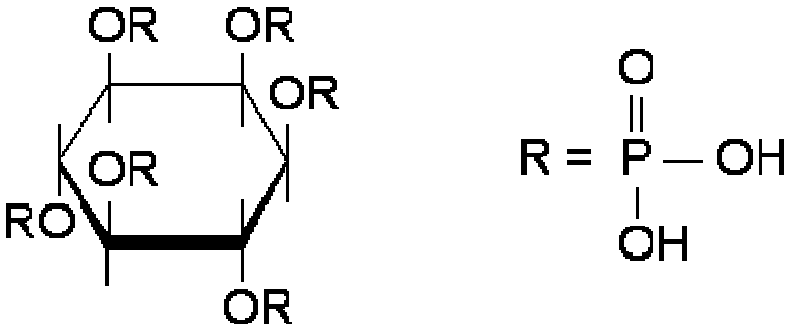

Figure 2. Phytic acid – myoinositol hexakis dihydrogen phosphate.

Jensen, Nash and their co-workers (1996; 1998) suggested a multistep process to facilitate the in-situ immobilization of metal and radionuclide contaminated substrates in which a solution containing IP6 is injected into an aquifer or sprayed on the land surface,

where it would then migrate through porous substrate and react with native polyvalent cations (e.g., Al, Fe, Ca, Mg) and precipitate. Immobilization of metals and radionuclides from solution then occurs either by precipitation of appropriate metal phytates or co-precipitation with phytates of common soil cations. Subsequent hydrolysis and mineralization of IP6, releasing orthophosphate, would then mimic the addition of HA. The proposed multistep process was largely evaluated in batch equilibration experiments.

Seaman et al. (2003) evaluated the efficacy of IP6 to potentially immobilize U, Ni, and other metals in contaminated sediments. The study pointed out differences in the efficacy of two IP6 salts, dodecasodium- and tetracalcium-IP6, and HA in decreasing the solubility of U, Ni, and other target metals. Further, knowledge of the effects of substances with solubilities and mobility in porous media higher than that of IP6 (e.g., cyclophosphate such as a trisodium trimetaphosphate, TP3) is limited. Trimetaphosphate does not adsorb appreciably to soil, whereas both of the hydrolysis products of the TP3 (Eqs. 3 to 5), orthophosphate and pyrophosphate [$H_2P_2O_7^{2-}$], which in turn hydrolyzes to orthophosphate (Eq. 5), do adsorb (Blanchar and Hossner, 1969b).

$$P_3O_9^{3-} + H_2O \rightarrow H_2P_3O_{10}^{3-} \qquad \textbf{Equation 3.}$$

$$H_2P_3O_{10}^{3-} + H_2O \rightarrow H_2P_2O_7^{2-} + H_2PO_4^- \qquad \textbf{Equation 4.}$$

$$H_2P_2O_7^{2-} + H_2O \rightarrow 2H_2PO_4^- \qquad \textbf{Equation 5.}$$

Metaphosphate hydrolysis to pyrophosphate and finally to orthophosphate can occur in addition to hydrolysis by acid or basic solutions catalyzed enzymatically by trimetaphosphate hydrolase, or chemically by dissolved Ca^{2+}, Mg^{2+} (Busman and

Tabatabai, 1985). The rate of the hydrolysis can be higher for field-moist soil when compared to once air-dried soil, presumably due to difference in microbial activity (Dick and Tabatabai, 1986). Blanchar and Hossner (1969a) reported a soil half life for TP3 of five hours. Immobilization of metals then occurs either by binding of pyrophosphate and orthophosphate to metal ions in solution (Al, Mg, Pb), or co-precipitation during the equilibration period (Dick and Tabatabai, 1987; Hossner et al., 2004).

Objectives of this Study

The purpose of this study was: (i) to evaluate the effects of various P sources on the solubility of Pb, Cu, and Zn in coarse-textured soil and U and Ni in fine-textured sediment as compared to HA, and (ii) to asses the long term stability of the immobilized Pb, Cu, Zn, U, and Ni as assessed by chemical extraction and solid-phase characterization methods.

3. MATERIALS AND METHODS

Sample Description

Lead Contaminated Soil: The soil material for this study was collected from a contaminated site in Jacksonville, FL, which began as a gasoline station, then became a salvage yard, and lastly has been used as a lead-acid battery recycling facility. Detailed description of the site was provided in the previous work of Cao et al. (2003c). Soil from a nearby undisturbed location was classified as a Spodosol (sandy, siliceous, thermic Ultic Alaquod). Industrial activities resulted in high levels of Pb, Zn, and Cu that are restricted mostly to the surface horizon. The soil was collected from the surface horizon rich in soil organic matter (Table 1), where mineralogical characterization revealed the presence of calcite ($CaCO_3$) and cerussite ($PbCO_3$) (Cao et al., 2002). Relatively high pH and the presence of free calcite are most likely the result of lime addition. Lime has been added most likely with an intention of lowering Pb solubility through precipitation of cerussite in the absence of phosphate anion (Fig. 1). Soil was air dried and sieved (2-mm) and stored in a plastic zip-lock bag.

Uranium Contaminated Sediment: The sediment material for the study was collected from the lower Tims Branch watershed on the Savannah River Site (SRS), former nuclear weapons production facility in Aiken, South Carolina, which drains eventually to the Savannah River after joining with Upper Three Runs Creek. The A/M area of the SRS was used for production of aluminum-clad uranium targets for nuclear weapons from 1958 until 1985, with production peaking in second half of 1960s. This

study site has been extensively studied and the history of the site is described in several publications (Batson et al., 1996; Punshon et al., 2003b; Punshon et al., 2004; Punshon et al., 2003c; Sowder et al., 2003). Briefly, Tims Branch watershed received a portion of the waste water discharge from the A/M processing area while the rest was diverted into an M-area settling basin. Most of the contaminants settled out in the Steed Pond, a pre-Cold War era farm pond with a wooden spillway in the lower Tims Branch watershed. The waste water contained large quantities of U and Al and other associated metals, chiefly Ni and smaller quantities of Cr, Cu, Zn, and Pb. Cumulative release of U into the Steed Pond was estimated in the vicinity of 44 Mg and although cumulative Ni release is unknown, the estimates based on the M-area settling basin suggests a similar amount.

Table 1. Selected physical and chemical properties collected for the contaminated soil from a decommissioned lead-acid battery recycling plant (Jacksonville, FL).

	Mean	SD
pH[§], n = 12	6.44	0.05
Organic carbon[#], %	3.91	0.90
Soil texture[†], n = 5	——— % ———	
Sand	97.12	1.25
Clay	2.27	1.15
Selected elements[‡], n= 4	——— mg kg^{-1} ———	
Aluminum	6931	384
Manganese	182	2
Iron	17835	2,016
Copper	1329	549
Zinc	1675	377
Lead	5155	970

[§] 10:1 solution/soil ratio in 0.01 *M* $CaCl_2$ (McLean, 1982)
[#] Walkley-Black Procedure (Nelson and Sommers, 1982) from (Cao et al., 2002)
[†] Hydrometer method (Gee and Bauder, 1986)
[‡] HF/HNO_3 microwave assisted digestion at 827 kPa (USEPA methods manual SW-846).

Table 2. Selected physical and chemical properties of the contaminated sediment collected from the surface soil in the lower Tims Branch watershed on the Savannah River Site near Aiken, SC.

	Mean	SD
pH[§], n = 3	4.44	0.01
Organic carbon[#], %, n = 1	6.91	
Soil texture[†], n = 3	%	
Sand[†], %	40.74	7.48
Clay[†], %	33.13	1.61
Selected elements, n = 4	mg kg^{-1}	
Nickel[‡]	340	26
Nickel[¢]	361	14
Uranium[‡]	1,273	99
Uranium[¢]	1,380	39

[§] 10:1 solution/soil ratio in 0.001 *M* $CaCl_2$ (McLean, 1982)
[#] Dry combustion (Leco, St. Joseph, MI) (Zabinski, 2006)
[†] Hydrometer method (Gee and Bauder, 1986)
[‡] HF/HNO_3 microwave assisted digestion at 827 kPa (USEPA methods manual SW-846).
[¢] HNO_3 microwave assisted digestion at 827 kPa (USEPA methods manual SW-846)

While the use of the M-area settling basin was later discontinued and basin was eventually capped, Steed Pond remained in its original state. The wooden spillway eventually gave way in 1984 when some of the highly contaminated sediment spilled to the lower Tims Branch watershed. Steed Pond became a wetland, subject to periodic erosion that contributed to the movement of the sediment downstream. Extent of the contamination in the lower watershed was studied on several occasions, and it was determined that the contamination varied greatly as a function of geomorphology, especially elevation and curvature, and other physical characteristics such as sediment pH (Borden, 2006; Punshon et al., 2003b; Zabinski, 2006). Mineralogy of the finest, highly reactive clay-sized sediment fraction is dominated by goethite (α-FeOOH) and,

presumably also due to the high effluent Al concentration, by three Al-bearing minerals (i.e., mainly kaolinite and lesser amounts of hydroxy-interlayered vermiculite and gibbsite) (Arey et al., 1999). Significant quantities of kaolinite were identified by the same authors also in the coarser, silt-sized fraction. The present study was conducted on the contaminated sediment sample with the highest total U and Ni content, designated TB6 (Table 2), that was collected from the surface of the soil in the lower watershed by Zabinski (2006). I do not know precise sampling location of the TB6. Sediment was stored at 4°C in field moist state in a plastic zip-lock bag.

Total Digestion

Subsamples (≈ 0.25 g dry weight) of 2-mm sieved Pb soil or TB6 sediment (Tables 1 and 2) were weighed into PFA-Teflon pressure vessels, each sample with four replicates. Microwave-assisted digestion (MDS-2000, CEM Corp., Matthews, NC) of samples was conducted in a mixture of 9 ml HNO_3 with 3 ml of HF according to the US EPA method 3052 (USEPA, 1996). Uranium contaminated sediment TB6 was in addition to HF/HNO_3 mixture digested in 10 ml of HNO_3, also in four replicates, to determine degree of eventual incorporation of U into the silicate minerals because this treatment is unable to dissolve those kinds of mineral assemblages. In order to avoid clouding of the sediment HF/HNO_3 digests after dilution with DI water, which was most likely caused by precipitation of metals in the form of fluorides, samples were treated immediately after cooling with 25 mL of 4% w/v boric acid (H_3BO_3) solution. Sealed pressure vessels were heated in microwave for ten more minutes at 160°C and 2.41 MPa to dissolve fluoride precipitates (Kingston et al., 1997; Strucken et al., 1988). Total concentrations of metal

and radionuclide in solution were measured by inductively coupled plasma mass spectrometry (ICP-MS, Elan 6000) and optical emission spectrometry (ICP-OES, Optima 4300 DV, PerkinElmer, Norwalk, CT). Element recovery of each digest was compared with the certified values of an applicable Standard Reference Material (SRM) produced by the National Institute of Standards and Technology (NIST), i.e., SRM 2709 San Joaquin soil and RM 8704 Buffalo River sediment for the Pb contaminated soil and U contaminated sediment, respectively (NIST, 2000; NIST, 2003).

Batch Equilibration

Four P amendments were evaluated in batch equilibrations and are listed in order of decreasing solubility: trisodium trimetaphosphate [TP3: $Na_3(PO_3)_3$], reagent-grade dodecasodium phytate [Na-IP6: $Na_{12}(CH(PO_4))_6$], precipitated calcium phytate [Ca-IP6: $Ca_{4.85}Na_{0.06}H_{2.24}(CH(PO_4))_6 \bullet nH_2O$, n ≈ 6.5] and reagent-grade hydroxyapatite [HA: $Ca_5(PO_4)_3OH$]. Ca-IP6 was used rather than commercially available monocalcium phytate [$CaH_{16}(C(PO)_4)_6 \bullet nH_2O$, $n \approx 3.1$] because it causes a significant decrease in pH and increases contaminant metal solubility (Seaman et al., 2003). The Ca-IP6 was produced as outlined by Nash et al. (1998) and Seaman et al. (2003) with one exception, oven drying at 60˚C was replaced by freeze drying. The surface area of each amendment material was determined using the Brunauer-Emmett-Teller (BET) method with N_2 as the probe gas (ASAP 2000, Micromeritics Instrument, Norcross, GA). Crystallinity of precipitated Ca-IP6 was evaluated by X-ray diffraction (XRD) (Scintag Inc. USA, Cupertino, CA). Surface area and XRD results were compared with those of Ca-IP6 prepared for a previous study by Seaman et al. (2003).

Three grams of sieved (2-mm) soil or sediment (Tables 1 and 2) were placed in Oak Ridge centrifuge tubes and amended with the appropriate P source. Six P based treatment levels, i.e., mass of P per mass of soil (approx. 0, 1, 2, 4, 8, 12 g kg^{-1}), were evaluated for the Pb contaminated soil and four levels (approx. 0, 2, 4, 10 g kg^{-1}) for the U contaminated sediment. Addition in excess of 10% by the dry weight of soil (65 g kg^{-1}) that could lead to a misinterpretation of the P addition effect due to physical dilution was not in exceeded. Sets with no soil or sediment added were also tested as controls. Each treatment consisted of six replicates for HA, Na- and Ca-IP6 and three replicates for TP3 for the Pb contaminated soil and three replicates for all four treatments in the U contaminated sediment. The amended soil or sediment was equilibrated in 15 ml of 0.01 *M* or 0.001 *M* $CaCl_2$ for the Pb or U contaminated samples, respectively on a reciprocal shaker for 170 hours at room temperature to establish quasiequilibrium conditions (Seaman et al., 2003). Following equilibration, the suspensions were then centrifuged at 10,000 rpm (11,952 g) for 20 min (RC5B, Sorval Kendro Laboratory Products, Newton, CT) and the pH was measured on the supernatants. Supernatants were filtered (0.22-μm nylon filters) prior to analysis for dissolved organic carbon (DOC, TOC-5000A, Shimadzu, Kyoto, Japan). The remaining supernatant was acidified (1% HNO_3) and analyzed for elemental composition by ICP-MS and ICP-OES. Residual soil within the centrifuge tubes were air-dried and saved for subsequent analysis.

Toxicity Characteristic Leaching Procedure

Changes in trace element partitioning resulting from the soil amendments were assessed using the USEPA Toxicity Characteristic Leaching Procedure (TCLP) (Davis et

al., 1990; USEPA, 1992). The TCLP procedure is used as a regulatory indicator of contaminant leachability in a municipal solid waste landfill under slightly acidic conditions. The TCLP reagent was prepared by diluting 5.7 mL of glacial acetic acid (CH_3COOH) and 64.3 mL of 1.0 *M* sodium hydroxide (NaOH) up to 1 liter with de-ionized water (18.3 MΩ cm) for a final pH of 4.93. Fifteen milliliters of the TCLP solution were added to a 0.75-g subsample of air-dried homogenized residual soil or sediment from each replicate of the treated and untreated soils and sediments described previously "to extract the solid phase with an amount of extraction fluid equal to 20 times the weight of the solid phase" (USEPA, 1976). In addition, U containing samples were analyzed in duplicate for each replicate. Samples were agitated on a reciprocal shaker for 18 hours at 25ºC, centrifuged, and the supernatant was filtered, acidified, and analyzed for elemental composition as described above. The TCLP extractable concentrations were corrected for any metal removed during the initial equilibration in 0.01 *M* or 0.001 *M* $CaCl_2$ in the case of Pb and U contaminated soils, respectively (Seaman et al., 2001b; Seaman et al., 2003).

Sequential Extraction

Subsamples (0.7500 g) of the air-dried residual soil or sediment from the batch equilibration were also assessed for treatment derived changes in trace element partitioning using a modified sequential extraction (SE) procedure consisting of eight steps listed from least to most aggressive in Table 3 (Arey et al., 1999; Miller et al., 1986). Miller's SE procedure has been altered for extraction of this soil and sediment by eliminating lead nitrate [$Pb(NO_3)_2$] reagent in the 'specifically adsorbed' (also called

Table 3. Sequential extraction steps used to asses trace element partitioning listed from least to most aggressive (Arey et al., 1999; Miller et al., 1986).

Step	Targeted fraction	Reagent	pH	Time, h	Note
W	Water soluble	deionized nano-pure water	5.5	16	
Ex	Exchangeable	0.5 *M* $Ca(NO_3)_2$ calcium nitrate	5	16	
Ac	Acid soluble	0.44 *M* glacial CH_3COOH + 0.1 *M* $Ca(NO_3)_2$ acetate reagent	2.5	8	
Hh	Mn-oxide occluded	0.01 *M* NH_2OH-HCl + 0.1 *M* HNO_3 acidified hydroxylamine hydrochloride	1.2	0.5	
Py	Organically bound	0.1 *M* $Na_4P_2O_7$ sodium pyrophosphate	10	24	
Ox	Amorphous Fe-oxide occluded	0.175 *M* $(NH_4)_2C_2O_4$ + 0.1 *M* $H_2C_2O_4$ ammonium oxalate	3	4	Darkness
Di	Crystalline Fe-oxide occluded	0.15 *M* $Na_3C_6H_5O_7$ + 0.05 *M* $C_6H_8O_7$ + 0.5 g $Na_2S_2O_4$ sodium dithionate in citrate buffer	5	0.5	50°C
Re	Residual (USEPA, 1996)	HF/HNO_3 microwave assisted digestion hydrofluoric/nitric acid digestion	< 1	0.16	180°C, 827 kPa

'inner-sphere complexed') fraction and 'crystalline Fe-oxide occluded' fraction was reduced solely by dithionite ($Na_2S_2O_4$) in a citrate ($C_6H_5O_7^{3+}$) buffer (Arey et al., 1999). Subsamples (0.2 g) of the residuals after the extraction of dithionite-extractable fraction were dissolved in duplicate according to the US EPA method 3052, microwave assisted digestion for siliceous materials (USEPA, 1996).

It is also important to emphasize that pyrophosphate, a TP3 hydrolysis product (Eq. 4), is the selective extractant for the 'organically bound' fraction of trace elements, the fifth step of the SE procedure. When hydrolyzed, the maximum amendment level for TP3 would correspond to 0.026 *M* pyrophosphate solution, which is approximately ¼ strength of the organically bound trace element extractant. After each extraction step, the samples were centrifuged, and the supernatants were filtered, acidified if necessary, and analyzed for metals as described above. The most soluble fraction, i.e., the water-soluble fraction, was corrected for any metal removed during the initial equilibration in 0.01 *M* or 0.001 *M* $CaCl_2$ in the case of Pb and U contaminated soil and sediment, respectively.

X-ray Spectrometry in the Electron Microscope

Treatment-derived changes in HA and Ca-IP6 amended Pb contaminated soil samples and metal enrichment of mineral grain coating in the same soil were evaluated using Energy Dispersive Spectrometry (EDS) and Wavelength Dispersive Spectrometry (WDS) in the electron microprobe (JEOL 8600 Superprobe, JEOL USA, Peabody, MA). Air-dried residual soil from the batch equilibration treated at the highest P amendment level, 12 g kg^{-1}, in the form of either HA or Ca-IP6 were deposited on glass slides treated with epoxy and cured at 135ºC. Grain mounts (each approximately 1 cm^2) on the glass

slides were subsequently ground until a uniform thickness was achieved – mechanically and by hand at 600 and 1000 mesh, polished, and carbon-coated. The quality of the polish was verified using a reflected light microscope. Three mounts were prepared for each studied amendment for total of six slides.

Mounted samples were imaged and analyzed with a Noran EDS X-ray microanalysis system (Thermo Electron Corporation, Minneapolis, MN) automated with PGT Avalon 4000 multi-channel analyzer running PGT Excalibur software (Princeton Gamma-Tech Instruments, Rocky Hill, NJ). The microprobe was also equipped with four WDS CITZAF1 V4.01 detectors (Geller MicroAnalytical, Topsfield, MA, Copyright by California Institute of Technology, Pasadena, CA). Beam parameters were as follows: current 15 nA, acceleration voltage 15 keV, spot size 5 μm, EDS collection time 30 live-time sec (45 to 60 real-time sec), and WDS dwell time 5 μsec. Inevitably higher energy lines will excite lower energy lines of lighter elements thus increasing counts of those elements. High Pb content (Table 1) made it prone to creation of additional signal for Mn, Fe, Cu, and Zn, but analytical software should correct for such interferences (Reed, 1996).

Slides were randomly, visually searched for grains with a visible coating. Whole grains were imaged in backscattered mode and elemental composition of spots with high Pb fluorescence signal was later recorded by WDS. Two different WDS analyses were conducted. First, oxide standards were used to quantify major elements present in precipitates and second, the elemental form of the standards for Zn, Cu, and Pb to analyze for their presence within the secondary precipitates.

Synchrotron Element Mapping and X-Ray Micro-Diffraction

Beamline Instrumentation

Synchrotron-based measurements were conducted on the X26A beamline at the National Synchrotron Light Source, Brookhaven National Laboratory, Upton, NY. The X-ray beam was monochromatized with a Si (111) crystal channel-cut to 7-mm gap. Monochromatic beam was then micro-focused to an approximately 9 × 7 μm spot by two 100-mm long, dynamically bent, rhodium coated silica mirrors arranged in Kirkpatrick–Baez geometry. The incident beam was optimized at 17.2 keV.

Fluorescence radiation for element mapping was recorded by a Radiant Vortex-EX silicon drift detector, whereas micro-diffraction patterns were recorded on a Bruker SMART 1500 charge-coupled device area detector utilizing Bragg techniques. The silicon drift detector was situated at 90° to the incident micro-beam in order to optimize signal/noise ratio by utilizing low intensity of scattered X-rays of the incident micro-beam at this angle. A diffraction detector equipped with a silver beam stop was positioned in transmission geometry. The sample stage was situated at 45° and viewed in normal incidence by an optical microscope with TV attachment.

Data Collection and Analytical Software

Only HA and Ca-IP6 amended Pb contaminated soil and U contaminated sediment samples from the batch equilibration were compared with an unamended soil (or sediment) unequilibrated in the background $CaCl_2$ solution because of their effect decreasing Pb, Cu and Zn or Ni and U solubility. Samples amended at 4 g kg^{-1} were selected because there was little decrease in contaminant solubility at higher treatment

levels. Air dried samples of the whole untreated and treated soils were lightly dusted on and sealed between pieces of Kapton tape. Two slides were prepared for each amendment studied for each soil, a total of eight slides. Micro-X-ray fluorescence element maps of randomly selected particles with detectable Pb fluorescence signals were recorded with a 7-μm step size and 2-s dwell time per pixel. Automated mapping included the following elements: Ca, Ti, Mn, Fe, Ni, Cu, Zn and Pb. Possible inference encountered in fluorescence emission measurements was an overlap between K-lines of Ti and L-lines of Ba, especially because either anatase (TiO_2) or barite ($BaSO_4$) can be relatively common soil particles. Fortunately, both anatase and barite present in the soil were highly crystalline and could be easily identified from the micro X-ray diffraction patterns.

Element maps were viewed in X26A_Plot, a general beamline plotting routine, and pixels with the highest element μ-XRF signal per particle were selected for diffraction analysis. Diffraction ring patterns from selected pixels were collected subsequently by exposing a single frame for 60 seconds with beam energy tuned to 17.374 keV with corresponding wavelength (λ) of 0.07136 nm. The large active input area combined with highest available spatial resolution optimizes this diffraction system for collection of diffraction rings out to higher 2θ angles on even weakly diffracting samples. The combination of the collimated micro-beam with high sensitivity/high resolution diffraction setup enables data collection on crystals as small as 10-μm. Area data (diffraction rings) were integrated to 1-D, i.e., intensity vs. 2θ angle, in the Fit2D program (Hammersley, 1997; Hammersley et al., 1996). Diffraction device settings (beam center, camera distance and non-orthogonality) were optimized using the known wavelength and combination of the α-Al_2O_3 and silver behenate ($AgC_{22}H_{43}O_2$) standard

diffraction patterns (Hammersley et al., 1994; 1989). A threshold mask was applied when deemed necessary to eliminate overly bright spots on or off the diffraction rings in order to aid the integration algorithm. Application of threshold masks was determined necessary by empirical observation when it was noticed that an excessively bright spot on or slightly off the diffraction ring resulted in a shift in the true position of the diffraction line, whereas 'lonely' bright spots resulted in an unjustified peak in the integrated 1-D pattern. Application of the mask was necessary especially in the case of the weakest 2-D diffraction patterns, frequently obtained for the phosphate treated soil samples, to eliminate as much noise as possible.

Identification of crystalline minerals from the integrated patterns was partially computerized (Match!, 2003; PDF-2, 2003). Where doubts existed about identity of the phases after the application of the computerized search routine, μ-XRF elemental composition of the diffracted pixels was taken into account to eliminate the presence of improbable mineral phases. Sometime uncertainty persisted despite the search and match procedure and knowledge of the elemental composition. In these instances, a minimalistic principle was applied and unidentified diffraction lines were assigned to phases already identified in the other, well-defined patterns from pixels of similar elemental composition for the same type of sample, i.e., untreated, HA or Ca-IP6 treated.

4. RESULTS AND DISCUSSION

A. Lead Immobilization in Phosphate Amended Soil

Batch Equilibration of Lead Contaminated Soil

Phosphorus and metal, Zn, Cu, and Pb, concentrations in solution originating from batch equilibration are plotted as a function of added P to soil ratio. Error bars represent one standard deviation of the treatment means. The 'reactivity' of the P amendments followed the expected trend with trisodium trimetaphosphate (TP3) and sodium phytate (Na-IP6) being much more reactive than precipitated calcium phytate (Ca-IP6) and reagent-grade hydroxyapatite (HA) (Fig. 3). The term 'reactivity' is used throughout this dissertation to cover both solubility and kinetic limitations of amendment dissolution and phosphate precipitation. From 30 to 80% and 0 to 50% of the P added in the form of TP3 and Na-IP6, respectively, was recovered in the supernatant at the end of the batch equilibration. High recovery of P from TP3 and Na-IP6 amended samples left much smaller amount of P to react during subsequent extractions. Also, concentrations of P in solution in the case of HA and Ca-IP6 were most likely lower due to the 'common ion effect' of Ca in the background solution (Arey et al., 1999; Seaman et al., 2001b). In the presence of soil, concentration of P in solution decreased when compared with the control: significantly in the case of Ca-IP6 (nearly forty times) and HA (five times) and only slightly at the three lowest amendment levels in the case of Na-IP6 and TP3 (data not shown). The presence of soil also resulted in less Ca remaining in solution when

compared to control: Na-IP6 (ten times) and TP3 (nearly two-fold), whereas Ca-IP6 and HA stayed approximately the same (data not shown).

The low inherent buffering capacity of the coarse-textured soil resulted in large differences in the measured pH values for the various treatments after equilibration. The

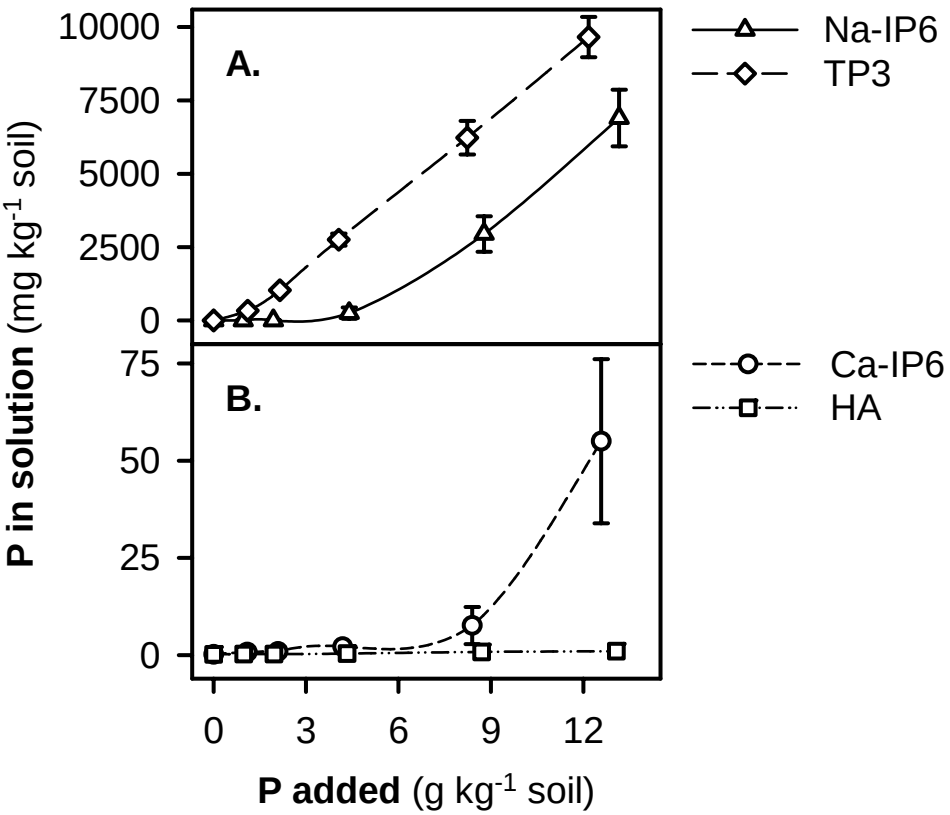

Figure 3. Effect of addition of calcium phytate (Ca-IP6), hydroxyapatite (HA), sodium phytate (Na-IP6), and trisodium trimetaphosphate (TP3) to the soil from a lead-acid battery recycling facility (Jacksonville, FL) on soluble phosphorus (*A* and *B*) after equilibration for 170 hours in 0.01 *M* $CaCl_2$ on a reciprocal shaker. Error bars represent one standard deviation of the treatment level means. Splines were included to improve data readability and do not represent exact trends.

pH for the HA treatments remained essentially constant, Na-IP6 increased pH nearly to 10 and addition of both, Ca-IP6 and TP3, lowered pH from 6.4 to 5.7 (Fig. 4). Rapid hydrolysis of the TP3 to pyrophosphate catalyzed by Ca in the background solution and slower hydrolysis of pyrophosphate to orthophosphate could be responsible for the rapid decrease in pH. Pyrophosphate would effectively buffer the solution because of the relatively low pKa_1 and pKa_2 values for the pyrophosphate, 0.85 and 1.96, respectively (Busman and Tabatabai, 1985; Manahan, 1990).

The maximum dissolved organic carbon (DOC) increase resulting directly from the phytate (IP6), an organophosphoric compound, addition would be just over 1 mg L^{-1}.

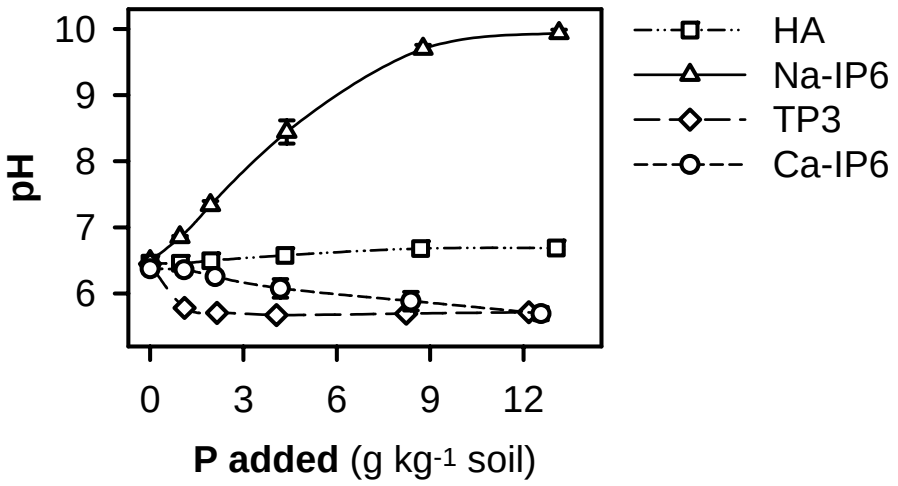

Figure 4. Effect of addition of calcium phytate (Ca-IP6), hydroxyapatite (HA), sodium phytate (Na-IP6), and trisodium trimetaphosphate (TP3) to the soil from a lead-acid battery recycling facility (Jacksonville, FL) on pH after equilibration for 170 hours in 0.01 *M* $CaCl_2$ on a reciprocal shaker. Error bars represent one standard deviation of the treatment level means. Splines were included to improve data readability and do not represent exact trends.

On one hand, an increase in DOC up to 2100 mg L^{-1} was observed with increasing Na-IP6, presumably because of the dispersion of soil organic matter (SOM) resulting from the large increase in pH combined with high Na concentration in solution, over 3 g kg^{-1}

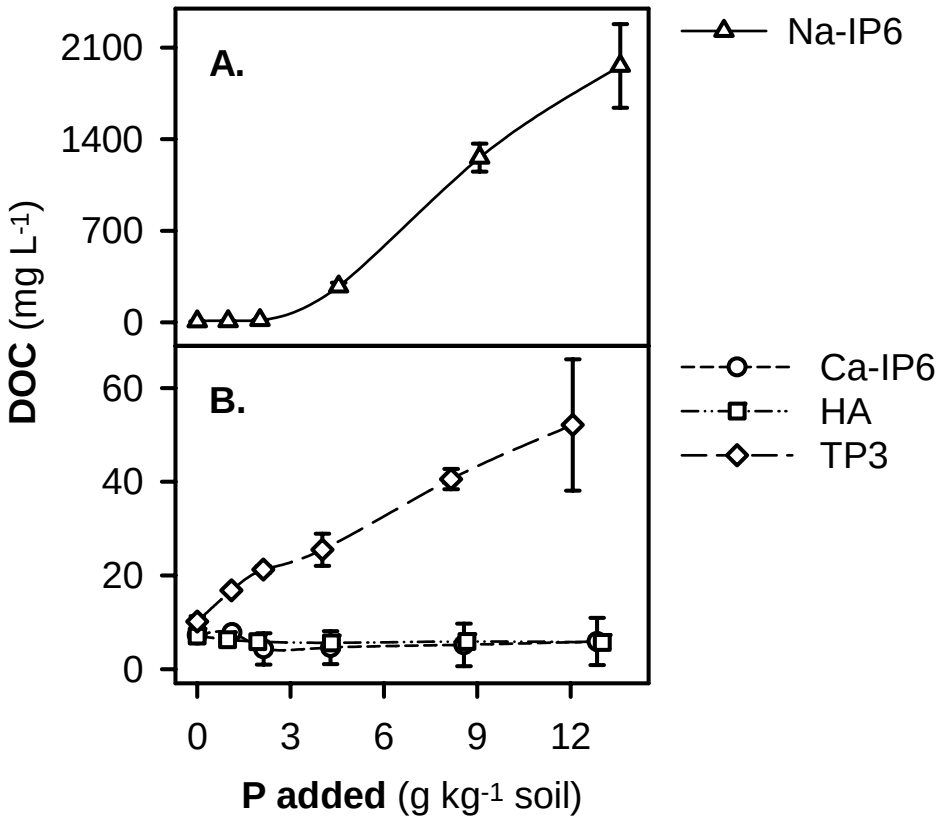

Figure 5. Effect of addition of calcium phytate (Ca-IP6), hydroxyapatite (HA), sodium phytate (Na-IP6), and trisodium trimetaphosphate (TP3) to the soil from a lead-acid battery recycling facility (Jacksonville, FL) on dissolved organic carbon (DOC, *A* and *B*) after equilibration for 170 hours in 0.01 *M* $CaCl_2$ on reciprocal shaker. Error bars represent one standard deviation of the treatment level means. Splines were included to improve data readability and do not represent exact trends.

soil (Seaman et al., 2003). On the other hand, DOC fluctuated, similar to HA treatment, around 6 mg L^{-1} for Ca-IP6 probably due to the strong affinity of IP6 for iron oxides and the flocculating power of the Ca containing background solution (De Groot and Golterman, 1993). A more moderate increase in DOC was observed for TP3 and was presumably caused by the following two factors, not necessarily in this particular order (Fig. 5): (i) a suppression of SOM adsorption on mineral surfaces because of the competition with TP3 hydrolysis products, i.e., pyrophosphate and orthophosphate, and (ii) a decrease in the number of the sorption sites due to the dispersion of the SOM by the pyrophosphate, which is used as a selective extractant for the organically bound trace metals (Table 3). Pyrophosphate solubilizes soil organic matter through polyvalent metal complexation (i.e., Al, etc.) that facilitates SOM dispersion (Papp et al., 1991). Concentration of Al in solution increased from much less than 1 to nearly 30 mg g^{-1} with increasing TP3 application and concentration of Fe in solution remained unchanged, around 15 mg g^{-1}. It needs to be emphasized that Na-IP6 turned out to be a more effective dispersant than pyrophosphate.

Metal Solubility after Equilibration Period

As observed in numerous previous studies (Arey et al., 1999; Kaplan and Knox, 2004; Knox et al., 2003; Ma et al., 1993; Ma et al., 1994a; Ma et al., 1994b; Seaman et al., 2001b; Seaman et al., 2003; Xu and Schwartz, 1994; Xu et al., 1994), HA decreased the solubility of Zn, Cu, and Pb with increasing amendment levels (Figs. 6 to 8). The solubility of the trace metals decreased as a result of the application of any P source for the lowest amendment level with only one exception: Cu after the addition of TP3 (Fig.

7). This exception could be explained by a greater strength of Cu-SOM complexes compared to Pb- and Zn-SOM complexes (Karapanagiotis et al., 1991), predominant association of Cu with SOM when compared to Zn and Pb (Bang and Hesterberg, 2004), and a competition between SOM and large dissolved pyrophosphate concentration for

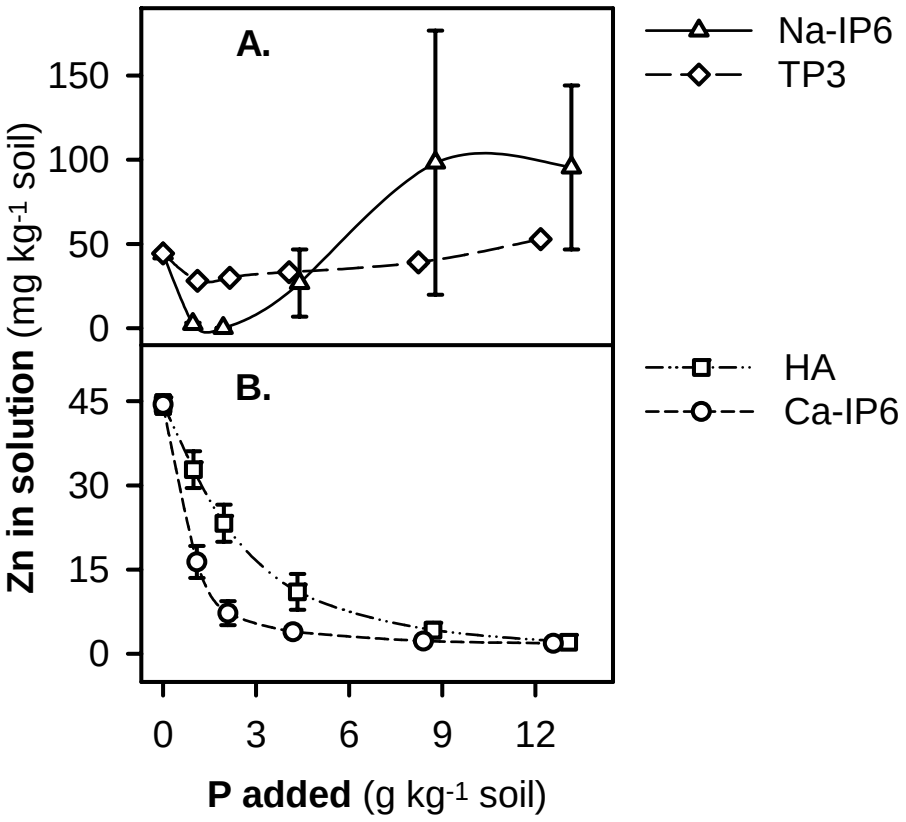

Figure 6. Effect of addition of calcium phytate (Ca-IP6), hydroxyapatite (HA), sodium phytate (Na-IP6), and trisodium trimetaphosphate (TP3) to the soil from a lead-acid battery recycling facility (Jacksonville, FL) on soluble zinc (*A* and *B*) after equilibration for 170 hours in 0.01 *M* $CaCl_2$ on a reciprocal shaker. Error bars represent one standard deviation of the treatment level means. Splines were included to improve data readability and do not represent exact trends.

adsorption sites (Fig. 3). Effects of the further addition differ for each amendment. Precipitated Ca-IP6 was even more efficient in lowering Zn solubility than HA, from 45 to around 2 mg kg^{-1}, than HA. Seaman et al. (2003) indicated that precipitated Ca-IP6 performed similarly to HA. The higher efficiency of the Ca-IP6 in our case, especially in the case of Zn (Fig. 6), was probably caused by its higher 'reactivity'. This conclusion was supported by differences in measured BET (N_2) surface areas and crystallinity of precipitated Ca-IP6. Oven-drying decreased the BET surface area on average by 2.5 m^2 g^{-1} to approximately 23 m^2 g^{-1} and facilitated crystal structure formation as verified by XRD (data not shown).

Most striking was the difference in trace metals solubility between precipitated Ca-IP6 and Na-IP6. On one hand, the solubility of all trace metals in the beginning decreased with increasing Ca-IP6 application and only concentration of Cu in solution increased over the control level at P amendment levels over 2 g kg^{-1}. On the other hand, Na-IP6 addition increased the solubility of all of the trace metals at P amendment levels over 2 g kg^{-1} and the most sensitive was again Cu. Dramatic increases in metal solubility at Na-IP6 amendment levels over 4 g kg^{-1} resulted from the aforementioned dispersal of the SOM (Figs. 4 and 5). The high variability observed for the trace metals at the three highest Na-IP6 levels (Figs. 6 to 8) reflects the complexity of the system characterized by the large increase in pH and DOC. No effort was made to decouple the effect of Na-IP6 addition from dynamics of metals in solution and DOC after pH adjustment with a strong base (e.g., sodium hydroxide: NaOH) in unamended soil, but it is assumed that at least some increases in DOC and metals in solution would be observed as pH increased for two reasons. Firstly, all studied metals tend to be at least to some extent associated with

SOM (Karapanagiotis et al., 1991). And secondly, SOM fractionation is frequently determined from proportions solubilized after pH manipulation with a strong base and strong acid (McBride, 1994). It was determined experimentally that recovery of various metals in a model solution of metal salts and purified humic acids (Sigma-Aldrich, St.

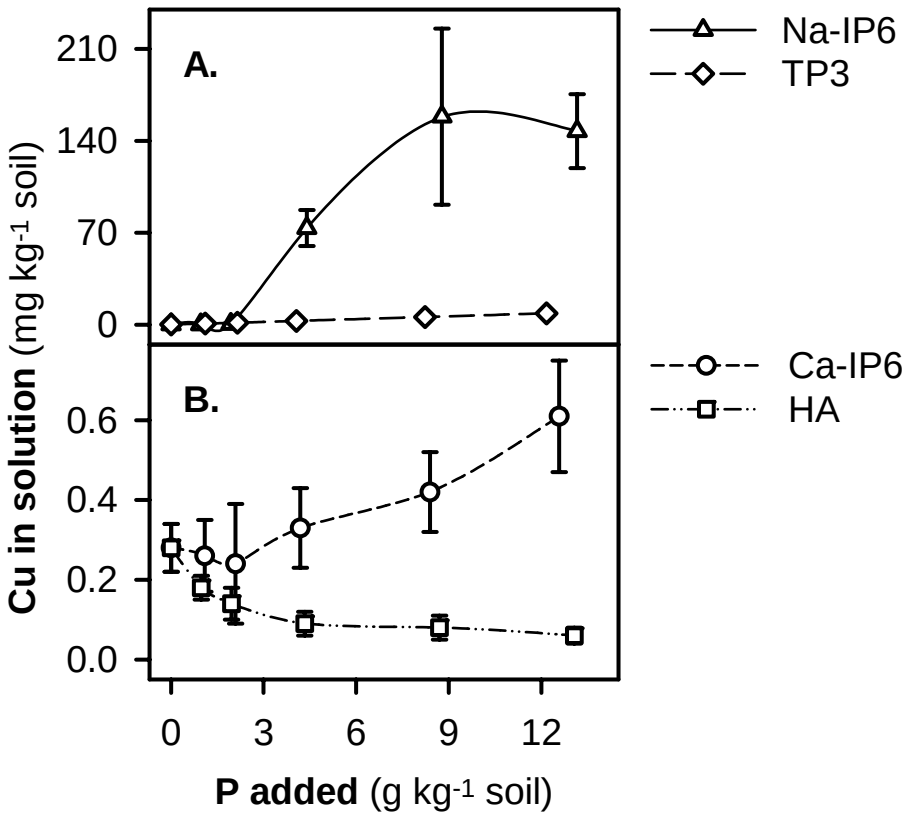

Figure 7. Effect of addition of calcium phytate (Ca-IP6), hydroxyapatite (HA), sodium phytate (Na-IP6), and trisodium trimetaphosphate (TP3) to the soil from a lead-acid battery recycling facility (Jacksonville, FL) on soluble copper (*A* and *B*) after equilibration for 170 hours in 0.01 *M* $CaCl_2$ on a reciprocal shaker. Error bars represent one standard deviation of the treatment level means. Splines were included to improve data readability and do not represent exact trends.

Louis, MO) in the 0.001 *M* $CaCl_2$ background solution at pH around 10, after filtration with 0.22-μm nylon filter, increased with increasing level of purified humic acid, an arbitrarily determined fraction of SOM, followed by pH adjustment from approximately 3 to 10 by sodium hydroxide (data not shown). Increased recovery was attributed to the

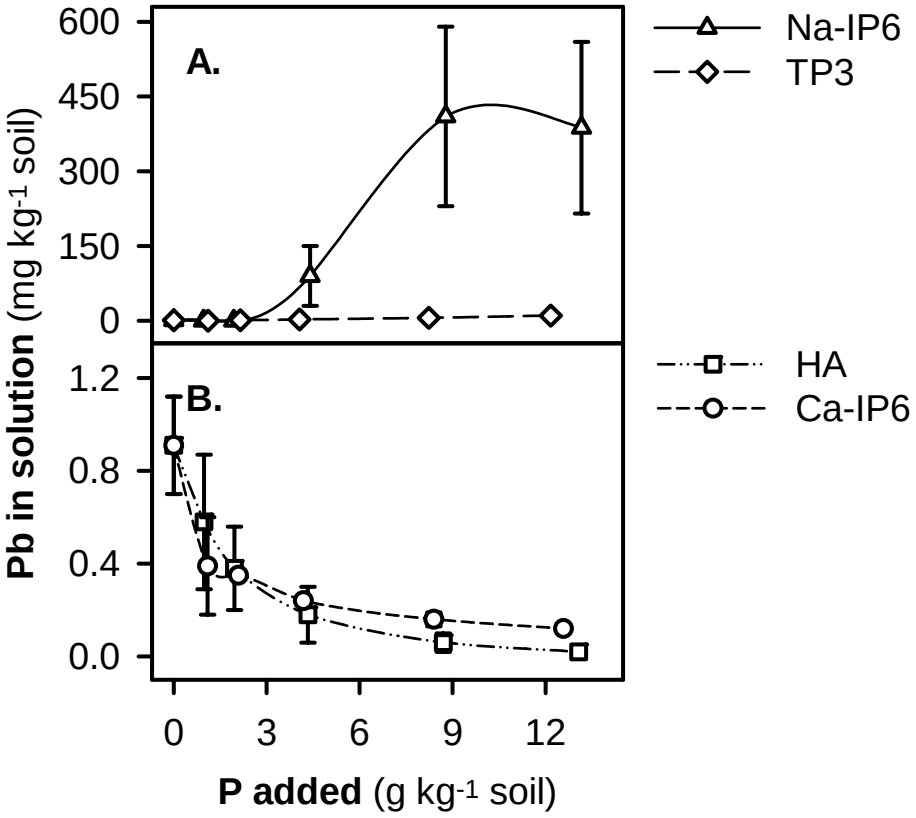

Figure 8. Effect of addition of calcium phytate (Ca-IP6), hydroxyapatite (HA), sodium phytate (Na-IP6), and trisodium trimetaphosphate (TP3) to the soil from a lead-acid battery recycling facility (Jacksonville, FL) on soluble lead (*A* and *B*) after equilibration for 170 hours in 0.01 *M* $CaCl_2$ on a reciprocal shaker. Error bars represent one standard deviation of the treatment level means. Splines were included to improve data readability and do not represent exact trends.

chelation potential of humic acid, which lowered metal content available for precipitation (as pure or mixed metal hydroxides) in the background solution depleted in Ca upon increase in pH. Importance of each of the three proposed steps: (i) Ca consumption from solution, (ii) pH increase, and (iii) DOC increase, which most likely take place simultaneously, is hard to determine due to complex and unknown kinetics of the chemical reactions. In comparison, TP3, the most soluble amendment, caused just a moderate increase in metal solubility: Pb and Cu at amendment levels over 4 and Zn at 12 g kg^{-1}. Organically bound trace metals were most likely selectively extracted by the pyrophosphate, a TP3 hydrolysis product, from the organically bound fraction. This conclusion was further supported by a moderate increase in DOC in TP3 amended samples (Figs. 5 to 8).

Toxicity Characteristic Leaching Procedure of the Contaminated Soil

The leachable fraction was corrected for the removal of metals during the initial equilibration (Seaman et al., 2001b; Seaman et al., 2003). Leachability of the trace metals from the treated soil under slightly acidic (pH ≈ 4.93), weak ligand (acetate), conditions of the TCLP extractant decreased to some extent with increasing amendment levels. All of the amendments tested were efficient in decreasing trace metal leachability for the two lowest addition levels as compared to control soil. However, the effect of SOM dispersal and metal complexation by IP6 and TP3 hydrolysis products in Na-IP6 and TP3 treated soil, respectively, affected the corrected TCLP-leachable fraction. Overall, the solubility of the trace metals in the treated soil samples was below that of the control soil except for Cu for the Na-IP6 and TP3 treatments over 4 g kg^{-1}.

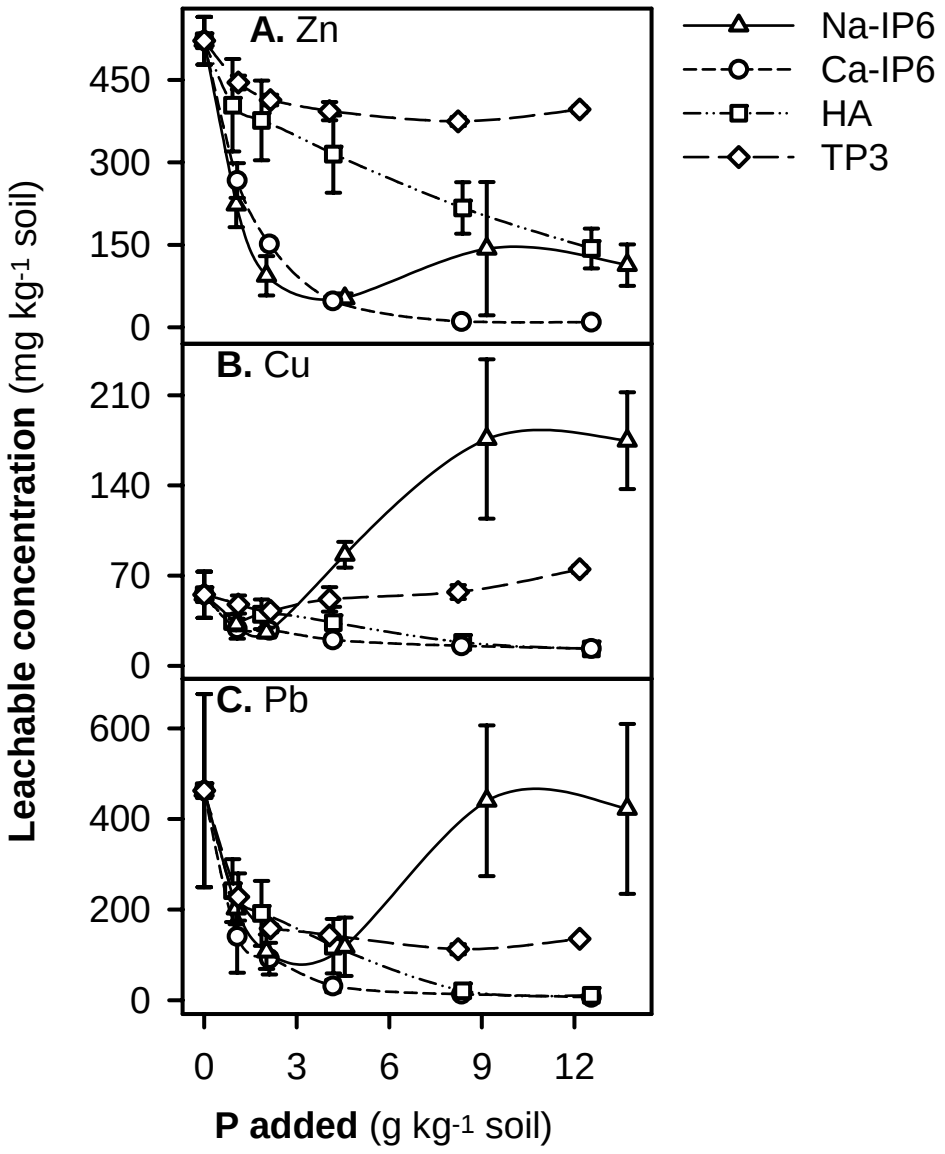

Figure 9. Toxicity Characteristic Leaching Procedure (TCLP) extractable zinc (*A*), copper (*B*), and lead (*C*) for the soil from a lead-acid battery recycling facility (Jacksonville, FL) amended with calcium (Ca-IP6) and sodium phytate (Na-IP6), hydroxyapatite (HA) and trisodium trimetaphosphate (TP3). Error bars represent one standard deviation of the treatment level means. Splines were included to improve data readability and do not represent exact trends.

Hydroxyapatite and Ca-IP6 treated soil samples behaved similarly with regards to lowering TCLP-leachability of the trace metals (Fig. 9). Not only does Ca-IP6 dissolve better than HA, but De Groot and Golterman (1993) also reported that IP6 adsorbs preferentially onto goethite [Fe(OOH)] when compared to orthophosphate. The higher efficiency of precipitated Ca-IP6 in this study when compared with Seaman et al. (2003) could have resulted from difference in Ca-IP6 'reactivity' attributed to the drying method, with freeze-drying yielding a product with a high surface area and lower crystallinity when compared to oven-drying.

This soil contaminated during a recycling of waste (i.e., spent lead-acid batteries) would be categorized as a 'hazardous waste' under the Resource Conservation and Recovery Act due to its toxicity (USEPA, 1992). Such categorization would be granted on basis of the TCLP leachable Pb concentration (Fig. 9C) as the other contaminant metals present at this site are not listed. The TCLP regulatory level for Pb is 5 mg L^{-1} (USEPA, 1992), which translates in the case of this extraction's liquid to solid ratio of 20 to 1 to 100 mg kg^{-1} soil. Clearly, only Ca-IP6 or HA addition at the three or two highest amendment levels, respectively resulted in lowering of the TCLP extractability of Pb below the regulatory level (Fig. 9C). However, additional dissolution of residual amendments in the aggressive TCLP reagent could have resulted in formation of Pb-bearing phosphates during the extraction procedure itself (Scheckel et al., 2003; Scheckel et al., 2005). The data about the stability of Zn, Cu, and especially Pb thus need to be interpreted with caution.

Sequential Extraction of the Lead Contaminated Soil

A refined operational assessment of metal solid-phase associations in the soil was conducted by successively dissolving less chemically labile fractions and the associated metals (Table 3) (Arey et al., 1999; Miller et al., 1986). Extracted mass of Al, Mn, Fe, Cu, Zn, and Pb for the untreated control soil sample were depicted as a portion of total mass extracted in the eight-step SE procedure (Fig. 10). This total extracted mass, so called pseudo-total, for each element was compared to the HNO_3/HF digestion of the whole sample (Table 1 and Fig. 10). Treated soil samples, including the untreated control, were grouped for each sequential extraction step in order to easily identify trends in metal solubility (Figs. 11 to 13).

On one hand, relatively small differences between the SE pseudo-totals and whole sample digest values were observed for Mn and Zn. On the other hand, rather large differences were observed for Al, Fe, Cu, and Pb. Small difference could be attributed to a low soil content in the case of Mn (Table 1) and nature of solid phase speciation and an extended equilibration time in the case of Zn. Zinc was extracted in two easily extractable fractions, i.e., Ex and Ac (Fig. 10). Synchrotron solid phase speciation by X-ray absorption near-edge spectroscopy (XANES) of Zn and Cu in two similar, coastal plain, sandy soils from North Carolina determined that Zn was usually adsorbed on Al- and Fe-oxide minerals, whereas Cu was mainly bound to soil organic matter (Bang and Hesterberg, 2004). Adsorbed Zn could be mobilized by fluctuations in soil solution composition, move through the soil and over time enrich more or less equally various adsorption surfaces, while Cu stayed strongly bound by the SOM. Unfortunately, we do not know when contamination of the Jacksonville site with these metals occurred and

Figure 10. Sequentially extracted aluminum (*A*), manganese (*B*), iron (*C*), copper (*D*), zinc (*E*), and lead (*F*) from a contaminated soil collected from a decommissioned lead-acid battery recycling facility (Jacksonville, FL). Samples were equilibrated for 170 hours in 0.01 *M* $CaCl_2$ on a reciprocal shaker. Sequential extraction steps are listed from the least to the most aggressive step (Table 3). Extracted metal concentrations were reported as a percentage of total concentration, which is represented by the number next to the element symbol in mg kg^{-1} soil, inserted in parenthesis is one standard deviation of the mean. Percentages represent difference between the sum of all extraction steps for each element and HF/HNO_3 digestion of the whole soil. Error bars represent one standard deviation of the fraction means. Please note different Y-axis scales on each row of graphs.

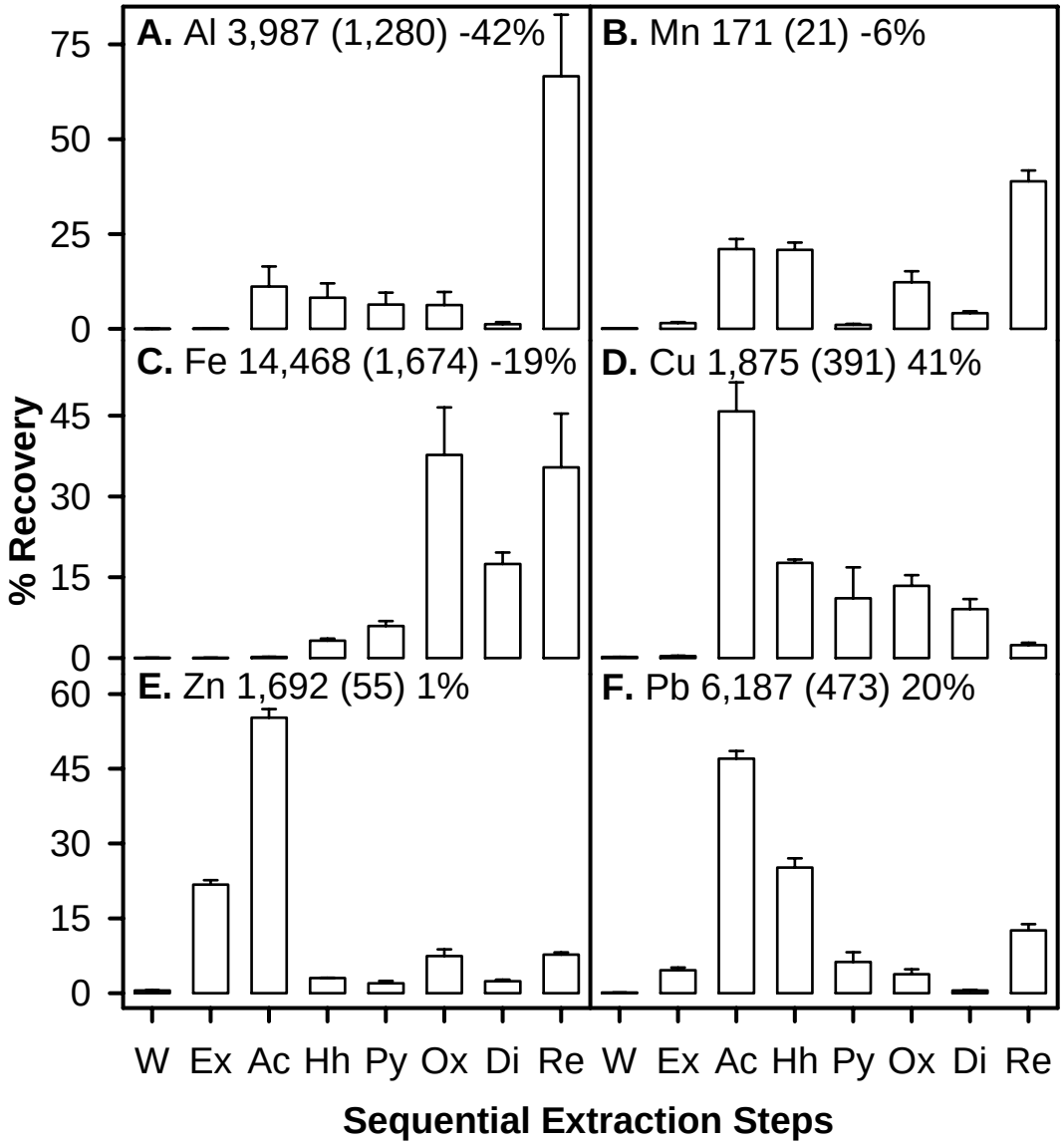
A. Al 3,987 (1,280) -42%
B. Mn 171 (21) -6%
C. Fe 14,468 (1,674) -19%
D. Cu 1,875 (391) 41%
E. Zn 1,692 (55) 1%
F. Pb 6,187 (473) 20%
% Recovery
0
15
30
45
60
75
W Ex Ac Hh Py Ox Di Re W Ex Ac Hh Py Ox Di Re
Sequential Extraction Steps

cannot thus deliberate, whether at least some of the differences in the pseudo-totals can be attributed to the temporal factor. Zinc response to the addition of HA and Ca-IP6 amendments was the most pronounced among the contaminants and could be attributed to the emergence of fresh abundant adsorption surfaces (Fig. 6). The dominance of the acetate-extractable over the calcium nitrate-extractable fraction could be to some extend artifactual as re-adsorption of Zn liberated by high ionic strength solution of neutral salt (1 *M* $MgCl_2$) to acetate-extractable fraction was illustrated (Gomez-Ariza et al., 1999), but it is hard to discuss this particular outcome since either reagent in our SE procedure was different (Table 3).

Large difference in Cu pseudo-total could be attributed to the presence of a few grains with a rich SOM coating particularly enriched in Cu and pyrophosphate-extractable or associated with pure Cu-bearing phases or amorphous and easily reducible Fe and Mn oxides soluble in acidic acetic acid and hydroxylamine hydrochloride reagents (Table 3), respectively (Fig. 10). Latter would also be true for Pb as diagnostic XRD diffraction peaks of Pb carbonate mineral (i.e., cerussite), whose solubility is highly pH dependent (Fig. 1), were observed even in the bulk soil from this site (Cao et al., 2002; Cao et al., 2003b). This fact was further exacerbated by a fact that microwave assisted digestion allows only for a small sample mass of 0.25 g soil per replicate. Conducive to this explanation are large values of standard deviation for both whole soil means, i.e., Cu 1,329 (549) and Pb 5,155 (970) mg kg^{-1} (Table 1), and the fact that mean sums of all SE steps for both elements, i.e., Cu 1,875 (391) and Pb 6,187 (473) mg kg^{-1} (Fig. 10), fall within or very close to one SD of the whole soil means. Very large differences in case of Fe and especially Al or 19% and 42%, respectively are then definitely a function of

heterogeneity of this coarse-textured soil. Nearly ¾ of all Al were extracted in the residual fraction with the rest generally associated with fractions between acetate- and oxalate-extractable fractions (Fig 10). The same proportion of Fe (~75%) was extracted in three least soluble fractions, i.e., Ox, Di and Re at 35%, 15%, and 30% respectively. On one hand, large amount of Fe in the residual (silicate lattice) fraction when compared to the Di is somewhat troubling and could be considered to be an indicator of an incomplete reduction of Fe by dithionite in citrate buffer in the preceding step. An incomplete reduction would be also supported by a sizeable proportion of the residual Mn. On the other hand, Miller et al. (1986) also extracted sizeable proportions of Fe and Mn in soils with low and medium Fe and Mn contents that were comparable to our values (Table 1). It is indeed possible that the overall low Mn content in this highly weathered soil was indicative of presence of mostly recalcitrant Mn solids.

Zinc: The majority of Zn was associated with more labile forms, with the bulk of the Zn in acetate- (60%) and calcium nitrate-extractable (< 25%) fractions. Less soluble, but redox sensitive forms, from hydroxylamine- to dithionite-extractable fractions, contained together around 20% and the residual fraction contained up to 10% of the total Zn content. An increase in the two most soluble fractions of Zn with increasing levels of P amendment in the form of TP3 was compensated by a decrease in the acetate-extractable fraction (Fig. 11A). The increase in the solubility of the most soluble fraction for the other readily soluble P source, Na-IP6, caused by the dispersion of SOM, was so large that it decreased Zn-recovery in all other SE fractions (Fig. 11B). Further, no other clear Zn-recovery trends were observed in less soluble fractions for either highly soluble P amendment. Apparently, higher added phytate concentration, a known chelate of

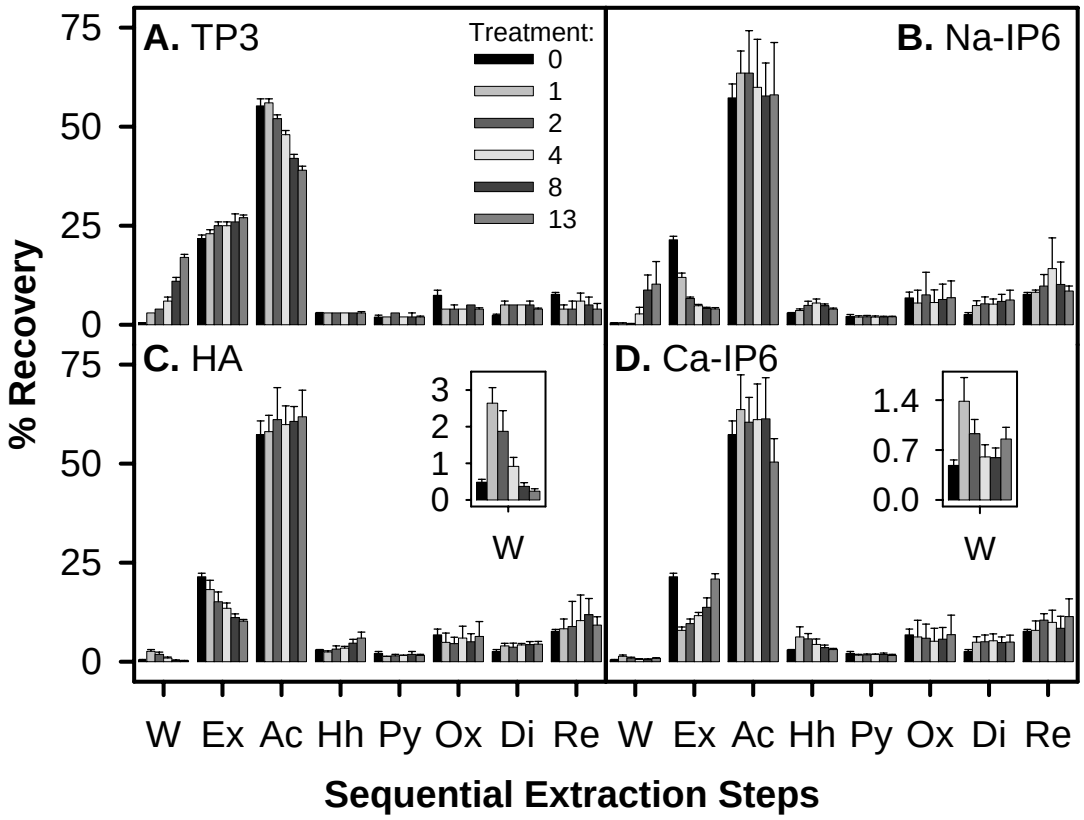

Figure 11. Sequentially extracted zinc from contaminated soil amended with trisodium trimetaphosphate (*A*), sodium phytate (*B*), hydroxyapatite (*C*), and calcium phytate (D). Samples were equilibrated for 170 hours in 0.01 *M* $CaCl_2$ on a reciprocal shaker. Sequential extraction steps are listed from the least to the most aggressive step (Table 3). Inserts reflect the expanded scale for the 'water-soluble' fraction of the given graphs. Extracted metal concentrations were reported as a percentage of total concentration. Unit for legend are treatment levels reported as mass of phosphorus added per mass of soil in g kg^{-1}. Error bars represent one standard deviation of the fraction means.

divalent metal ions, counterbalanced any positive effect of Ca-IP6 on the water-soluble fraction by increasing the calcium nitrate-extractable fraction (Fig. 11D) (He et al., 2006). Hydroxyapatite behaved conservatively by decreasing Zn-solubility in the two most soluble fractions which were compensated by increases in the next two less soluble fractions (Fig. 11C). This decrease might have been function of redistribution of Zn liberated by the calcium nitrate reagent to HA adsorption surfaces. Some of the adsorbed Zn might have been liberated from HA surfaces by the acidic acetate and hydroxylamine reagents and some was carried over to the two most recalcitrant fractions.

Copper: When compared to Zn most of Cu was in the six least soluble fractions, with the bulk in the acetate-extractable (50%) fraction and five ≈10%-portions in the following less soluble, but again redox sensitive, fractions. Copper's response to the soluble amendments Na-IP6 and TP3 in some instances resembled that of Zn probably because of similar mechanisms of interaction (Figs. 12 A and B). It was hard to observe any clear solubility trend for Ca-IP6 amended soil samples (Fig. 12D). Hydroxyapatite once again lowered the solubility of Cu, now in only the most soluble fraction (W), when compared with only two of the most soluble fractions in the case of Zn. This decrease was counterbalanced by an increase in Cu solubility in hydroxylamine-extractable fraction. Copper recovery also increased in the oxalate-extractable and residual fractions (Fig. 12C).

Lead: Most of the Pb was associated with acetate- (30-50%) and hydroxylamine-extractable (20-40%) fractions and the residual (15%) fraction (Fig. 13). Dodecasodium phytate and TP3 treatments, which increased Pb solubility during initial equilibration and had the least effect on decrease of the Pb TCLP leachability behaved similarly. A high

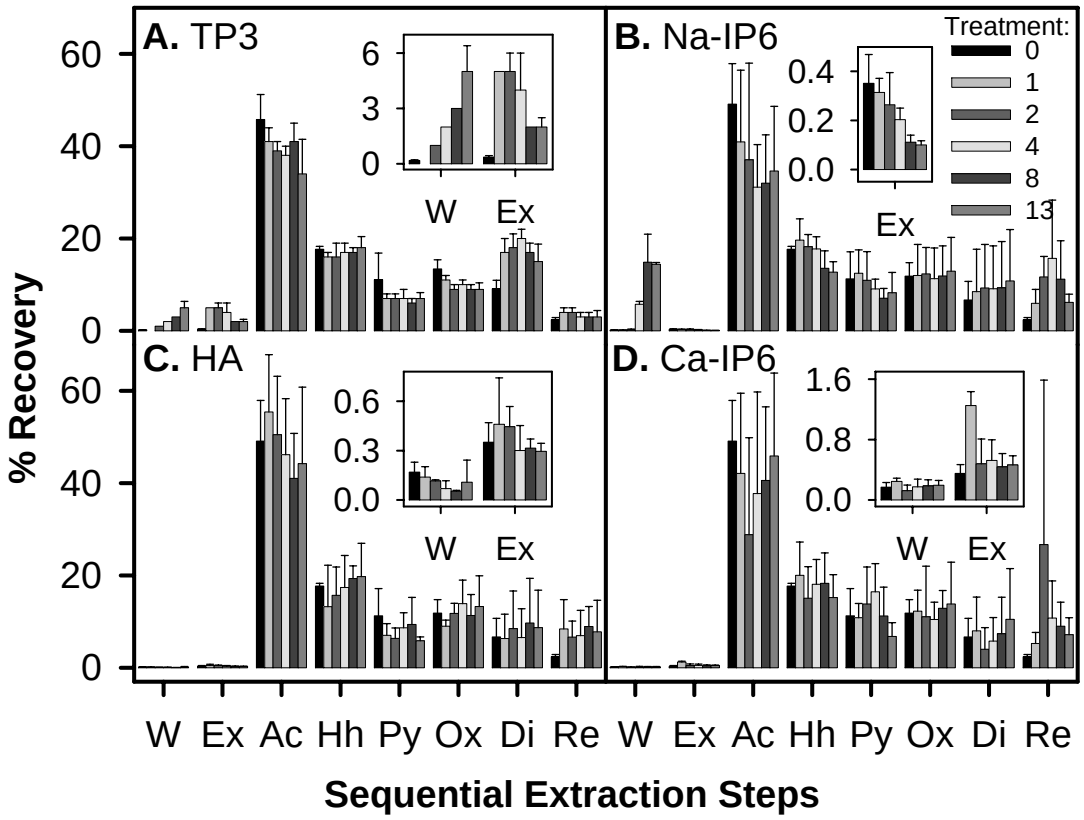

Figure 12. Sequentially extracted copper from contaminated soil amended with trisodium trimetaphosphate (*A*), sodium phytate (*B*), hydroxyapatite (*C*), and calcium phytate (*D*). Samples were equilibrated for 170 hours in 0.01 *M* $CaCl_2$ on a reciprocal shaker. Sequential extraction steps are listed from the least to the most aggressive step (Table 3). Inserts reflect the expanded scale for the 'water-soluble' and 'exchangeable' fractions of the given graphs. Extracted metal concentrations were reported as a percentage of total concentration. Unit for legend are treatment levels reported as mass of phosphorus added per mass of soil in g kg^{-1}. Error bars represent one standard deviation of the fraction means.

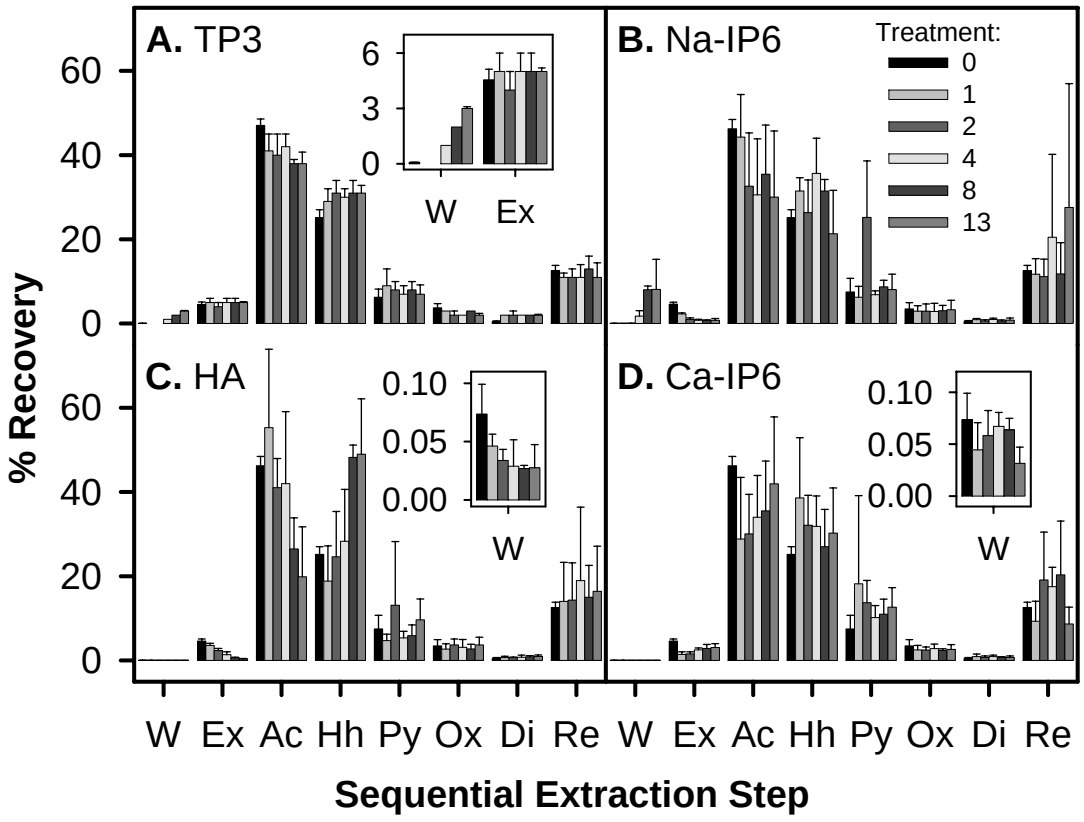

Figure 13. Sequentially extracted lead from contaminated soil amended with trisodium trimetaphosphate (*A*), sodium phytate (*B*), hydroxyapatite (*C*), and calcium phytate (*D*). Samples were equilibrated for 170 hours in 0.01 *M* $CaCl_2$ on a reciprocal shaker. Sequential extraction steps are listed from the least to the most aggressive step (Table 3). Inserts reflect the expanded scale for the 'water-soluble' and 'exchangeable' fractions of the given graphs. Extracted metal concentrations were reported as a percentage of total concentration. Unit for legend are treatment levels reported as mass of phosphorus added per mass of soil in g kg^{-1}. Error bars represent one standard deviation of the fraction means.

water-soluble Pb for the Na-IP6 treated soil, once again attributed to SOM dispersion would have been extracted later with the calcium nitrate- and acetate-extractable fractions (Fig. 13B). A decrease in Pb solubility in the HA amended soil was a function of the shift from the water-, calcium nitrate-, and acetate-extractable fractions to less soluble hydroxylamine- and to a lesser degree to the pyrophosphate-extractable fractions (Fig. 13C). On the contrary, increased Ca-IP6 addition, which also had a positive effect on water-soluble Pb, increased labile Pb associated with calcium nitrate- and acetate-extractable fractions at the expense of the hydroxylamine-extractable, the least soluble of the major Pb fractions (Fig. 13D). The aforementioned increase in Pb solubility could be ascribed to chelating potential of IP6 as well (He et al., 2006).

Overall, the solubility trends of all trace metals for individual treatments are nearly identical despite aforementioned differences in association of the eight SE fractions. Hydroxyapatite lowered solubility of all trace metals in two or three of the most labile fractions by facilitating the transformation to more recalcitrant fractions. An increase in trace metal solubility in the two most soluble fractions after TP3 addition was most likely caused by partial extraction of organically bound Zn and Cu by pyrophosphate, a TP3 hydrolysis product. Chelated forms may enhance the downward migration of contaminant metals in field settings. The degradation of soil hydraulic properties caused by the dispersion of SOM and the soil clay fraction may prohibit Na-IP6 field application (Seaman et al., 2005). The precipitated Ca-IP6 lowered the metal extractability, but facilitated the unwanted shift of Zn and Pb from more recalcitrant to a labile calcium nitrate-extractable fraction.

It is necessary, however, to point out, that the use of increasingly aggressive extractants may facilitate the artifactual redistribution of phosphate, IP6, and the target metal (Davidson et al., 2004; Gomez-Ariza et al., 1999; Meers et al., 2009; Tipping et al., 1985). Scheckel et al. (2003; 2005) pointed out the discrepancy between Pb enrichment in the residual fraction, coinciding with the pyromorphite formation during the extraction procedure itself, as determined by an exact spectrometric method. Therefore, data about the redistribution and long term stability of Zn, Cu, and Pb thus need to be interpreted with caution.

Summary of Lead Immobilization Study

Phosphate amendments applied to the soil from the lead-acid battery recycling plant with the purpose of lowering Pb, Cu, and Zn solubility behaved very differently. Hydroxyapatite additions lowered trace metal solubility and precipitated calcium phytate even outperformed hydroxyapatite with regards to lowering trace metal solubility, probably because of the higher initial 'reactivity'. Trimetaphosphate caused immediate, but moderate increases in contaminant solubility, which was attributed to partial extraction of organically bound metals and complexation with pyrophosphate, a TP3 hydrolysis product, whereas an increase in contaminant concentration in solution upon addition of sodium phytate could be described as tremendous. Dispersion of SOM and the clay-sized fraction due to the application of Na-IP6 may have also a degrading influence on the soil hydraulic properties. However, favorable immobilization trends need to be critically evaluated because of the possible trace metal redistribution in treated soil caused by aggressive extractants used in Toxicity Characteristic Leaching Procedure and

sequential extraction. Dispersion of soil organic matter and soil clay-sized fraction plus the chelating potential of phytate and pyrophosphate, hydrolysis products of metaphosphate, and dissolved organic carbon in general, can cause unforeseen complications upon addition of soil remediation amendments.

B. Solid Phase Speciation of Lead in Soil

Electron microscope and synchrotron-based measurements were conducted on samples prepared specifically for each technique, electron microscopy and synchrotron measurements. Analyzed spots were in both cases selected randomly after visual survey of exposed mineral grains and measurement of fluorescence signals of studied metals. Individual locations of measurement are summarized in tables and figures where they are marked by Roman numerals. It is important to point out that location marked by Roman numeral in a table or a figure is not identical with other location marked by the same Roman numeral e.g., Table 4 and 5, unless table or figure heading specifically implies so e.g., Table 5 and Figure 16.

Elemental Composition of Lead-Bearing Precipitates

Residual amendments were observed in samples treated with HA and Ca-IP6 and were identified by the characteristic Ca to P peak ratio in the recorded Energy Dispersive Spectrometry (EDS) spectra. Microprobe analysis of the mineral grain coating was complicated by an incomplete penetration of the resin through the grain coatings to the grains itself. Such grains were frequently plucked out, most likely during the mechanical grinding, while being stripped off of the coating. Grain ejection thus exposed for

microprobe analysis mostly the inner side of the coating. Phosphate enrichment of the inner side would be presumably lower then the outer side due to an indirect contact with the background solution during the batch equilibration process. Wide range in P enrichment could have been caused by limited diffusion of the background solution to the inner side of the grain coating. Quantitative analysis conducted by Wavelength Dispersive Spectrometry (WDS) might thus not be representative of the quasiequilibrium established between the solid and the solution.

Much of the contaminant metals were associated with Fe- or Mn-rich coatings of mineral grains (≥0.1 mm), even though some free-standing metal-rich particles were also observed. Elemental weight content of the analyzed points are summarized in Table 4 and can be divided to three major groups: Pb- (I-IV), Mn- (VI-VIII) and Fe-dominated (IX and X) environments. Exception among the analyzed spots was the 5th spots because it contained low Fe (<5%) and no Mn, but Pb weight content was at 25% very close to Mn-dominated spots. Aluminum weight content in all analyzed spots ranged from well over 1% to just a trace amount, 0.5% was the average content.

The Pb weight content between 50% and 57% (I-IV, Table 4) is well within the range of the 59% for drugmanite [$Pb_2(Fe,Al)H(PO_4)_2(OH)_2$], but the Fe content is well short of the stoichiometric 8% and P content is sufficient only in the spots I and III. Weight content of the 5th spot very nearly matches P and Pb content of corkite [$PbFe_3PO_4SO_4(OH)_6$] (Nriagu, 1984), but the Fe content is again well short of the required 25%. Presence of weathered metallic lead in this soil cannot be excluded because anode battery plates are manufactured of elemental Pb, but there was no corroboratory evidence found in the course of the microscopic and micro-diffraction

Table 4. Composition of coatings recorded on ten mineral grains from a hydroxyapatite and calcium phytate amended contaminated soil collected at a decommissioned lead-acid battery recycling plant (Jacksonville, FL). Results were obtained using wavelength dispersive spectrometry (Geller MicroAnalytical, Topsfield, MA) within electron microprobe (JEOL 8600 Superprobe, Peabody, MA).

	Al	Si	P	Ca	Mn	Fe	Cu	Zn	Pb
	elemental weight %								
I	0.1141	0.2375	12.61	2.77	BDL	6.74	BDL	0.2901	56.72
II	0.2227	0.1454	4.90	1.4094	BDL	0.2959	0.2241	0.4871	51.93
III	0.2750	0.4697	17.33	7.00	ND	1.5407	BDL	0.3058	50.42
IV	0.0967	0.0427	3.07	0.8391	0.1810	1.0702	ND	BDL	50.12
V	0.3284	0.3242	5.18	1.6590	ND	4.68	BDL	0.1051	24.53
VI	0.6007	0.2432	0.7195	0.9147	41.67	0.2435	4.50	1.7738	30.43
VII	1.0892	1.2743	0.7482	0.7581	39.81	0.8770	3.04	1.8237	10.10
VIII	1.2759	0.8253	2.80	2.34	31.38	5.31	1.4217	2.76	24.61
IX	0.7023	0.8337	1.9919	0.4965	0.2003	45.31	1.7347	0.3660	12.39
X	0.8547	2.40	5.14	1.3219	BDL	65.58	0.3403	2.74	13.78
mean	0.5560	0.680	5.45	1.95	22.65	13.2	1.88	1.18	32.50
SD	0.4168	0.715	5.40	1.91	20.86	22.9	1.65	1.09	18.20
CV, %	74.96	105	99.0	98.1	92.12	174	87.7	92.3	56.01
SE of mean	0.1318	0.226	1.71	0.605	6.598	7.24	0.521	0.346	5.757

ND – not detected
BDL – below detection limit

studies. Analysis for elemental forms of metal was complicated by the small size of all of the freestanding particles because the electron beam readily excites a sample volume larger than the particle of interest. Separated metal particles were on average 53% Pb with just traces of other elements included in a search procedure, which is again very close to the drugmanite value. Lead content was possibly overestimated due to the poor quality of the elemental Pb standard, because no other elemental Pb standard was available to verify WDS calibration.

Manganese dominated spots (VI-VIII, Table 4) were substantially enriched in Pb (between 10% and 30%) and also contained high levels of Cu (between 1.4% and 3%). It was surprising to identify three Mn-rich particles out of ten surveyed especially when the total Mn content of the soil was only 182 mg kg^{-1}, which is at the low end of the common soil content (Lindsay, 1979; McBride, 1994; Sparks, 2003). I propose following explanations for this phenomenon: mineralogical and biological. On one hand, the weight Pb and Mn content of two spots (VI and VIII) is indicative of pure Pb-bearing manganate coronadite [$Pb_2(Mn^{4+},Mn^{2+})_8O_{16}$] (McKenzie, 1989). On the other hand, rhizosphere bioaggregation of Pb on root epidermis or within root cortex, seems feasible especially because of the low Mn content of this soil (Cotter-Howells et al., 1999; Lanson et al., 2008). On other occasions, high contrast Mn- and Pb-rich particles were observed on a backscattered image of this soil (Fig. 14). These loaf-shaped particles were packed within approximately 10-µm wide grooves of a regularly ribbed surface of low backscatter matrix, presumably root fragments of monocotyledonous plant, e.g., grass. Lanson et al. (2008) hypothesized that similar particles, phyllomanganate, formed on an epidermis of grass roots as a part of defense mechanism against Zn phytotoxicity. Such bioaggregates

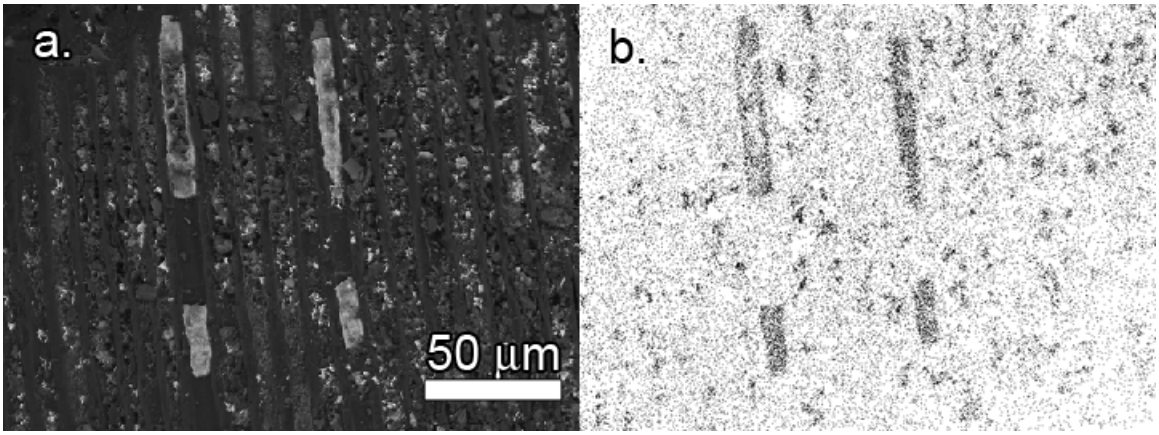

Figure 14. Backscattered image captured by electron microprobe (JEOL 8600 Superprobe, Peabody, MA) depicts a regularly ribbed surface of a low backscatter matrix, presumably a root fragment of a monocotyledonous plant, with four large bright manganese-rich nodules (*a*). Second image is a map of characteristic lead (Pb Mα) X-ray of the same area (*b*). Sample was collected from a contaminated soil at a decommissioned lead-acid battery recycling facility (Jacksonville, FL).

could have been incorporated into organo-mineral grain coatings, where they were found, from the bulk soil after root tissue decomposition. Biologically mediated sequestration of Cu, Zn and mainly Pb might have also been an important immobilization mechanism at this site.

It would be very interesting to compare biogenic phyllomanganate solubility with that of common soil Mn minerals and pedogenic ferromanganese nodules that also show very high affinity for metals and particularly high affinity for Pb (McKenzie, 1989). This soil contains according to the employed sequential extraction (SE) procedure around 40%

of its Mn in the residual fraction, which also contains sizeable Pb and Zn fractions (Fig. 10). If it is predominantly the phyllomanganates among the Mn minerals that are responsible for its share of Cu, Zn and Pb sequestration in the most resistant SE fraction then we have an important argument for re-vegetation of contaminated soils with metal tolerant members of *Poaceae* family and other members of the *Liliopsida* class who employ the same nutrient management strategy (Panfili et al., 2005). Nevertheless, even biogenic phyllomanganate with the highest observed loading ratio for divalent metal of 0.46 (Lanson et al., 2008) would not provide an explanation for the entire mass of Pb extracted in the residual fraction (3.737 mmol kg^{-1}). At best, the entire Mn mass in the residual fraction of 1.210 mmol kg^{-1} would correspond to mere 0.557 mmol kg^{-1} of Pb. The rest of the Pb (3.180 mmol kg^{-1}) must have been associated with other elements – most likely iron oxides (goethite, FeOOH) and kaolinite [$Al_2Si_2O_5(OH)_4$] or gibbsite [$Al(OH)_3$].

The last two spots (IX and X, Table 4) were dominated by Fe signal and were equally enriched in Pb (~13%) and contained variable amount of Cu and Zn and nearly no Mn. Weight Pb content between 10% and 15% places these two precipitates well short of any of the previously mentioned Pb minerals (Nriagu, 1984). Elemental composition of the phosphate-enriched precipitates indicates that reactive chemistry of mineral coating was dominated by Fe or Mn compounds rather than alumosilicates (e.g., kaolinite) even though localized dominance of alumosilicates cannot be excluded due to aforementioned spatial heterogeneity in precipitate composition and limited spatial resolution of the microprobe beam.

Figure 15. Backscattered image of typical detrital quartz grain with two distinct locations of phosphorus-rich coating (*a*) in the phosphate amended soil from a decommissioned lead-acid battery recycling plant (Jacksonville, FL) together with two overlaid energy dispersive spectra (*b*) (Thermo Electron Corporation, Minneapolis, MN) within electron microprobe (JEOL 8600 Superprobe, Peabody, MA). Spectra were obtained from two different locations of the same grain; black spectrum was collected for the coating on the right and grey spectrum, which is offset by approximately 150 counts per second, on the left side of the grain, respectively.

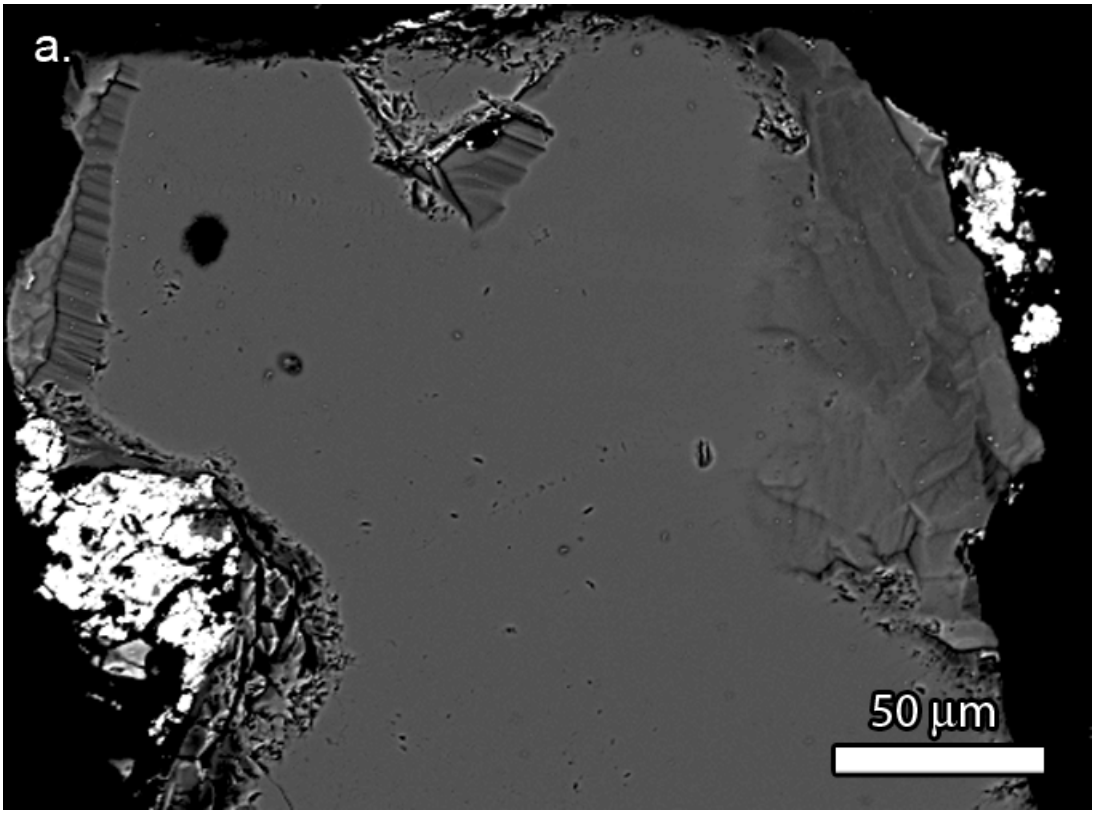
a.
50 µm

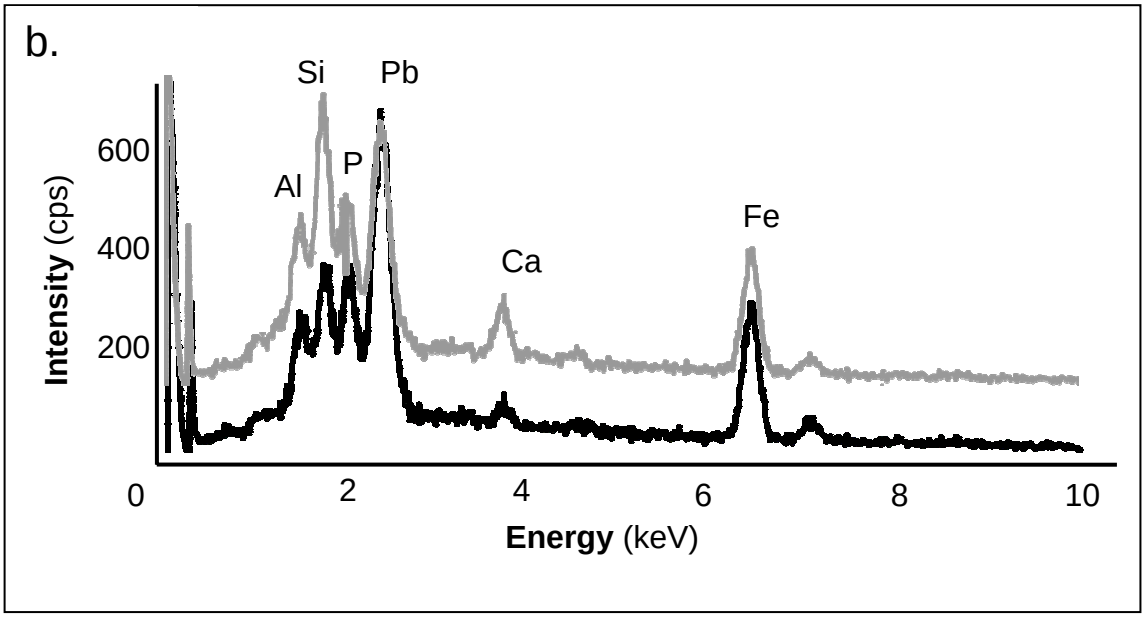
b.
Si
Pb
Al
P
Ca
Fe
600
400
200
Intensity (cps)
0
2
4
6
8
10
Energy (keV)

The elemental composition of the precipitates was quite heterogeneous even for two measurements on the same grain. Differences in Pb content are illustrated by overlaid EDS spectra taken at two different locations of the same quartz grain (Fig. 15). The disparity in Pb content was most likely a function of the proximity to the weathering Pb fragment. An increase in the Si signal can be attributed to adjacent quartz particle within the sample volume excited by an electron beam. Disproportionate ratios of P to Ca, otherwise characteristic for pure HA or Ca-IP6, together with WDS elemental analysis of precipitates provides reasonable evidence of immobilization of trace metals due to the formation of secondary precipitates in the case of both low solubility amendments (Seaman et al., 2003). Xu and Schwartz (1994) indicated pyromorphite-like [$Pb_5(PO_4)_3(OH, F, Cl)$] mineral co-precipitation as the mechanism of Pb immobilization by HA, which was favorable both thermodynamically, as based on reaction mechanism calculation, and kinetically with the limiting step being apatite dissolution. Weight composition of our richest Pb precipitates (I-V, Table 4) suggests drugmanite or corkite to be more important in this amended soil. Surface adsorption to the residual amendment is also used as a plausible immobilization mechanism (Xu et al., 1994) especially in the two, Fe-dominated spots.

Solid Phase Speciation of Lead Precipitates in Untreated Soil

Eleven micro X-ray diffraction (μ-XRD) patterns were collected for the untreated soil (Table 5 and Fig. 16). Goethite was identified in six (I-V and VII, Fig. 16) patterns and its presence in the others cannot be ruled out. The most common Pb-bearing crystalline phase, present in all eleven patterns, was plumbojarosite

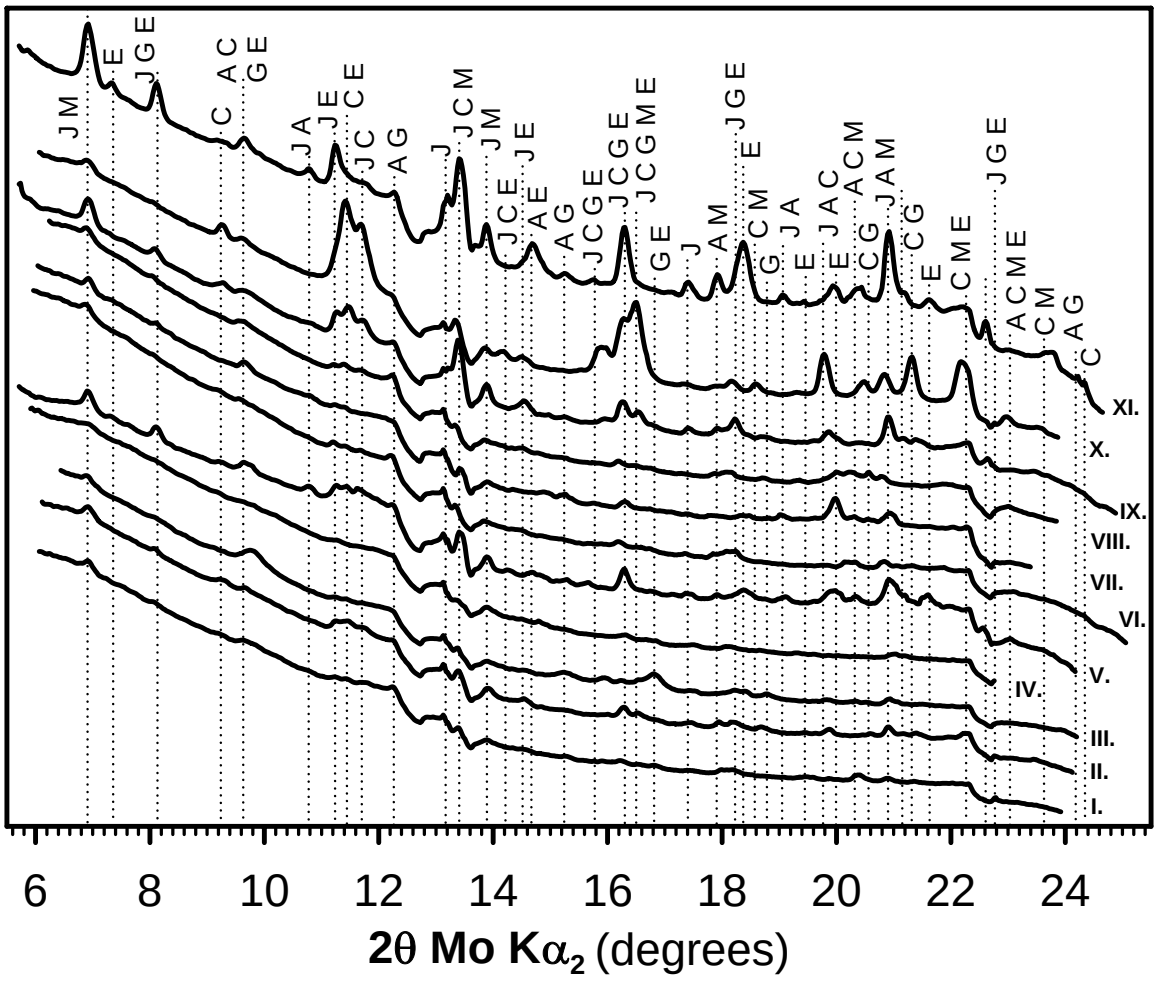

Figure 16. Eleven synchrotron micro-X-ray diffraction patterns for untreated, lead contaminated soil (Jacksonville, FL). These patterns are plotted with a staggered offset (~100 cps) against 2θ degrees Mo $K\alpha_2$, which correspond to beam energy 17.374 keV and wavelength 0.07136 nm. Minerals identified were A – anglesite, C – cerussite, E – chenite, G – goethite, J – plumbojarosite and possibly also M – massicot.

Table 5. Crystalline lead-bearing and associated phases identified from eleven synchrotron micro-X-ray diffraction patterns obtained for untreated, Pb contaminated soil (Jacksonville, FL). Detail information for each diffraction pattern as identified by computerized (Match!, 2003) and manual search routines can be found in part (*A*) and summary in part (*B*). Integrated diffraction patterns can be found plotted with staggered offset in Fig. 16. Relative elemental content is examined when chenite was identified.

A.	Notes[#]	Identified phases
I		anglesite, cerussite, goethite, plumbojarosite
II		anglesite, cerussite, goethite 16.7°, plumbojarosite
III		goethite, plumbojarosite
IV		anglesite, cerussite, goethite, plumbojarosite
V	↓Ti, some Fe, some Cu	anglesite, cerussite, chenite, goethite, plumbojarosite
VI		anglesite, plumbojarosite
VII	↓Ti, some Fe, some Cu	anglesite, chenite, goethite, plumbojarosite
VIII	↑Ti, ↓Fe, ↑Cu	anglesite, chenite, plumbojarosite
IX		cerussite, plumbojarosite
X		cerussite, plumbojarosite
XI	↓Ti, some Fe, some Cu	anglesite, chenite, plumbojarosite

[#] Elemental content was obtained from the X-ray fluorescence for the diffracted pixels

B. n = 11	Chemical formula	Times identified in 11 patterns
Anglesite	$PbSO_4$	8
Cerussite	$PbCO_3$	6
Plumbojarosite	$PbFe_6(SO_4)_4(OH)_{12}$	11
Chenite	$CuPb_4(SO_4)_2(OH)_6$	4
Goethite	FeOOH	6

$[Pb(Fe)_6(SO_4)_4(OH)_{12}]$. The other common Pb minerals were anglesite and cerussite identified in eight (I, II, IV-VIII and XI, Fig. 16) and six (I, II, IV, V, IX and X, Fig. 16) patterns, respectively. Identification of chenite $[CuPb_4(SO_4)_2(OH)_6]$ is deemed justified

despite weak diffraction pattern by enhanced Cu content, low to moderate Fe content and at least in one case very high Ti content in and around the diffracted hotspot (V, VII, VIII and XI, Fig. 16). Elevated Cu as well as Mn, Fe, and Zn in the vicinity of the hotspot were rather common even in the other patterns. Even though the diffraction patterns, especially for plumbojarosite and chenite, were somewhat weak, unique identification features and multi-line fit (Match!, 2003) aided with the identification (Table 5, Fig. 16). Positive identification of those two minerals might be also attributed to the used analytical techniques [i.e., synchrotron-based μ-XRD and micro-X-ray fluorescence (μ-XRF)] because electron beam and vacuum induced sample degradation was observed during extended viewing and analysis under vacuum in the electron microscope (Hochella et al., 1999).

Observed mineralogical diversity of the surveyed particles reflect a micro-morphological environment characterized by the adsorption surfaces e.g., anatase (TiO_2), goethite, kaolinite and to a large extent availability of ferric iron (Fe^{3+}) in solution that determined the type of mixed basic sulfate (i.e., chenite vs. plumbojarosite). Presence of massicot cannot be completely ruled out because its diffraction peaks coincide with that of the other minerals. However, its presence is unlikely as solubility of this oxide by far exceeds that of any other Pb mineral (Lindsay, 1979; Nriagu, 1984) and would have been much enhanced by an extremely low pH and high sulfate content at the time of contamination (Fig. 1). These conditions, however, would have been highly conducive to a formation of other Pb-bearing basic sulfates (e.g., plumbojarosite and chenite). Although only these two mixed basic Pb-bearing sulfates were identified on the basis of diffraction patterns, I do not exclude the presence of others (e.g., Zn mixed sulfates),

especially considering the co-occurrence of other elements identified in μ-XRF search procedure at sizeable amounts and the rather qualitative nature of this work.

Natural specimens of chenite have been identified as a weathering product in galena (PbS_2) ore mine with chalcopyrite ($CuFeS_2$) inclusions and in an old slag dump nearby (Paar et al., 1986). It was hypothesized on the basis of close association of chenite with other Pb- and Cu-bearing minerals that chenite is only thermodynamically stable in environments low in carbonic acid. Plumbojarosite is a relatively common mineral in oxidized zones of galena ore deposits, where it forms the mature, stable phase on the surface of other Pb-bearing minerals, and in precipitates associated with sulfate-rich acid mine drainage from oxidized tailings from ore extraction (Bigham et al., 1992; Chapman et al., 1983; Davis et al., 1993). Plumbojarosite was identified as free-standing plumbojarosite crystals rather than iron oxide/plumbojarosite complexes (Hochella et al., 1999). While ample Fe^{3+} in solution, high sulfate and acidic pH, induced by oxidation of ferrous iron and/or sulfides, are common threads of these types of environments, these conditions are not commonly met in aerobic soils and had to be caused by spilled electrolyte during lead-acid battery recycling. I hypothesize that processes that started with an introduction of spilled electrolyte and dissolved or particulate Pb from the surface of battery plates resulted in pedogenic formation of chenite or plumbojarosite (Eqs. 6 and 7).

$$4Pb^{2+} + Cu^{2+} + 2HSO_4^- + 6H_2O \rightarrow Pb_4Cu(SO_4)_2(OH)_6 + 8H^+ \qquad \textbf{Equation 6.}$$

$$Pb^{2+} + 6Fe^{3+} + 4HSO_4^- + 12H_2O \rightarrow PbFe_6(SO_4)_4(OH)_{12} + 16H^+ \qquad \textbf{Equation 7.}$$

Thermodynamic calculation reveals that as sulfate leaches out and pH increases over time plumbojarosite becomes unstable with regards to lead sulfate and carbonates and soil Fe^{3+} hydroxide or its crystalline equivalent, goethite (Allison et al., 2006; Kashkay et al., 1975; Lindsay, 1979), either of which is thought to control Fe^{3+} solubility in most soils. However, exact prediction of Pb solubility as controlled by plumbojarosite dissolution is quite difficult, because of wide range of predicted solubility constants ((Chapman et al., 1983; Kashkay et al., 1975), see also discussion in Hochella et al. (1999)). In line with this, plumbojarosite was identified at pH above 4 (Bigham et al., 1992). Furthermore, Hochella et al. (1999) did not observe any dissolution features on plumbojarosite crystals even at pH 6.6, which is nearly identical with this pH value. This extreme, however, might be attributed to encapsulation of the crystals in associated iron oxide, ferrihydrite $Fe_2O_3 \bullet 0.5H_2O$.

Persistence of plumbojarosite and chenite, and eventually other basic sulfates, at a near neutral pH of this soil (Table 1) could be explained by a frequent co-occurrence of anglesite and cerussite in diffraction patterns. Their formation could be kinetically favored over dissolution of plumbojarosite as pH gradually increased from that of battery electrolyte to current value, which would lead to fouling of plumbojarosite surfaces and an incomplete dissolution. Liberated Fe, Pb, and SO_4 would be sequestered from solution in the form of goethite and anglesite or cerussite. This explanation is supported by a historical evidence of liming, presumably to lower trace metal solubility by increased adsorption and co-precipitation (Cao et al., 2003c). Under an equilibrium condition finite amounts of calcite and plumbojarosite in low-ionic strength solution (0.01 *M* $CaCl_2$)

dissolve and Pb in solution is then controlled by hydrocerussite or cerussite near control values observed in our batch experiment (Allison et al., 2006).

Solid Phase Speciation of Lead Precipitates in Treated Soil

Nine and sixteen diffraction patterns were collected for hydroxyapatite (HA) and calcium phytate (Ca-IP6) treated soil samples, respectively (Figs. 17, 18, 19, and 20). Collected μ-XRD patterns generally identified much lower degrees of crystallinity for the Pb-bearing phases in the treated samples than in the patterns obtained from the untreated soil samples. Outcomes of the automated search procedure with μ-XRF elemental composition had to be repeatedly scrutinized to eliminate unlikely phases. The most common mineral in both treatments was corkite, identified in seventeen out of twenty five recorded diffraction patterns. Pyromorphite, which is frequently proposed as the main Pb sink in phosphate amended soils, was identified only three times, twice in HA and once in Ca-IP6 amended soil samples (Tables 6 and 7). For the purpose of this study it was assumed that all identified pyromorphite is chloropyromorphite [$Pb_5(PO_4)_3Cl$] rather than hydroxypyromorphite or fluoropyromorphite [$Pb_5(PO_4)_3F$]. All theses analogs were identified in the automated search procedures, but weak diffraction patterns and lack of μ-XRF data for fluorine and chlorine did not allow for decisive identification. Chloropyromorphite was selected because experimental evidence indicates that hydroxypyromorphite converts readily to thermodynamically more stable chloropyromorphite in a chloride background solution (Nriagu, 1973). In all practicality I cannot decisively exclude the presence of solid solution type pyromorphite with partial substitution of fluoride and hydroxyl ion for chloride.

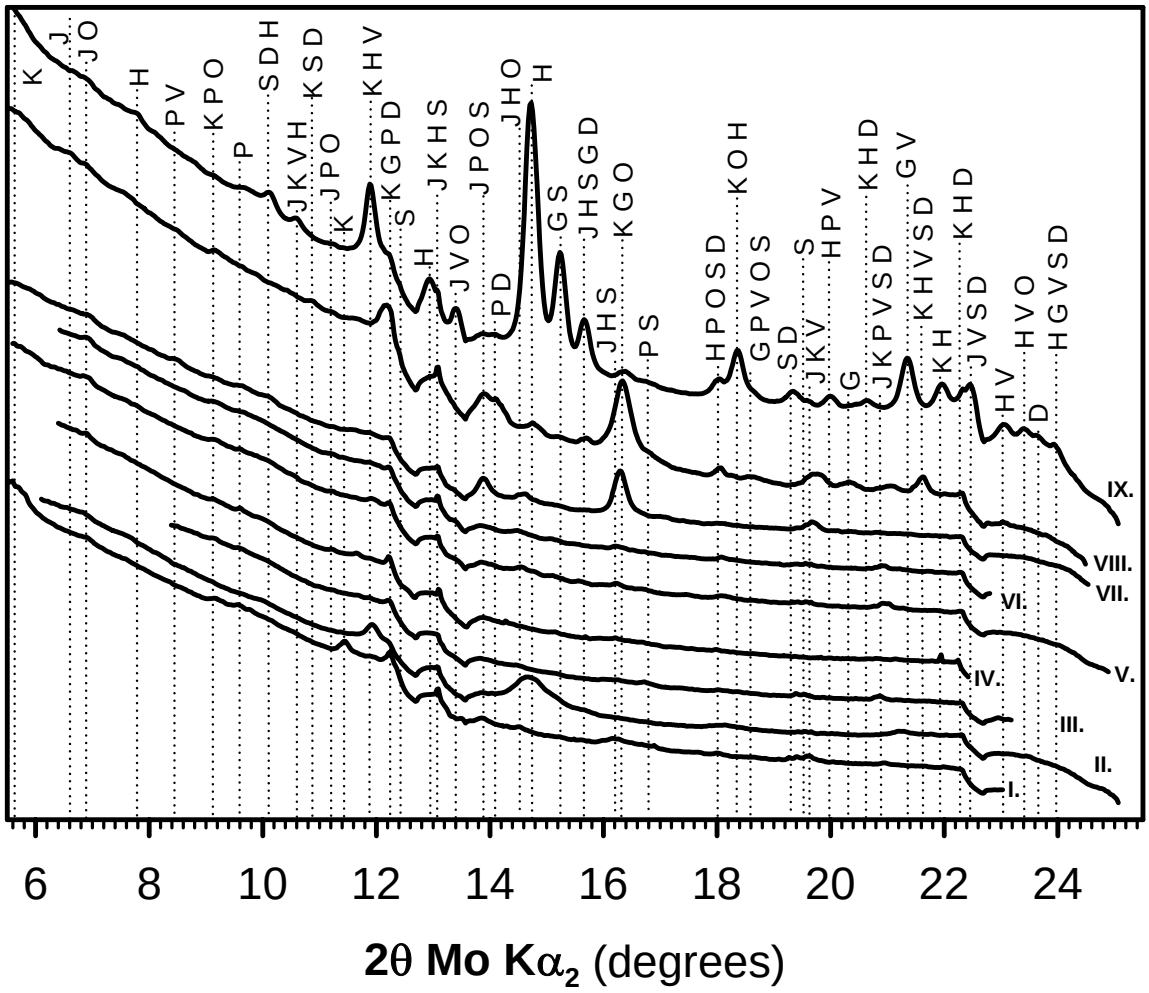

Figure 17. Nine synchrotron micro-X-ray diffraction patterns for lead contaminated soil (Jacksonville, FL) treated with hydroxyapatite. These patterns are plotted with a staggered offset (~100 cps) against 2θ degrees Mo $K\alpha_2$, which correspond to beam energy 17.374 keV and wavelength 0.07136 nm. Minerals identified were D – drugmanite, G – goethite, H – hydroxyapatite, K – kaolinite, O – corkite, P – pyromorphite, S – strengite, V – variscite and possibly also J – plumbojarosite.

Table 6. Crystalline lead-bearing and associated phases identified from nine synchrotron micro-X-ray diffraction patterns for Pb contaminated soil (Jacksonville, FL) treated with hydroxyapatite. Detail information for each diffraction pattern as identified by computerized (Match!, 2003) and manual search routine can be found in part (*A*) and summary in part (*B*). Integrated diffraction patterns can be found plotted with staggered offset in Fig. 17.

A.	Identified phases
I	goethite, kaolinite 5.7°
II	hydroxyapatite
III	corkite, kaolinite (low angles unavailable)
IV	corkite, kaolinite (low angles unavailable), strengite
V	corkite, hydroxyapatite
VI	corkite, drugmanite, hydroxyapatite
VII	corkite, goethite, strengite
VIII	corkite, goethite, hydroxyapatite, pyromorphite, strengite
IX	corkite, drugmanite, hydroxyapatite, pyromorphite

B. n = 9	Chemical formula	Times identified in 9 patterns
Corkite	$PbFe_3PO_4SO_4(OH)_6$	7
Pyromorphite	$Pb_5(PO_4)_3Cl$	2
Drugmanite	$Pb_2(Fe,Al)H(PO_4)_2(OH)_2$	2
Strengite	$FePO_4•2H_2O$	3
Hydroxyapatite	$Ca_5(PO_4)_3OH$	5
Kaolinite	$Al_2Si_2O_5(OH)_4$	3
Goethite	FeOOH	3

Drugmanite was the only other Pb-bearing phosphate identified in HA treated soil in two samples (VI and IX, Fig. 17). Somewhat problematic, even upon close scrutiny, was identification of strengite ($FePO_4•2H_2O$) and variscite ($AlPO_4•2H_2O$) because of the lack of unique, strong diffraction line and an overlap between lines around 19.6° 2θ Mo

$K\alpha_2$ (Figs. 17 and 18). Furthermore, neither presence of variscite nor the presence of Al-drugmanite could be corroborated with μ-XRF data because the mapping routine did not include either Al or any other element lighter than Ca. Variscite precipitation was previously indicated in Pb immobilization studies on basis of the solution oversaturation with respect to this mineral (Ma et al., 1994b; Seaman et al., 2001b). However, analytical Al levels in solution for this soil were below the inductively coupled plasma mass spectrometry detection level (0.2 μg L^{-1}) for both HA and Ca-IP6 amended soil. Common sorbent phases identified in diffraction patters for treated soil included anatase, apatite, goethite, and kaolinite. Identification of kaolinite was frequently complicated by an incomplete diffraction patterns with the low 2θ Mo $K\alpha_2$ angles (<6.5°) with the strongest, 001, diffraction missing (Tables 6 and 7, Figs. 17 and 18). Low diffraction angles are frequently missing due to the setup of the diffraction system, which is optimized for collection of diffraction rings out to higher 2θ angles.

Frequency of corkite's occurrence was not altogether surprising for at least two reasons. Firstly, there are considerable chemical similarities between corkite and plumbojarosite, the most common Pb mineral identified in the untreated soil (Tables 5, 6 and 7). Incongruent dissolution of plumbojarosite to corkite could be kinetically favorable over stoichiometric ionization of jarosite and subsequent neoformation of Pb-bearing phosphates. And secondly, solutions become saturated with respect to corkite at or above pH 5 with much lower phosphate level than those required for precipitation of pyromorphite (Davis et al., 1993; Nriagu, 1984). Limited solubility of hydroxyapatite would be thus conducive to corkite formation in presence of sufficient SO_4 (Ma et al., 1993). Transformation of plumbojarosite to corkite is completed through isomorphous

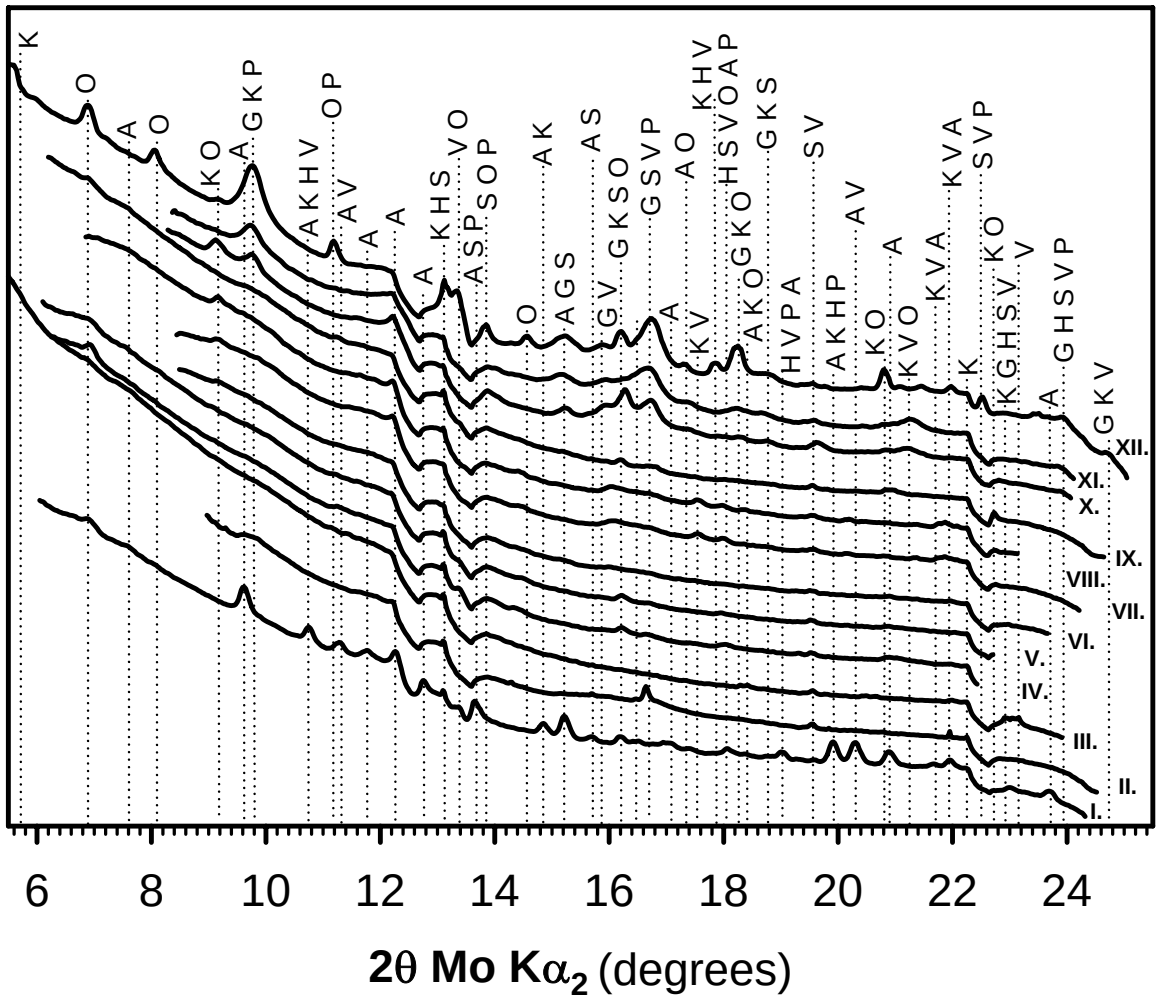

Figure 18. Twelve synchrotron micro-X-ray diffraction patterns for lead contaminated soil (Jacksonville, FL) treated with calcium phytate. These patterns are plotted with a staggered offset (~100 cps) against 2θ degrees Mo $K\alpha_2$, which correspond to beam energy 17.374 keV and wavelength 0.07136 nm. Minerals identified were A – anglesite, G – goethite, H – hydroxyapatite, K – kaolinite, O – corkite, P – pyromorphite, S – strengite, and V – variscite.

substitution of two phosphate anions for two sulfate anions (Jambor, 1999). Increased net-negative charge from the substitution is satisfied by another Pb cation, which effectively sequesters dissolved Pb in this sparingly soluble mineral (Nriagu, 1984). Excess Pb required for corkite formation as well as Pb needed for formation of far less common pyromorphite and drugmanite came most likely from dissolution of cerussite and anglesite, because cerussite was not identified in amended soil at all and anglesite only on a single occasion (Tables 6 and 7). Lack of hinsdalite [$PbAl_3PO_4SO_4(OH)_6$] in diffraction patterns further emphasizes the aforementioned scarcity of Al in this soil or kinetic advantage of plumbojarosite/corkite transformation because this mineral shares the same stability field with relatively common corkite (Nriagu, 1984). Prevalence of Pb-bearing phosphates in diffraction patterns over their Cu and Zn counterparts can be explained by two main factors: much higher initial Pb content of the soil and the ability of Pb to outcompete Zn for available phosphate (Cotter-Howells and Caporn, 1996).

Hydroxyapatite: Diffraction patterns for the HA treated soil are summarized in Table 6 and can be divided in three groups (Fig. 17) defined by a common soil sorbent, namely residual HA (II, V, VI, VIII and IX), goethite (I, VII and VIII), and kaolinite (I, III and IV). There is also some evidence of particle aggregation in two of the patterns with an apparent contribution from goethite (I and VIII). Sorbent provided nucleation sites for formation of metal phosphates directly (i.e., apatite), or indirectly through phosphate groups adsorbed on surfaces of the sorbent. Such is the case of kaolinite and goethite, both of which show very high affinity for orthophosphate (Celi et al., 1999). Although adsorption of Zn, Cu and especially Pb on surfaces of the residual hydroxyapatite grains would seemed to be mechanism responsible for sequestering these

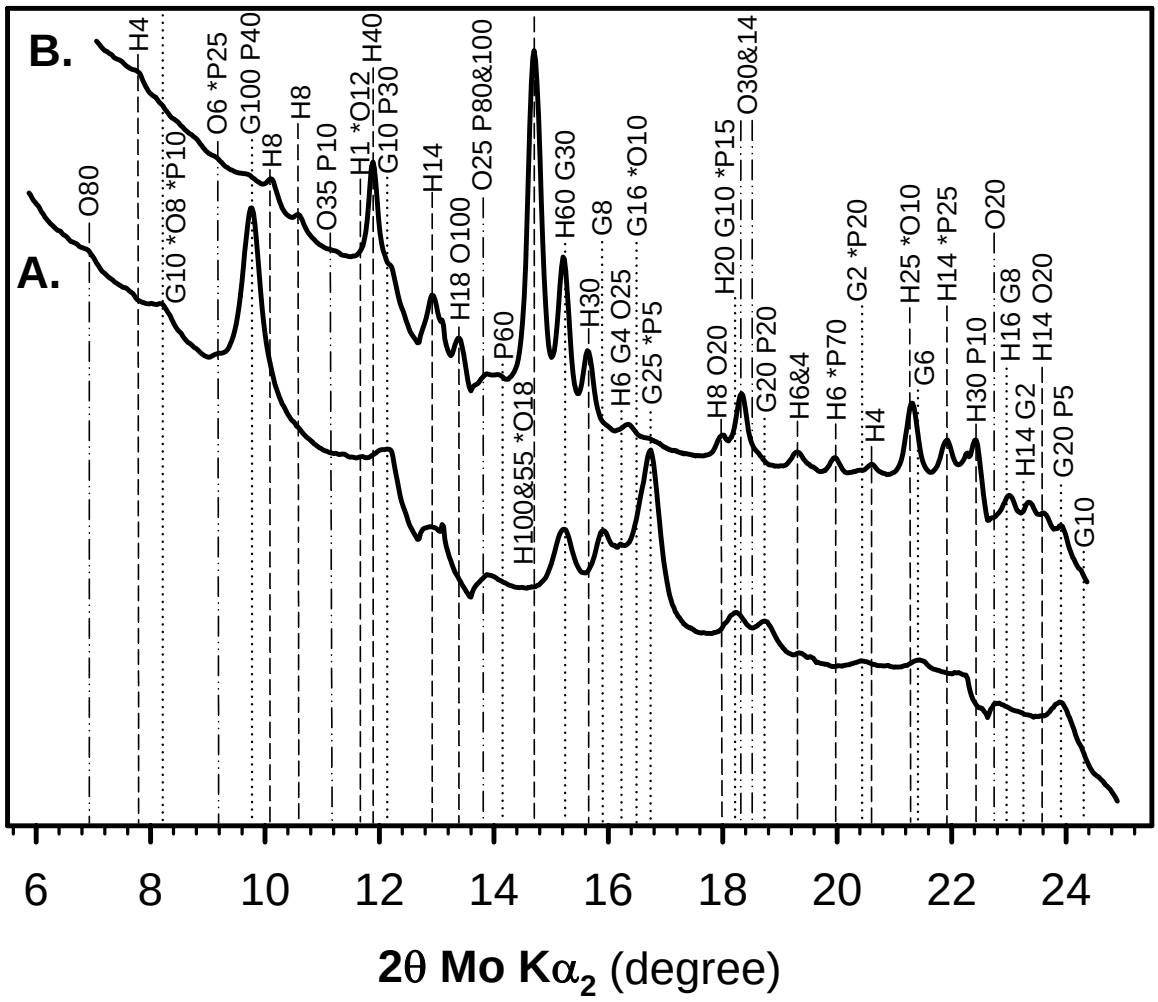

Figure 19. Two synchrotron micro-X-ray diffraction patterns obtained from spots with the highest Fe (*A*) and Pb (*B*) counts on a single iron-rich particle from lead contaminated soil (Jacksonville, FL) treated with calcium phytate at 4 g kg^{-1} soil to lower metal solubility. Minerals identified were G – goethite, H – hydroxyapatite, O – corkite, and P – pyromorphite. Relative intensity of each line obtained from ICDD powder diffraction files is recorded after the letter symbol for mineral. Where one diffraction line is right next to another line of the same element or lines of multiple minerals overlap only one drop line was used. Asterisk marks slightly larger distance between overlapping lines.

and other metals, it was encrustation of the HA grains in phosphate precipitates that was supported by μ-XRD analysis. The most common Pb-bearing minerals identified by the automated search procedure with the help of the μ-XRF elemental composition (Table 6), and not only on HA grains, was corkite (III-IX, Fig. 17), and twice each pyromorphite (VIII and IX, Fig. 17) and drugmanite (VI and IX, Fig. 17). Even the presence of corkite's precursor jarosite in the especially weak diffraction patterns cannot be completely ruled out due to overlap with diffraction lines of the other minerals. Jarosite's presence in HA treated soil could possibly be explained by formation of a solid solution between this mineral and corkite. Strengite was identified three times in diffracted pixels (IV, VII, and VIII, Fig. 17) and was always accompanied by corkite. This result might be interpreted in two possible ways. Firstly, available Pb was incorporated into the structure of precipitated strengite, i.e., co-precipitation. And secondly, strengite and corkite co-exist, each as a separate entity, below 10-μm scale.

Calcium Phytate: Sixteen diffraction patterns collected for Ca-IP6 amended soil were summarized in Table 7 and plotted in three figures (Figs. 18, 19 and 20). Anatase was added to the list of sorbents for the Ca-IP6 treated soil (Table 7 and Fig. 20), but it was not the only time in the course of this study that a Ti-rich particle was observed. Goethite was this time the most common sorbent identified in nine of sixteen patterns (II, IV, V, VI and X-XII, Fig. 18, A and B, Fig. 19). Kaolinite was identified four times (Table 7), but identification again suffered from a limited extent of two diffraction patterns at the low 2θ Mo $K\alpha_2$ angles (VII and VIII, Fig. 18). Corkite was again the most frequent mineral, identified ten times (Table 7, Figs. 18 and 19A). Other minerals identified in Pb rich spots were pyromorphite (Fig. 19B), strengite (IV, V and X-XII, Fig.

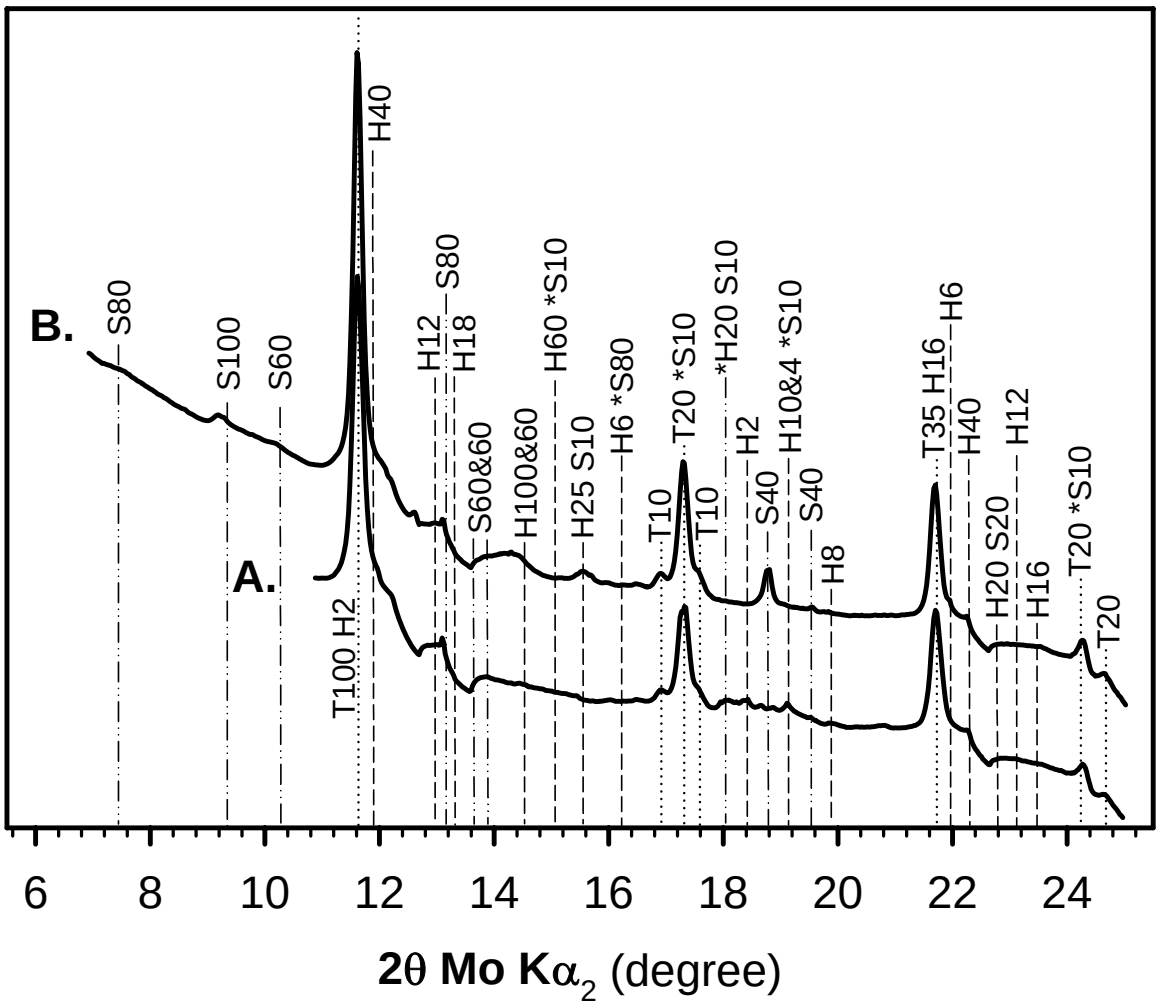

Figure 20. Two synchrotron micro-X-ray diffraction patterns obtained from spots with the highest Pb (*A*) and Ti (*B*) counts on a single titanium-rich particle from lead contaminated soil (Jacksonville, FL) treated with calcium phytate at 4 g kg^{-1} soil to lower metal solubility. Minerals identified were H – hydroxyapatite, S – strengite, T – anatase. Relative intensity of each line obtained from ICDD powder diffraction files is recorded after the letter symbol for mineral. Where one diffraction line is right next to another line of the same element or lines of multiple minerals overlap only one drop line was used. Asterisk marks slightly larger distance between lines.

Table 7. Crystalline lead-bearing and associated phases identified from sixteen synchrotron micro-X-ray diffraction patterns for Pb contaminated soil (Jacksonville, FL) treated with precipitated calcium phytate. Detail information for each diffraction pattern as identified by computerized (Match!, 2003) and manual search routine can be found in part (*A*) and summary in part (*B*). Integrated diffraction patterns can be found plotted with staggered offset in Figs. 18, 19 and 20.

A.	Figure	Identified phases
I	18	anglesite (9.6°, 11.8°, 23.7°), corkite (6.9°, 13.4°)
II	18	goethite, variscite, ↑Zn and ↑Cu counts[#]
III	18	kaolinite 5.7°, variscite
IV	18	corkite, goethite, strengite/variscite 19.6°
V	18	corkite (6.9°, 14.5°), goethite, strengite/variscite 19.6°
VI	18	corkite, goethite, hydroxyapatite
VII	18	corkite 14.5°, kaolinite (low angles unavailable)
VIII	18	corkite, kaolinite (low angles unavailable)
IX	18	corkite 6.9°
X	18	corkite, goethite, strengite/variscite 19.6°
XI	18	goethite, strengite/variscite 19.6°
XII	18	corkite, goethite, kaolinite 5.7°, and possibly strengite
XIII	19 A	corkite (6.9°, 22.7°), goethite
XIV	19 B	goethite, hydroxyapatite, pyromorphite 14.1°
XV	20 A	anatase, hydroxyapatite, strengite
XVI	20 B	anatase, hydroxyapatite, strengite

[#] Elemental content was obtained from the X-ray fluorescence for the diffracted pixels

B. n = 16	Chemical formula	Times identified in 16 patterns
Corkite	$PbFe_3PO_4SO_4(OH)_6$	10
Pyromorphite	$Pb_5(PO_4)_3Cl$	1
Anglesite	$PbSO_4$	1
Strengite	$FePO_4 \cdot 2H_2O$	7
Variscite	$AlPO_4 \cdot 2H_2O$	2
Apatite	$Ca_5(PO_4)_3$(OH, F, Cl or Br)	4
Kaolinite	$Al_2Si_2O_5(OH)_4$	4
Anatase	TiO_2	2
Goethite	FeOOH	9

18, A and B, Fig. 20), and variscite (II and III, Fig. 18). Lowering of the metal solubility due to the presence of metal phytates in Ca-IP6 amended soil cannot be excluded because metal phytates are in general not crystalline (Cotter-Howells et al., 1999).

Absolutely unexpected among sorbents in Ca-IP6 treated soil was presence of apatite (VI, Fig. 18, Fig. 19B, and Fig. 20). Apatite presence was surprising all the more because XRD analysis of the freeze-dried Ca-IP6 precipitate used in this study did not reveal the presence of any crystalline material. I can only hypothesize that microcrystalline HA formed during the precipitation of the Ca-IP6 or during the week-long equilibration period of the batch experiment through a hydrolysis of phytate. Firstly, if apatite formed during the precipitation of Ca-IP6, freeze-drying probably preserved highly reactive microcrystalline apatite surfaces and might be responsible for higher 'reactivity' in comparison with the oven-dried Ca-IP6 (Seaman et al., 2003). Direct comparison of the freeze-dried to the oven-dried Ca-IP6 precipitate indicated smaller BET (N_2) surface area and crystallinity in the oven-dried variety. Apatite's presence in the Ca-IP6 amended soil samples explains, at least partially, similarities in metal solubility trends with HA amended samples in this study. Secondly, if apatite precipitated from the hydrolysis products during the equilibration period together with strengite and variscite (Table 7, Figs. 18 and 20) it is evidence of formation of orthophosphates of abundant metals upon phytate application to soil (Jensen et al., 1996; Nash et al., 1998).

Surface Heterogeneity of Studied Grains in Treated Soil

This section further illustrates spatial heterogeneity of surface coating on an individual mineral grain already partially illustrated by the EDS and WDS measurements

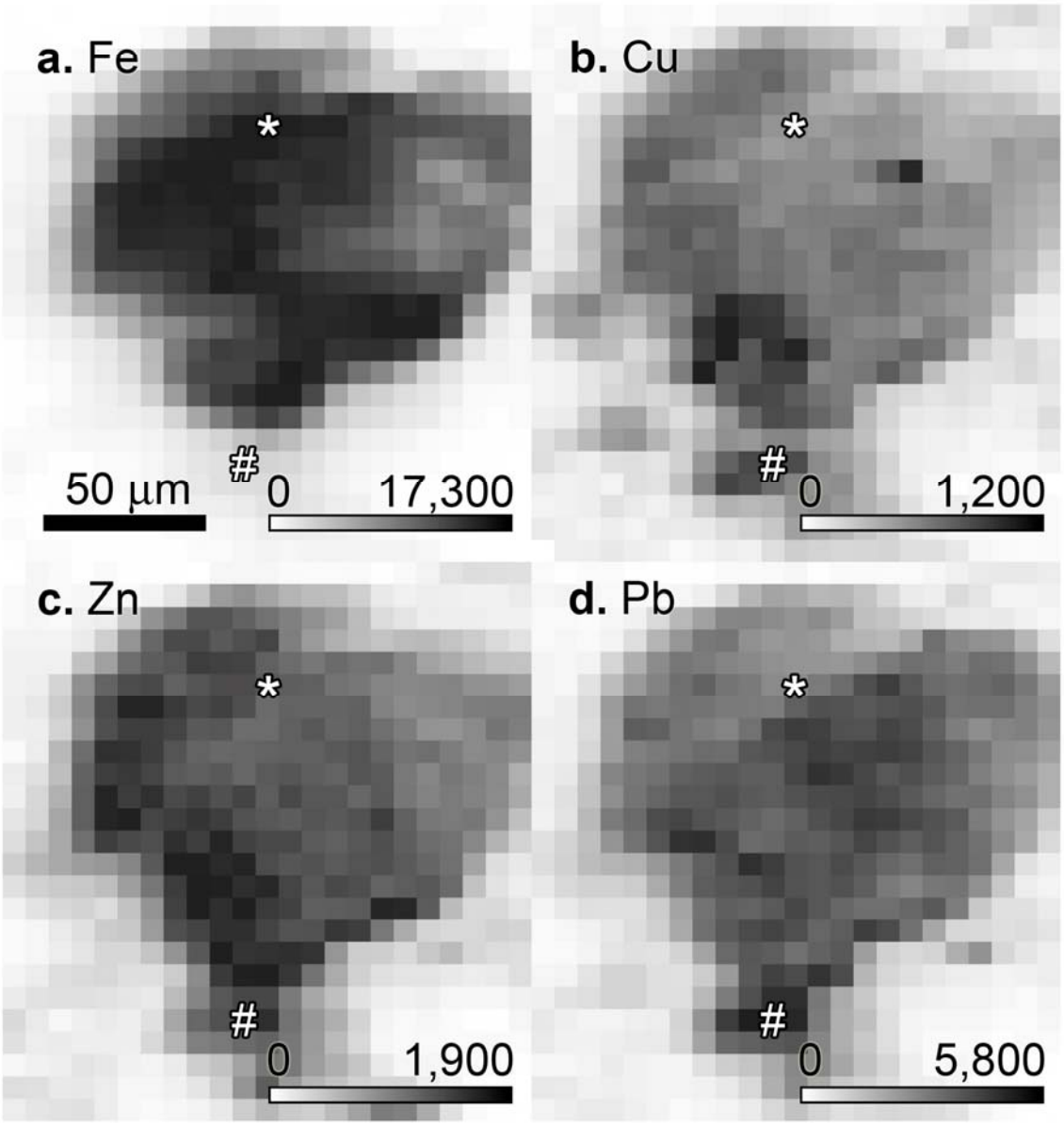

Figure 21. Element synchrotron micro-X-ray fluorescence maps, Fe Kα (*a*), Cu Kα (*b*), Zn Kα (*c*), and Pb Lα (*d*) of a single, Fe-rich particle from lead contaminated soil (Jacksonville, FL) treated with calcium phytate at 4 g kg^{-1} soil to lower metal solubility. Scale bar units are counts per second. Spots with the highest Fe and Pb counts were selected for micro-X-ray diffraction and are marked by an asterisk (*****) and number (#) signs, respectively. Scale bar = 50 µm.

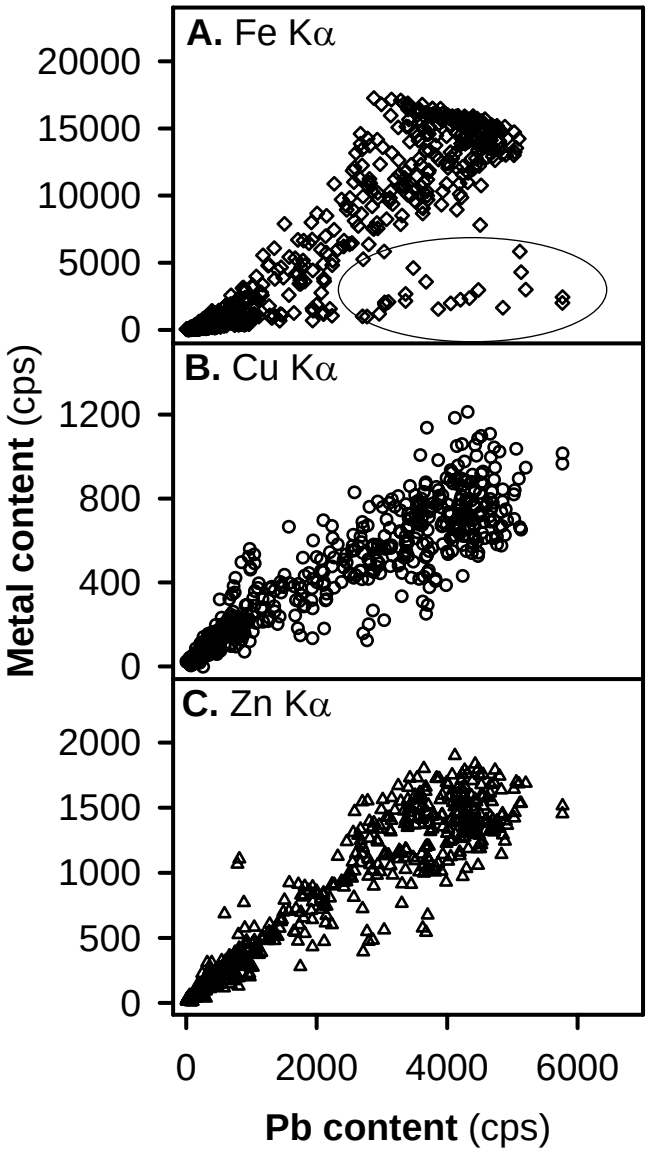

Figure 22. Correlations between Fe (*A*), Cu (*B*), and Zn (*C*) plotted against lead content of a single iron-rich particle from lead contaminated soil (Jacksonville, FL) with calcium phytate at 4 g kg^{-1} soil to lower metal solubility. Elemental content was measured by synchrotron micro-X-ray fluorescence.

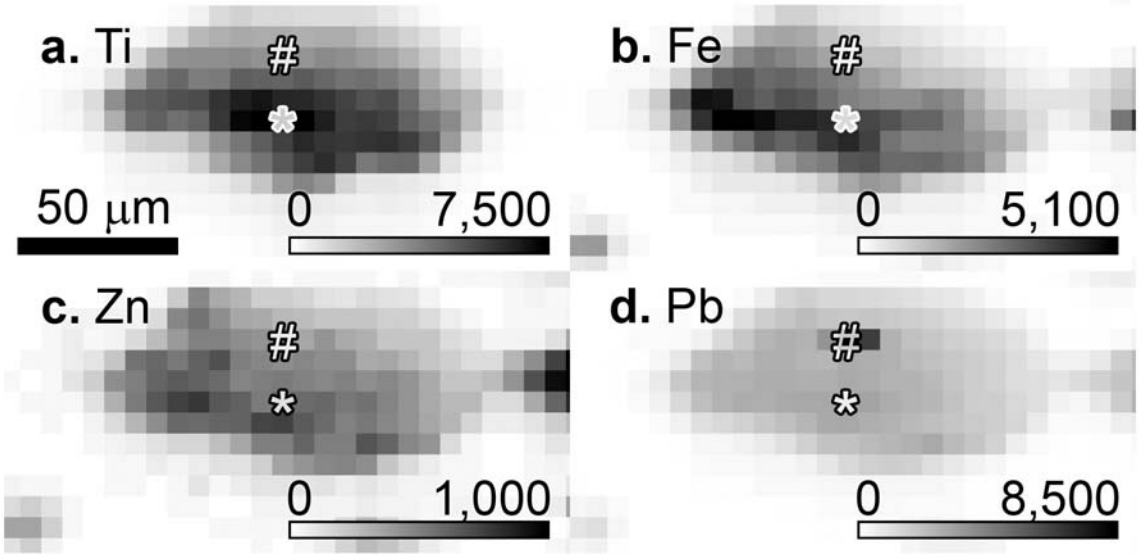

Figure 23. Element synchrotron micro-X-ray fluorescence maps, Ti Kα (*a*), Fe Kα (*b*), Zn Kα (*c*), and Pb Lα (*d*) of titanium-rich particle from lead contaminated soil (Jacksonville, FL) treated with calcium phytate at 4 g kg^{-1} soil to lower metal solubility. Scale bar units are counts per second. Spots with the highest Ti and Pb counts were selected for micro-X-ray diffraction and are marked by an asterisk (*) and number (#) signs, respectively. Scale bar = 50 μm.

(Table 4 and Fig. 15). Two mineral grains in the sample amended with Ca-IP6, one dominated by Fe and the other by Ti, are captured in a series of μ-XRF maps for abundant chemical elements (Figs. 21 and 23). Number sign denotes in both figures a pixel with the highest Pb content and an asterisk marks pixels with the highest Fe or Ti content, respectively. Two diffraction patterns were collected from the marked pixels on each grain and are plotted in Figs. 19 and 20, respectively. Elemental maps demonstrate

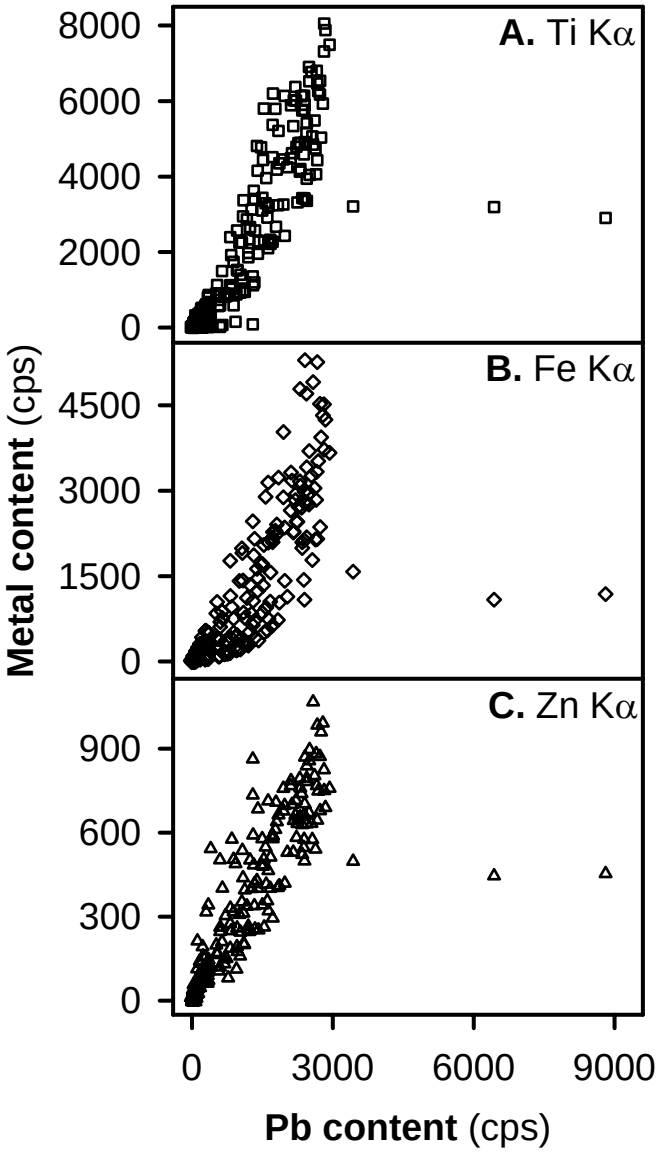

Figure 24. Correlations between Ti (*A*), Fe (*B*), and Zn (*C*) plotted against lead content of a single titanium-rich particle from lead contaminated soil (Jacksonville, FL) with calcium phytate at 4 g kg^{-1} soil to lower metal solubility. Elemental content was measured by synchrotron micro-X-ray fluorescence.

the chemical heterogeneity of the analyzed surfaces, the highly localized nature of metal enrichment of the sorbent surface in the treated soil, and the multi-phase contribution to the diffraction signal recorded in each of the patterns. Series of correlation plots between Pb and the other elements plotted in the μ-XRF maps illustrates relationship between goethite adsorption surface and metal contaminants (Fig. 22). Disproportionately enriched pixels, high Pb and low Fe counts along the X-axis (Fig. 22A), are indicative of formation of Pb-bearing phase(s) as they stand out of otherwise proportionally enriched surface of the particle. Lead enrichment corresponded proportionally with Cu and Zn signal, which indicates the same disproportionate relationship between those two elements and goethite adsorption surface (B and C, Fig. 22). Localized Pb enrichment of the grain surface is visible in Figure 23, where Pb signal from three pixels, which correspond approx. to an area of 20 × 10 μm, by far exceeds that of the rest of the particle. Relationship between Ti adsorption surface (i.e., anatase) and Pb, Fe and Zn, provides interesting insight into relationship between primary and secondary adsorption surfaces. Microcrystalline apatite might have formed or have become associated with the anatase adsorption surface through adsorption of colloidal Ca-IP6/HA (Fig. 20) and subsequently served as a secondary adsorption surface for the identified metals (Fig. 23). The only other crystalline orthophosphate in addition to apatite identified in the Pb enriched pixel is Fe-bearing strengite (Fig. 20) despite very high Pb content and similar element correlation trends (Fig. 24). It is entirely possible that Zn and Pb were sequestered in form amorphous orthophosphates or Fe simply precipitated all hydrolyzed orthophosphate and the other two metals formed amorphous Zn- and Pb-phytates that do not tend to be crystalline (Cotter-Howells et al., 1999).

Summary of Solid-Phase Speciation

Chemistry of this highly weathered sandy soil is most likely dominated by active surfaces of ferric and to a lesser degree also manganese compounds with possible contribution from other minerals, such as layered alumosilicates, titanium oxide and barium sulfate to name a few. The advanced weathering stage is responsible for formation of the iron-rich coating on mineral grains that was largely responsible for sequestration of copper, zinc, and lead in this contaminated soil. Apatite and calcium phytate addition to the soil resulted in phosphate enrichment of the active surfaces. However, WDS elemental composition of the analyzed mineral grain coatings does not reflect the quasiequilibrium formed during the batch equilibration due to the overexposure of the inner side after the ejection of grains from the epoxy during polishing stage of the sample preparation. Lead speciation in the solid phase of the contaminated soil changed after apatite and calcium phytate addition and equilibration in background solution. Unamended soil showed strong diffraction patterns for lead sulfate and carbonate, i.e., anglesite and cerussite. Mixed basic lead sulfates, plumbojarosite and chenite, were also commonly identified. The frequency of plumbojarosite presence in diffraction patterns was surprising because this mineral should dissolve at near neutral pH of this soil in favor of goethite precipitation. Anglesite and cerussite mostly dissolved during the equilibration of the soil with apatite or calcium phytate amendments. Decreases in lead solubility were accompanied by formation of new lead-bearing phases, mostly corkite and to a lesser extent drugmanite and pyromorphite. Preferential formation of corkite over the other two minerals was likely facilitated by low solubility of the phosphate amendments used, because the solution becomes over-saturated with respect to

corkite at lower phosphate levels. Strengite and variscite were also identified in diffraction patterns of the lead-rich spots. However, it is impossible to say, mostly due to the inadequate spatial resolution, whether these minerals simply co-existed side by side with the other lead-bearing minerals or served as an active sink of lead via co-precipitation and adsorption of lead to those newly precipitated surfaces. Plumbojarosite was most likely transformed to corkite through isomorphous substitution of phosphate for sulfate and incorporation of lead to satisfy the excess negative charge. Another lead sequestering mechanism was either bioaggregation in manganese-rich grains or precipitation of Pb- and Mn-bearing mineral coronadite. The goal of lead immobilization strategy through phosphate addition was achieved through precipitation of mixed basic phosphate sulfate and not by frequently proposed precipitation of pyromorphite.

C. Uranium Immobilization in Phosphate Amended Sediment

This sediment was collected from the lower Tims Branch watershed (Zabinski, 2006), just downstream of the Steed Pond, which was a primary source of the lower Tims Branch contamination (Batson et al., 1996). Analysis of the whole sediment as well as the results of Ni and U immobilization experiments were compared to those obtained for the Steed Pond sediment amended with hydroxyapatite (HA), dodecasodium phytate (Na-IP6), and calcium phytate (Ca-IP6) (Seaman et al., 2003). This Tims Branch sediment had in comparison with the Steed Pond sediment (Seaman et al., 2003) higher soil organic matter (SOM) content (6.91% and 4.9%, respectively) and a different texture. The Tims Branch sediment contained 40.7% sand and 26.2% silt (Table 2) compared to Steed Pond sediment, which was 19.2% sand and 45.2% silt (Seaman et al., 2003). The

clay-sized content for both sediments (33.1% and 35.6%) was similar. Observed textural differences were most likely function of mode of the sediment transport, mixing with the coarse soil of the lower Tims Branch watershed, and geomorphology of the alluvial plane (Borden, 2006).

Total digestion of Tims Branch sediment revealed slightly lower levels of Ni and U (Table 2) in HF/HNO_3 treatment despite the addition of boric acid that should have dissolved any fluoride precipitates (Kingston et al., 1997; Strucken et al., 1988). These mean concentrations were, however, within or near one standard deviation of replicate mean for the HNO_3-only digests and the difference was thus minimal. Fluoride salts precipitation should affect mainly alkaline earth and rare earth metals (Kingston et al., 1997) and indeed that is where major differences in total concentrations (Mg, Ca, Ba; data not shown) between treatments were observed. Total Ni and U content (350 and 1300 mg kg^{-1}, respectively) was much lower than in the Steed Pond sediment (1922 and 2260 mg kg^{-1}; (Seaman et al., 2003). Differences in the contaminant content might be also partially contributable to the sediment transport and differences in SOM content and sediment texture, but the main reason for the sharp drop in Ni content in comparison with U is its mobility in this environment as illustrated by much higher transfer of Ni into woody and herbaceous plant tissues (Punshon et al., 2003a; Punshon et al., 2003b; Sowder et al., 2003).

Batch Equilibration of Uranium and Nickel Contaminated Sediment

Concentrations of P, Ni and U in solution from batch equilibration are plotted as a function of added P to sediment. Concentrations of P in solution from HA and Ca-IP6

amended sediment samples equilibrated in 0.001 *M* $CaCl_2$ were 15 and 60 mg kg^{-1} sediment, which was higher than in the Pb immobilization experiment (1 and 8 mg kg^{-1} sediment in 0.01 *M* $CaCl_2$), respectively (Figs. 3B and 25B). The increase was most likely caused by lowering of the common ion effect after tenfold decrease in Ca content

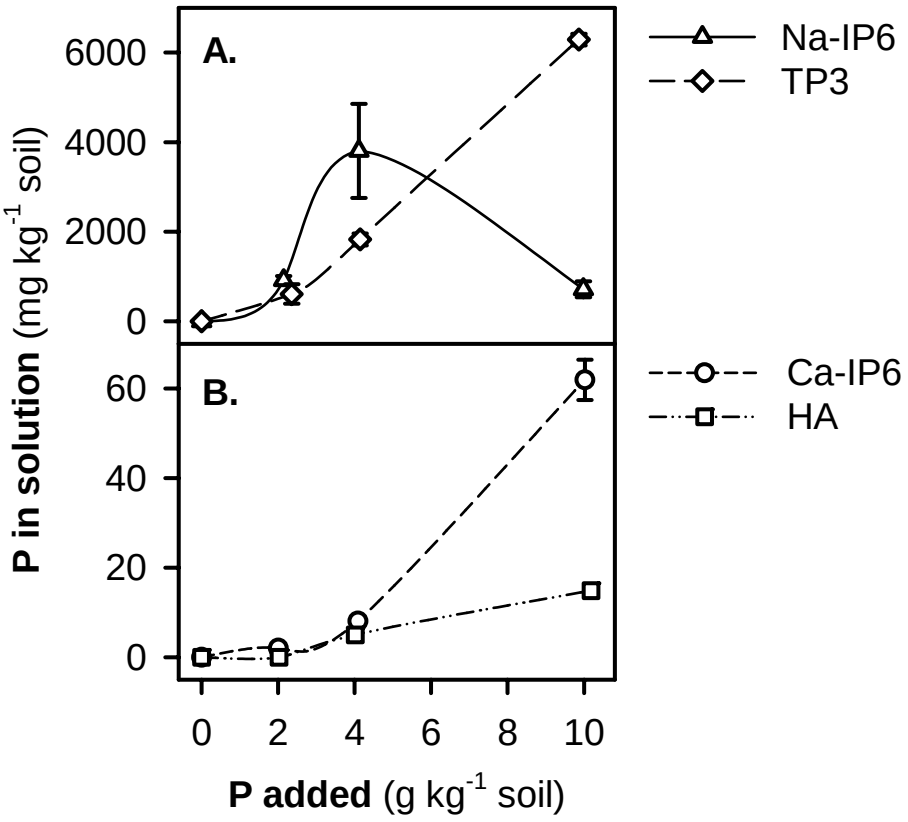

Figure 25. Effect of addition of calcium phytate (Ca-IP6), hydroxyapatite (HA), sodium phytate (Na-IP6), and trisodium trimetaphosphate (TP3) to the Tims Branch sediment on soluble phosphorus (*A* and *B*) after equilibration for 170 hours in 0.001 *M* $CaCl_2$ on a reciprocal shaker. Error bars represent one standard deviation of the treatment level means. Splines were included to improve data readability and do not represent exact trends.

of the background solution. The concentrations of P in solution in this Tims Branch sediment did not, however, completely correspond with HA and Ca-IP6 amendments to the sediment from a nearby Steed Pond in 0.001 *M* $CaCl_2$, which were 10 and 180 mg kg^{-1} sediment (Seaman et al., 2003). The threefold increase in the case of Ca-IP6 might be attributed to an inconsistency in preparation procedure and difference in drying technique, i.e., oven drying replaced by freeze drying in our case. Trisodium trimetaphosphate (TP3) and Na-IP6 were again much more reactive than the HA or Ca-IP6 and more than 50% of added TP3 was recovered in the supernatant at the end of batch equilibration (Fig. 25A). Very peculiar was behavior of Na-IP6, as nearly 100% was recovered for the 4 g kg^{-1} sediment amendment level, but less than 10% for the highest phosphate amendment level, 10 g kg^{-1} sediment. Similar decreases in concentrations in solution between these two treatment levels for Na-IP6 were observed for Al, Mn and to a lesser degree for Fe, with decreases from 3036 to 267, from 213 to 53, and from 1000 to 800 mg kg^{-1}, respectively. It might be indicative of precipitation of metal phytates, which tend to lack any crystallinity (Cotter-Howells et al., 1999). High phosphate recovery from the supernatant leaves very little phosphate to react with metals and radionuclides and vice versa.

Sediment samples were well buffered between pH of 5.1 and 5.5 upon addition of HA, Ca-IP6 and TP3 for all amendment levels, which was an increase of nearly one pH unit from 4.4 for the unamended control (Fig. 26). This pH increase corresponds well with other HA addition studies conducted on other sediment samples from the Steed Pond/Tims Branch area (Arey et al., 1999; Seaman et al., 2001b; Seaman et al., 2003). Sodium phytate addition resulted in substantially larger pH increase of up to two pH

units, but remained well short of the four unit jump for the poorly buffered Pb-contaminated soil. Comparable behavior of highly reactive TP3 with the less reactive HA and Ca-IP6 was probably caused by the abundance of Al adsorption surfaces in this sediment, namely kaolinite, hydroxy-interlayered vermiculate and gibbsite (Arey et al., 1999), which were instrumental in sequestering TP3 hydrolysis products, presumably mainly pyrophosphate, from the background solution. As these adsorption surfaces eventually became saturated with increasing P amendment level, the pH actually dropped slightly at the highest TP3 treatment level, 10 g kg^{-1} sediment (Fig. 26).

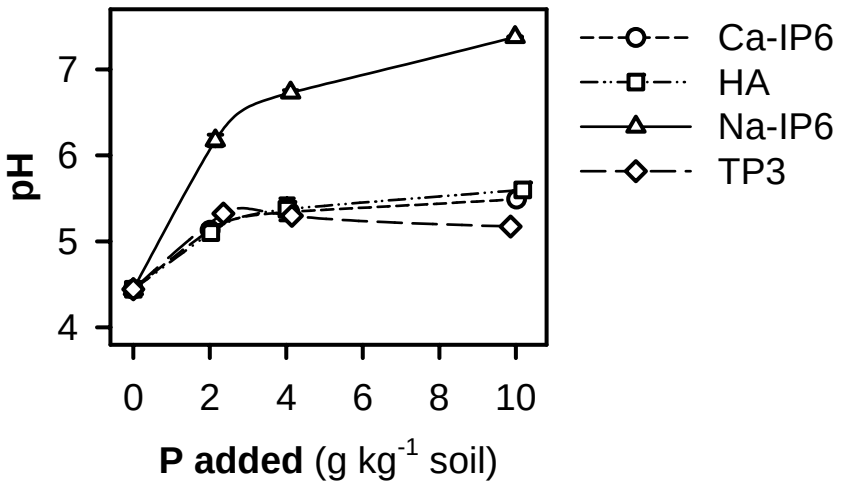

Figure 26. Effect of addition of calcium phytate (Ca-IP6), hydroxyapatite (HA), sodium phytate (Na-IP6), and trisodium trimetaphosphate (TP3) to the Tims Branch sediment on pH after equilibration for 170 hours in 0.001 *M* $CaCl_2$ on a reciprocal shaker. Error bars represent one standard deviation of the treatment level means. Splines were included to improve data readability and do not represent exact trends.

Progressively larger quantities of dissolved organic carbon (DOC) with increasing application rate were observed for all amendments (Fig. 27), when compared to the unamended control (60 mg L^{-1}), and were much above the maximum DOC increase resulting directly from the phytate (IP6), an organophosphoric compound, addition.

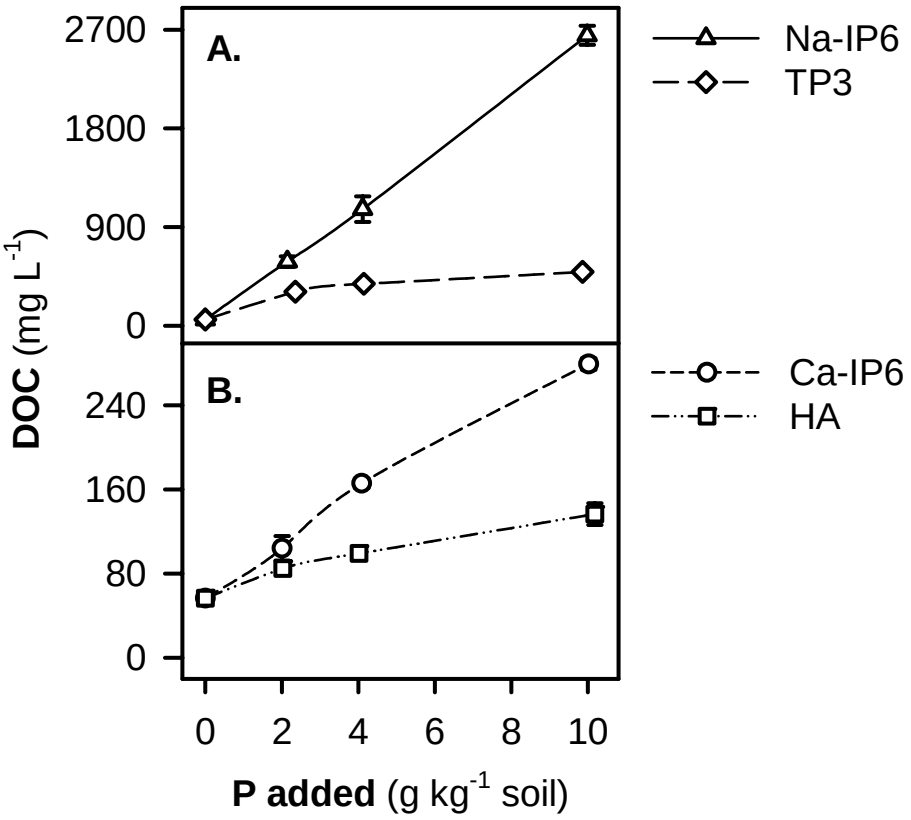

Figure 27. Effect of addition of calcium phytate (Ca-IP6), hydroxyapatite (HA), sodium phytate (Na-IP6), and trisodium trimetaphosphate (TP3) to the Tims Branch sediment on dissolved organic carbon (DOC, *A* and *B*) after equilibration for 170 hours in 0.001 *M* $CaCl_2$ on reciprocal shaker. Error bars represent one standard deviation of the treatment level means. Splines were included to improve data readability and do not represent exact trends.

Dissolved organic carbon increased linearly up to 2700 mg L^{-1} in samples amended with Na-IP6 despite the peculiar drop in P in solution at the highest amendment level (Fig. 25) that was accompanied by similar drop in solution levels of Al, Mn and Fe, solution levels of these metal up to this point increased with increasing Na-IP6 application rate. The other amendments caused smaller, but still sizeable increases in DOC, which were presumably the result of SOM desorption from mineral surfaces in direct competition with phosphate or phytate in solution. Trimetaphosphate hydrolysis product pyrophosphate most likely facilitated SOM dispersion through complexation of Al and Fe (Papp et al., 1991) and solution concentrations of both metals increased up to 250 and 120 mg kg^{-1} sediment, respectively. Hydroxyapatite addition lowered, or had no effect on, solution concentration of Al, Mn and Fe and Ca-IP6 behaved identically with an exception of a slight increase in concentration of Fe in solution from 1 to 3 mg kg^{-1} sediment. Application of amendment that caused dispersion of the SOM is thus undesirable as it results in liberation of metals associated with the SOM.

Nickel and Uranium Solubility after Equilibration Period

X-ray absorption spectroscopic studies have identified the dominant oxidation state of U in the Savannah River Site (SRS) sediments to be the more soluble hexavalent uranyl ion (Bertsch et al., 1994; Hunter and Bertsch, 1998). Phosphate treatments had variable effect on Ni and U solubility in the contaminated sediment studied. Hydroxyapatite addition to the contaminated sediment verified the hypothesis of decreasing Ni and U concentrations in solution with increasing amendment level (Figs. 28 and 29). Concentrations of Ni and U in solution dropped from nearly 6 to 1 mg kg^{-1}

sediment and from 0.6 to less than 0.2 mg kg^{-1} sediment, respectively. Our results agree with number of HA-based U and Ni immobilization studies conducted on the Steed Pond sediment (Arey et al., 1999; Seaman et al., 2001b; Seaman et al., 2003), which is a source for this lower Tims Branch sediment and other sediment collected at the SRS

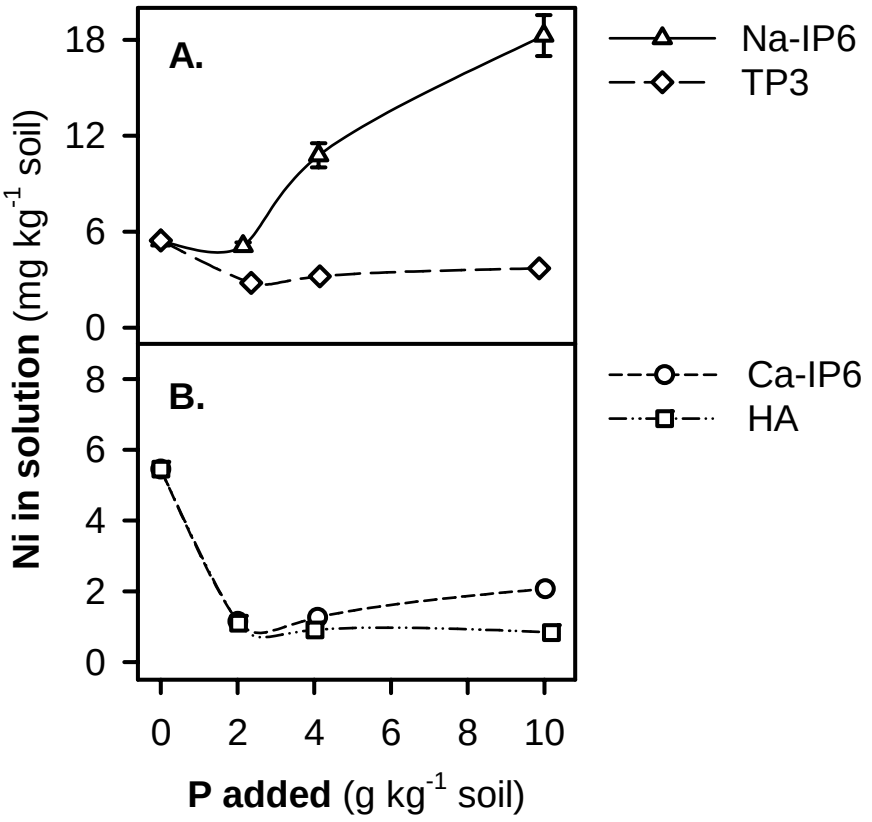

Figure 28. Effect of addition of calcium phytate (Ca-IP6), hydroxyapatite (HA), sodium phytate (Na-IP6), and trisodium trimetaphosphate (TP3) to the Tims Branch sediment on soluble nickel (*A* and *B*) after equilibration for 170 hours in 0.001 *M* $CaCl_2$ on a reciprocal shaker. Error bars represent one standard deviation of the treatment level means. Splines were included to improve data readability and do not represent exact trends.

(Seaman et al., 2001a). The concentration of U in solution decreased in a similar matter for the Ca-IP6 amended sediment, but Ni concentration rose slightly at the higher amendment levels to 2 mg kg^{-1} sediment after the initial drop to 1 mg kg^{-1} sediment at the lowest amendment level (Fig. 28), presumably due to the chelation of Ni by phytate or DOC. Nickel concentrations were also significantly depressed by TP3 in a manner similar to the Ca-IP, with a decrease to 3 mg kg^{-1} at the lowest treatment level followed by a gradual increase to 3.7 mg kg^{-1} at the highest treatment level, which is well below 6 mg kg^{-1} sediment for the unamended control (Fig. 28); TP3 was not effective in immobilizing U, as the analytical concentration rose steadily with increasing treatment levels (Fig. 29). Sodium phytate amendment was similarly ineffective in immobilizing of either Ni or U, even though Ni concentration dropped slightly at the lowest treatment level and the analytical level of U plummeted at the highest treatment level to 35 mg kg^{-1} sediment after an initial steep increase (Fig. 29).

The increased U concentration (Fig. 29) in Na-IP6 or TP3 amended sediment can be at least partially attributed to the increase in DOC upon addition of either amendment due to a strong binding potential between uranyl ion and DOC as has been illustrated for common DOC model compounds such as citric acid ($C_6H_8O_7$) or Suwannee River humic and fulvic acids (Lenhart et al., 2000). Uranium partitioning studies conducted on sediments collected in Steed Pond and lower Tims Branch watershed (including this TB6) have determined strong positive relationship between the DOC and analytical U concentrations as well (Jackson et al., 2005; Sowder et al., 2003). In addition to truly dissolved U and Ni in 0.2-mm filtrates of water extracts of the studied sediments, Jackson et al. (2005) identified two distinct complexes, DOC-U complex and Al-dominated

colloids. Colloid dispersal caused by charge reversal upon adsorption of IP6 or TP3 hydrolysis products (pyrophosphate) might be thus responsible for further increase in U and Ni concentration in solution. The sharp drop in concentration of U and P in solution at the highest Na-IP6 treatment level (Figs. 25 and 29) might be a result of overcoming

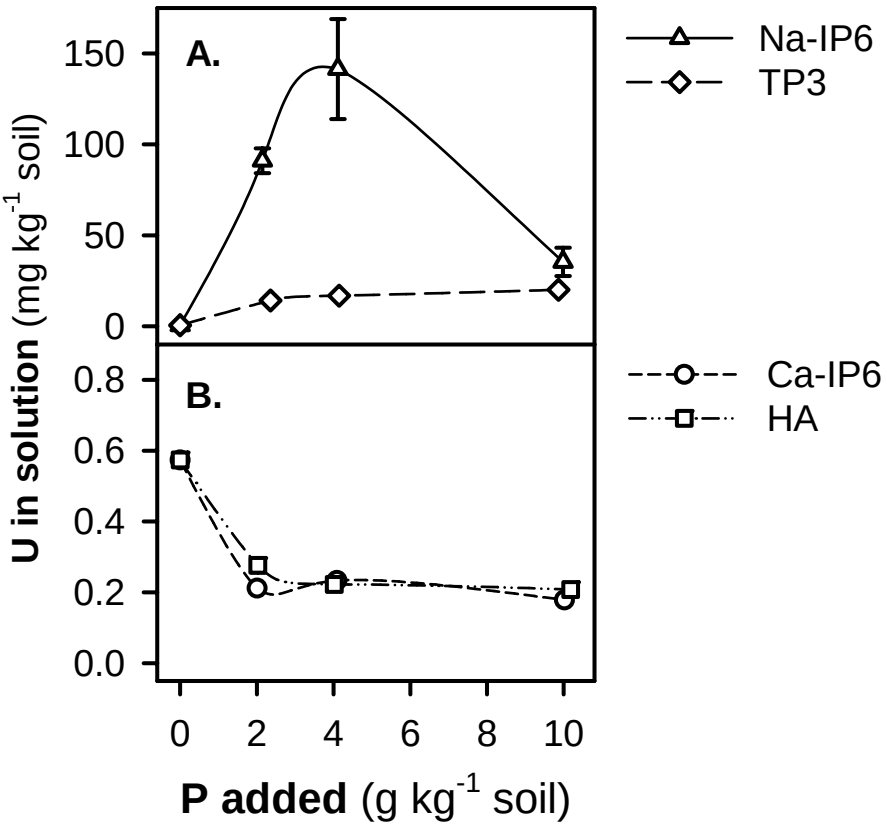

Figure 29. Effect of addition of calcium phytate (Ca-IP6), hydroxyapatite (HA), sodium phytate (Na-IP6), and trisodium trimetaphosphate (TP3) to the Tims Branch sediment on soluble uranium (*A* and *B*) after equilibration for 170 hours in 0.001 *M* $CaCl_2$ on a reciprocal shaker. Error bars represent one standard deviation of the treatment level means. Splines were included to improve data readability and do not represent exact trends.

certain critical level of the dissolved, dispersed, and complexed U and dissolved IP6, at which phytate precipitates free uranyl ions and some of the colloidal U, while leaving trends of DOC and Ni concentration in solution unchanged (Figs. 27 and 28). Similar trend was observed for Mg, Al, Ca, Mn, and Fe (figures can be found in appendix). The relatively low variability between replications observed for the concentrations of both contaminants in solution at all treatments reflects great buffering capacity of this sediment.

Toxicity Characteristic Leaching Procedure of the Contaminated Sediment

The TCLP extraction was carried out on all treated sediments, and extraction levels were corrected for the removal of contaminants during the seven-day equilibration (Seaman et al., 2001b; Seaman et al., 2003). Leachability of the contaminants from the treated sediments decreased to some extent with increasing treatment levels for all amendments except the Na-IP6 (Fig. 30), which was likely due to the enhanced dispersion of the SOM and associated contaminants during the batch equilibration (Fig. 28 and 29) and not by enhanced leaching in the mildly acidic, weak ligand TCLP extractant. It is important to point out that the decrease in contaminant TCLP leachability might be to some extent artifactual (Scheckel et al., 2003; Scheckel et al., 2005). A reason is the enhanced dissolution of the residual HA and Ca-IP6 amendments in the TCLP extractant due to the lower pH and presence of acetate, a known Ca complexation ligand. The resultant solubilized P was subsequently available to precipitate additional metals and U liberated by the TCLP extractant, in fact further stabilizing contaminants. Redistribution maintained corrected Ni and U levels close to 8 and 40 mg kg^{-1} in the TP3

treated sediment (A and B, Fig. 30), whereas an increased solution concentration of the phytate in the Ca-IP6 treated sediment in turn increased Ni levels above the TP3 values with increasing treatment level due to complexation and decreased analytical U concentration due to the phytate's high affinity for uranyl ion (Nash et al., 1998). The

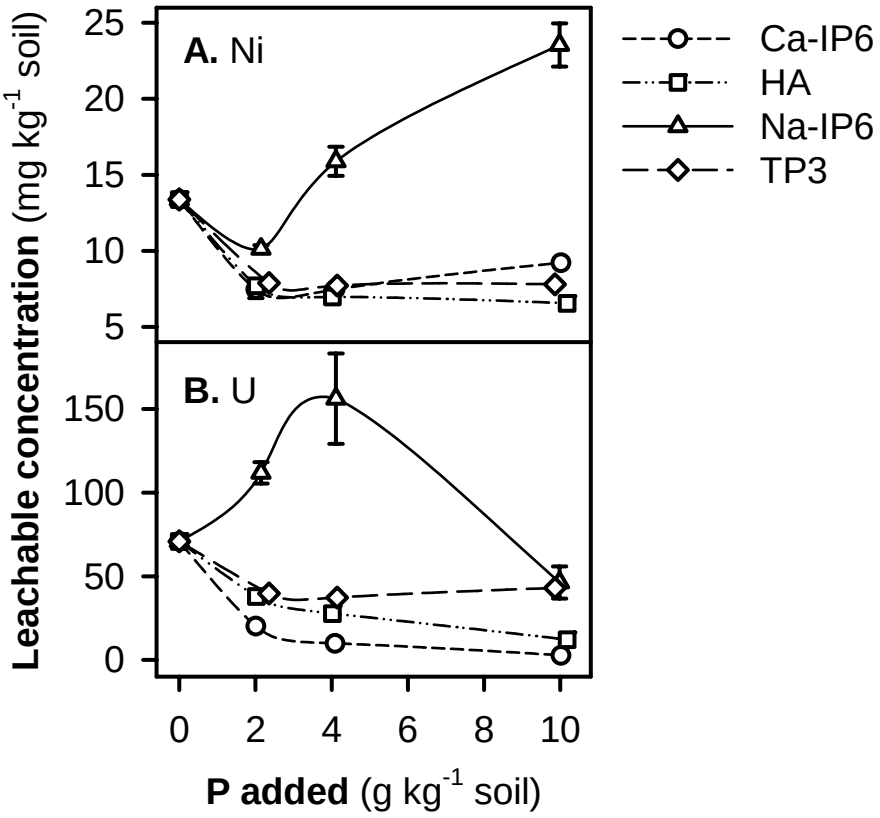

Figure 30. Toxicity Characteristic Leaching Procedure (TCLP) extractable nickel (*A*) and uranium (*B*) for Tims Branch sediment amended with calcium phytate (Ca-IP6), hydroxyapatite (HA), sodium phytate (Na-IP6), and trisodium trimetaphosphate (TP3). Error bars represent one standard deviation of the treatment level means. Splines were included to improve data readability and do not represent exact trends.

results of TCLP leachability suggest that all studied amendments except Na-IP6 are suitable for Ni and U immobilization at the smallest treatment level, but at the largest treatment level Ca-IP6 and TP3 had a negative effect on Ni and U solubility, respectively (Fig. 30).

Sequential Extraction of the Uranium and Nickel Contaminated Sediment

Sequential extractions provide a more refined operational assessment of fractionation of contaminants in this sediment. The selected procedure authored by Miller et al. (1986) and later altered by Arey and co-workers (1999) successively dissolves less and less chemically labile fractions of the studied contaminants (Table 3). Sowder et al. (2003) decided to eliminate the hydroxylamine-extractable step from the extraction procedure for contaminated and uncontaminated SRS sediments, pointing to the low total Mn content in them (between 100 and 600 mg kg^{-1} sediment). Omission of that extractant likely resulted in U contained in that fraction nearly completely extracted with the pyrophosphate-extractable and redistribution of Ni to the oxalate- and dithionite-extractable and residual fraction. Two things made me hesitant to follow in these footsteps; firstly, potentially important role Mn oxides played in Pb speciation in the Pb contaminated soil despite its low content (Table 4) and secondly, organic character of phytate molecule with its strong affinity for uranyl ion (Nash et al., 1998). We decided to maintain the original extraction procedure for two main reasons. The water-soluble fraction was corrected for the contaminants removed during the initial equilibration in the low ionic strength background solution, 0.001 M $CaCl_2$.

The average extracted mass that was summed for all extraction steps accounted for 107.99% and 100.31% of Ni and U, respectively, compared to single microwave-assisted digestions with HNO_3/HF mixture. Extracted mass of Ni and U for the treated soils were grouped for each sequential extraction step in order to identify trends in metal solubility (Figs. 31 and 32). Regardless of amendment applied, each studied contaminant represented a distinct SE pattern. Nickel, on one hand, was widely distributed throughout all SE fractions ranging from a few percent in the water-soluble, the acetate-extractable, and hydroxylamine-extractable fractions, and up to twenty percent in oxalate and residual fractions (Fig. 31). Uranium fractionation, on the other hand, was absolutely dominated by the hydroxylamine- and pyrophosphate-extractable fractions, i.e., 40% each (Fig. 32). The rest of the U was associated mostly with the acetate-extractable fraction (up to 10%), with consistently 3% in the oxalate-extractable fraction and a few percent in the four remaining fractions.

Nickel: While application of HA, Ca-IP6 and TP3 lowered Ni solubility at the end of the initial seven-day equilibration period in this contaminated sediment (Fig. 28), the amendment did not appear to affect the Ni distribution within the SE procedure. On a contrary, all of the phosphate amendments seem to shift the Ni solubility from the three most resistant fractions (oxalate-, dithionite-extractable and residual fractions) to less recalcitrant fractions (Fig. 31). The decrease in the resistant fractions might be a result of re-adsorption of Ni liberated by one of the less aggressive extractants to iron oxides in the untreated samples and to phosphates in the treated samples. Redistribution of Ni by a high ionic strength solution of neutral salt (1 *M* $MgCl_2$) as a function of SOM and Fe (hydr)oxide content has been illustrated (Gomez-Ariza et al., 1999). This evidence

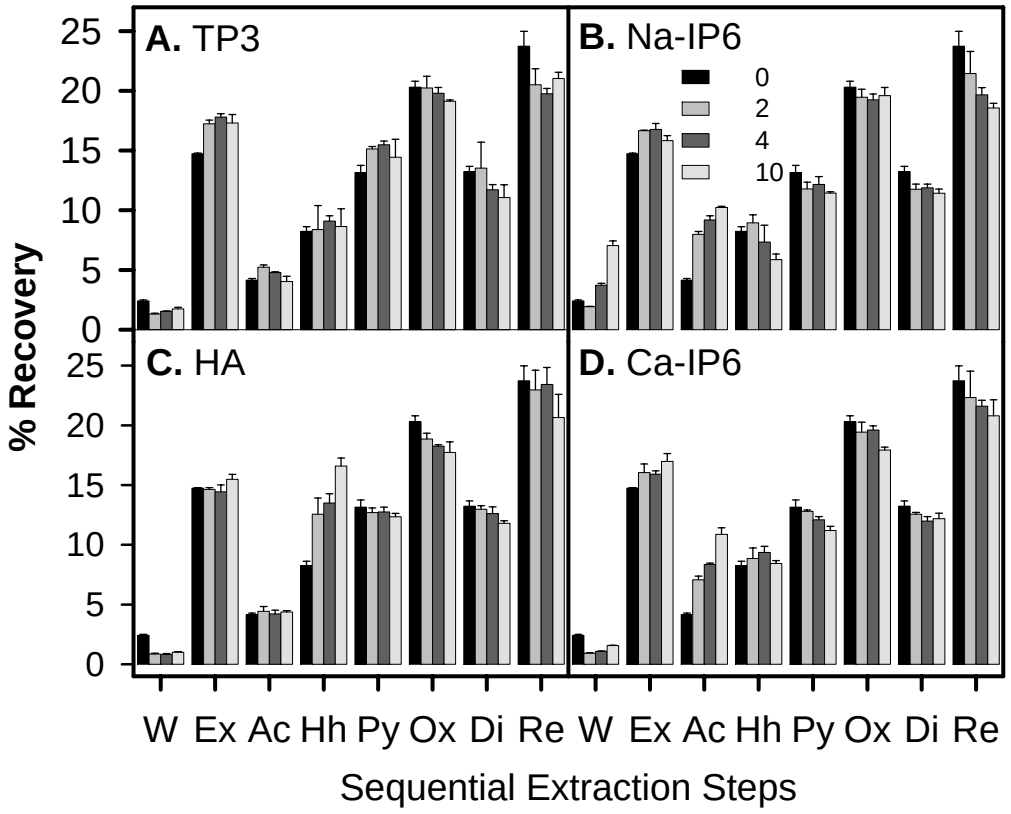

Figure 31. Sequentially extracted nickel from contaminated sediment amended with trisodium trimetaphosphate (*A*), sodium phytate (*B*), hydroxyapatite (*C*), and calcium phytate (*D*). Samples were equilibrated for 170 hours in 0.001 *M* $CaCl_2$ on a reciprocal shaker. Sequential extraction steps are listed from the least to the most aggressive step (Table 3). Extracted metal concentrations were reported as a percentage of total concentration. Units for legend are treatment levels reported as mass of phosphorus added per mass of sediment in g kg^{-1}. Error bars represent one standard deviation of the fraction means.

however, is not directly applicable to our SE protocol because it uses different and weaker salt reagent for the 'exchangeable' fraction [0.5 *M* $Ca(NO_3)_2$].

In the case of both phytate amendments Ni solubility increased mostly in the acetate-extractable fraction, with a smaller even in the calcium nitrate-extractable fraction (B and D, Fig. 31). Larger increase in calcium nitrate-extractable Ni was seen in the TP3 amended sediment which also increased slightly Ni in the pyrophosphate-extractable fraction (Fig. 31A). In the HA amended sediment the shift from the four most recalcitrant fractions was directed to the hydroxylamine-extractable fraction (Fig. 31C). Seamen et al. (2001b) suggested that the Ni-bearing phosphates that formed during the initial equilibration must have been susceptible to dissolution at the lower pH of the hydroxylamine reagent when compared to the acetate extractant, pH 1 and 2 (Table 3). The consistent increase in easily extractable fractions and consistent decrease in resistant fractions bring into question the efficacy of applying phosphates for immobilization of Ni in contaminated soils and sediments.

Uranium: Uranium speciation in this sediment is dominated by the uranyl ion (Bertsch et al., 1994; Hunter and Bertsch, 1998)which is most likely adsorbed to two phases in this sediment, the dissociated carboxyl groups of SOM and to a lesser degree to the most common mineral in the clay-sized fraction, kaolinite (Arey et al., 1999). Kaolinite and SOM are primary candidates for adsorption of positively charged uranyl ion because of their sheer abundance and negative charge that they carry at this pH value (Table 2), where identified oxides carry a positive charge (Langmuir, 1997c).

Large shifts in U extractability in the SE fractions illustrate the high affinity of phytate for uranyl ion (Fig. 32). Both the highly soluble Na-IP6 and the less soluble Ca-

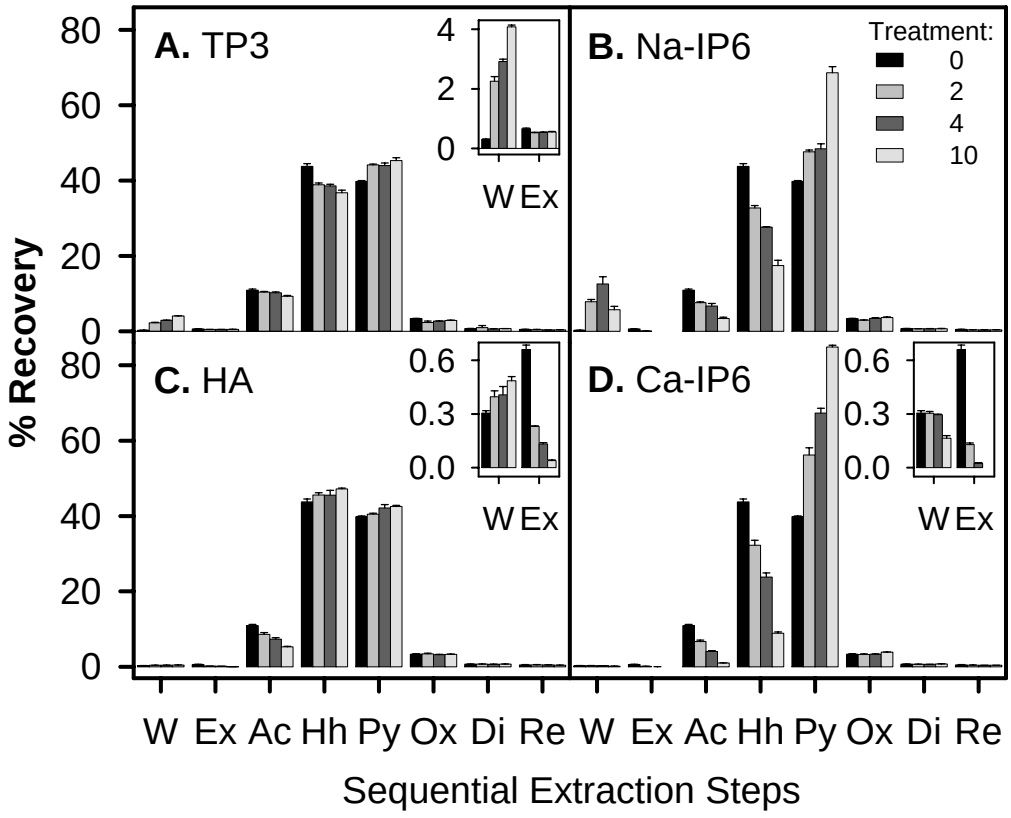

Figure 32. Sequentially extracted uranium from contaminated sediment amended with trisodium trimetaphosphate (*A*), sodium phytate (*B*), hydroxyapatite (*C*), and calcium phytate (*D*). Samples were equilibrated for 170 hours in 0.001 *M* $CaCl_2$ on a reciprocal shaker. Sequential extraction steps are listed from the least to the most aggressive step (Table 3). Inserts reflect the expanded scale for the 'water-soluble' and 'exchangeable' fractions of the given graphs. Extracted metal concentrations were reported as a percentage of total concentration. Unit for legend are treatment levels reported as mass of phosphorus added per mass of sediment in g kg^{-1}. Error bars represent one standard deviation of the fraction means.

IP6 decreased U extractability from the calcium nitrate- through hydroxylamine-extractable fractions and shifted this load to the pyrophosphate-extractable fraction; the effect of TP3 was similar, but a lot less dramatic (Fig. 32A). Hydroxyapatite addition caused SE distribution different from the other three amendments because the hydroxylamine-extractable fraction increased as well (Fig. 32C). Three most recalcitrant fractions showed very little amendment- and treatment-induced changes.

Manganese: It has been mentioned earlier in this section that total Mn content of the sediment was only 600 mg kg^{-1} and Sowder et al. (2003) questioned the necessity of including hydroxylamine hydrochloride extraction step on basis of relative 'unimportance' of Mn, especially in comparison to the large Fe content of the sediment (Table 2) and lack of identifiable Mn phases in SRS soils and sediments (Clark et al., 1996). This point would be especially valid had there been experimental evidence that the hydroxylamine hydrochloride extractant effectively lowered U solubility through reduction of uranyl U^{6+} to uranous U^{4+} ion. There is only one partial piece of evidence by Hunter et al. (1998), who observed a slight shift of the U-L_{III} absorption edge towards the U^{4+} potential after extraction of SRS sediment with hydroxylamine. This evidence, however, is unclear because, as authors of the previous paper recognized, it does not eliminate the possibility that the U^{4+} had been present in the sediment all along, but its presence became more pronounced after removal of the dominant U^{6+}.

Upon analyzing the hydroxylamine-extractable Mn and U in all the samples (except the Na-IP6 amended), it is clear that the U/Mn molar ratio is not excessively large. The mean value of U/Mn is 0.72 with 0.27 standard deviation based on 36 measured points. Manganese oxides could not be responsible for all U released in this

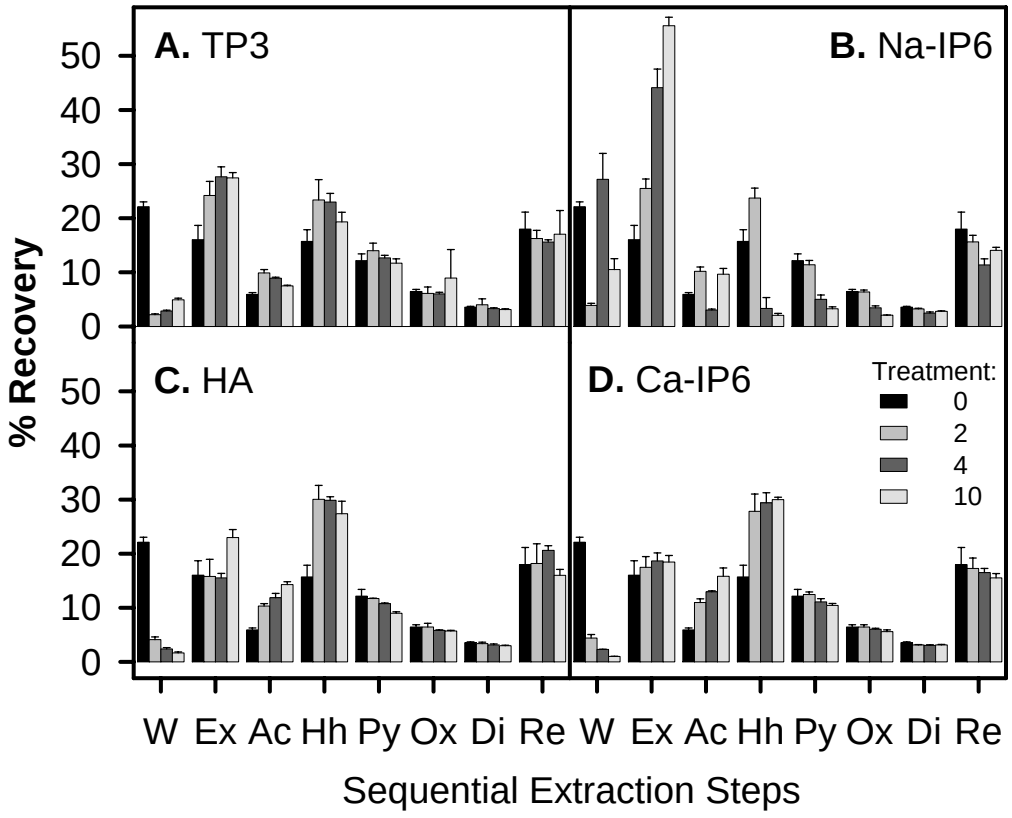

Figure 33. Sequentially extracted manganese from contaminated sediment amended with trisodium trimetaphosphate (*A*), sodium phytate (*B*), hydroxyapatite (*C*), and calcium phytate (*D*). Samples were equilibrated for 170 hours in 0.001 *M* $CaCl_2$ on a reciprocal shaker. Sequential extraction steps are listed from the least to the most aggressive step (Table 3). Extracted metal concentrations were reported as a percentage of total concentration. Unit for legend are treatment levels reported as mass of phosphorus added per mass of sediment in g kg^{-1}. Error bars represent one standard deviation of the fraction means.

fraction, but other U-bearing phases are likely involved. Little work has been done on U SE and solid phase solubilities are not well known for U. Sodium phytate amended sediment samples were excluded from the U/Mn molar analysis, because that amendment changed radically the distribution of Mn (Fig. 33) in favor of the calcium nitrate- and water-extractable fractions due to initial DOC dispersion (Fig. 27) at the expense of three more recalcitrant fractions: Hh, Py, Ox (Fig. 33 B).

Overall, the SE provided some insight into the U and Ni distribution in this sediment, e.g., illustrating the tremendous affinity of phytate for U. Nickel extractability seemed to be affected rather negatively as any phosphate amendment resulted in a shift from the most recalcitrant fractions to more soluble fractions. Uranium remained associated to a large extent with the same fractions, and no transfer to one of the most recalcitrant fractions occurred, just the proportions have changed in treated samples. Synchrotron-based X-ray micro-diffraction of the identified U hotspots, similar to one conducted for the Pb contaminated soil, did not identify any crystalline Ni- or U-bearing phase in treated sediment samples or the untreated control. The only identified crystalline phases were (the order does not signify abundance) anatase, gibbsite, goethite, kaolinite, quartz, and 2:1 phyllosilicates, e.g., mica, smectite, vermiculate.

Summary of Uranium and Nickel Immobilization Study

Treatment experiments designed to lower the solubility of two contaminants, Ni and U, by amending contaminated sediment with several phosphate compounds of varying solubilities revealed both similarities and differences. Whereas HA and Ca-IP6 lowered solution concentrations of both contaminants of interest, TP3 amendment was

effective only in lowering concentration of Ni in solution and Na-IP6 was not effective at all. The two latter named amendments were ineffective or less effective in immobilizing Ni and especially U, most likely because both dispersed progressively larger quantities of dissolved organic carbon and Al-dominated colloids to which U and Ni were adsorbed. The other two amendments, HA and Ca-IP6, caused much smaller dispersion of soil organic matter. The increase in concentration of U and Ni in solution might have been even more pronounced has it not been for the pH buffering capacity of this sediment. Both extraction techniques applied in this experiment, Toxicity Characteristic Leaching Procedure and sequential extraction, were likely burdened by extraction artifacts: aggressive extractants enhanced dissolution of the residual amendments, i.e.., HA and Ca-IP6, and facilitated redistribution of phosphates adsorbed during the initial batch equilibration. Despite these artifacts, which should have helped to further stabilize the contaminants, Ni fractionation was shifted by all amendments from most recalcitrant fractions to those extractable with relative ease (i.e., calcium nitrate- and acetate-extractable fractions). Uranium in the three most recalcitrant factions remained largely unaffected by any phosphate amendment, but proportions in two most abundant fractions, hydroxylamine- and pyrophosphate-extractable, shifted in favor of the more recalcitrant fraction. This shift was especially drastic for both phytate amended samples which was a function of tremendous affinity of phytate for uranyl ion, the dominant form of U in this sediment. Multi contaminant systems like this one pose significant difficulties in applying effective immobilization strategies, as stabilizing effects of the amendments on U were counterbalanced by increasing extractability of Ni.

5. SUMMARY AND CONCLUSIONS

Experiments were conducted to test the efficacy of proposed phosphate amendments, i.e., trisodium trimetaphosphate [TP3: $Na_3(PO_4)_3$], dodecasodium phytate [Na-IP6: $Na_{12}(CH(PO_4))_6$] and calcium phytate [Ca-IP6: $Ca_{4.85}Na_{0.06}H_{2.24}(CH(PO_4))_6 \bullet n H_2O$, n ≈ 6.5], for immobilization of multiple inorganic contaminants in a predominantly Pb-laden soil and U-laden sediment as compared to widely tested hydroxyapatite [HA: $Ca_5(PO_4)_3OH$]. Distinct contamination histories as lead-acid battery recycling and nuclear weapons production facilities left corresponding loads of Pb, Cu and Zn in the soil and Ni and U in the sediment. The soil was coarse textured, with medium content of organic matter, near neutral pH, poor buffering capacity and mineralogy of the clay-sized fraction dominated by iron hydroxides, whereas the sediment was fine textured, with high organic matter content, acidic pH, good buffering capacity and mineralogy of the same faction dominated by kaolinite [$Al_2Si_2O_5(OH)_4$] and other Al-bearing minerals.

The different phosphate amendment applied to the contaminated soil and sediment behaved very differently in a week-long batch equilibration. Hydroxyapatite additions in general lowered trace metal and U solubility with increasing treatment level. Precipitated Ca-IP6 behaved similarly and even outperformed HA with regards to lowering Zn solubility in the contaminated soil, probably because of the higher initial 'reactivity'. Nickel and Cu, however, were impacted to a various degree negatively by increasing treatment level of this phosphate amendment, presumably due to chelation

potential of phytate. Trimetaphosphate caused immediate, but moderate increases in Cu, Pb and U solubility, which was partially attributed to complexation with TP3 hydrolysis products, specifically pyrophosphate ($P_2O_7^{4-}$), and partially to an amendment-triggered, moderate dispersion of soil organic matter. The other two metals, Ni and Zn, were impacted by TP3 treatment in similar way, but solubility did not increase much beyond the control which would be indicative of lesser degree of association with the dispersed organic matter or lower affinity for the hydrolysis products. Much more serious dispersion of the soil organic matter and colloidal particles followed sodium phytate addition that was greatly enhanced by low buffering capacity of the Pb-laden soil. Not only did dispersion cause tremendous increase in all studied contaminants, but may have also had a degrading influence on the soil hydraulic properties.

An effort was made to estimate stability of the immobilized contaminants in the amended soil and sediment by use of the Toxicity Characteristic Leaching Procedure (TCLP) extractant and to gain a refined operational assessment of treatment-derived changes by sequentially extracting less chemically labile metal fractions. In the course of the TCLP and fractionation effort it became clear that results were to some extent confounded by redistribution of adsorbed phosphates and dissolution of residual, low solubility amendments such as hydroxyapatite and calcium phytate. Generally favorable TCLP leachability trends thus need to be viewed critically. While keeping in mind possible extraction artifacts, useful information can be obtained from the sequential fractionation of the contaminants. Copper and Pb fractionation were typically found in more recalcitrant forms (fractions liberated by more acidic or aggressive extractants), whereas Zn was extracted primarily in two easily extractable fractions, i.e., calcium

nitrate- and acetate-extractable. The other contaminant also dominated only by two fractions was uranium, but its distribution was split between the hydroxylamine- and pyrophosphate-extractable fractions ('Mn-oxides occluded' and 'organically bound'). Some authors eliminated the hydroxylamine extractant from the sequence while pointing to a low total Mn content in this sediment, but findings of this work suggest Mn-bearing phases as a part of the U sequestering mechanism until direct spectroscopic evidence proves otherwise. Uranium associated with the hydroxylamine-extractable fraction in phytate amended samples was highly prone to transfer to the pyrophosphate-extractable fraction, which must have been a function of tremendous affinity of this organophosphorus amendment for the dominant form of U in this sediment, uranyl ion (UO_2^{2+}). Sequential fractionation of the Ni in this sediment provides disconcerting evidence for a progressive shift from the three or four most recalcitrant fractions to relatively easily extractable fractions by all amendments. This occurred despite extraction artifacts that should have had stabilizing effect on the formation of Ni phosphates in the amended sediment.

In order to obtain more mechanistic understanding of the contaminant sequestration in the amended soil and sediment, both treated and untreated samples were subjected to X-ray spectroscopy analysis. Qualitative spectroscopy helped to identify common Pb-bearing and other closely associated phases in the untreated soil and helped to shed light on widely discussed mechanisms of solid phase Pb speciation changes upon phosphate addition. Spectroscopic studies of the sediment did not reveal the presence of any crystalline form of U or Ni. Chemistry of the highly weathered sandy soil was dominated by active surfaces of ferric and, to a lesser degree, Mn-bearing compounds.

Importance of the latter in sequestration of Pb in this soil was quite surprising due to the exceptionally low total Mn content of the soil and might be indicative of Pb bioaggregation in Mn-rich grains whose elemental composition resembled the Mn-bearing mineral coronadite [$Pb_2(Mn^{4+},Mn^{2+})_8O_{16}$]. Unamended Pb-contaminated soil showed strong diffraction patterns for anglesite ($PbSO_4$) and cerussite ($PbCO_3$), and the mixed basic lead sulfates, plumbojarosite [$Pb(Fe)_6(SO_4)_4(OH)_{12}$] and chenite [$CuPb_4(SO_4)_2(OH)_6$], were also commonly identified. The frequency of plumbojarosite presence in diffraction patterns was surprising because this mineral should dissolve at near neutral pH of this soil in favor of goethite precipitation. Decreases in Pb solubility with P additions were accompanied by formation of new Pb-bearing phases, mostly corkite [$PbFe_3PO_4SO_4(OH)_6$] and to a lesser extent drugmanite [$Pb_2(Fe,Al)H(PO_4)_2(OH)_2$] and pyromorphite [$Pb_5(PO_4)_3(Cl)$], which is usually proposed as the main sink of Pb in the phosphate amended soils.

Efforts aimed at lowering solubility of contaminant metals or radionuclides in multi contaminant systems such as this Pb-laden soil and U-laden sediment through precipitation of phosphates can meet with significant difficulties. Amendment selection and application rate have to take into account characteristics such as solubility, hydrolysis products, chelation potential and presence of contaminants in the amendment itself, as well as many aspects of the studied system, e.g., dominant form of targeted contaminant, presence of other contaminants, soil buffering capacity, and organic matter content. Outcomes of this study suggest that calcium phytate is suitable as an apatite substitute in immobilization of the studied contaminants with the exception of Cu and Ni. Nickel immobilization efforts might require other approach than phosphate addition because all

studied amendments shifted Ni distribution to more labile fractions. Two of the studied amendments, sodium phytate and metaphosphate, are not suitable for immobilization purposes as they caused dispersion of soil organic matter and soil colloids.

REFERENCES

Adriano, D.C. 2001. Trace elements in terrestrial environments: Biogeochemistry, bioavailability and risks of metals. 2nd ed. Springer-Verlag, New York, NY.

Allison, J.D., D.S. Brown, and K.J. Novo-Gradac. 2006. MINTEQA2/PRODEFA2, a geochemical assessment model for environmental systems: Version 3.0 user's manual. U.S. Environ. Prot. Agency, Athens, GA.

Antunes, S.C., D.R. de Figueiredo, S.M. Marques, B.B. Castro, R. Pereira, and F. Goncalves. 2007. Evaluation of water column and sediment toxicity from an abandoned uranium mine using a battery of bioassays. Sci. Total Environ. 374:252-259.

Arey, J.S., J.C. Seaman, and P.M. Bertsch. 1999. Immobilization of uranium in contaminated sediments by hydroxyapatite addition. Environ. Sci. Technol. 33:337-342.

ATSDR. 2008. Public health statement for uranium [Online]. Available by Cent. for Disease Control and Prevention www.atsdr.cdc.gov (posted August 2008; verified 11 June).

Bacon, J.R., and C.M. Davidson. 2008. Is there a future for sequential chemical extraction? Analyst (Cambridge) 133:25-46.

Bang, J.S., and D. Hesterberg. 2004. Dissolution of trace element contaminants from two coastal plain soils as affected by pH. J. Environ. Qual. 33:891-901.

Basta, N.T., R. Gradwohl, K.L. Snethen, and J.L. Schroder. 2001. Chemical immobilization of lead, zinc, and cadmium in smelter-contaminated soils using biosolids and rock phosphate. J. Environ. Qual. 30:1222-1230.

Batson, V.L., P.M. Bertsch, and B.E. Herbert. 1996. Transport of anthropogenic uranium from sediments to surface waters during episodic storm events. J. Environ. Qual. 25:1129-1137.

Belzile, N., P. Lecomte, and A. Tessier. 1989. Testing readsorption of trace-elements during partial chemical extractions of bottom sediments. Environ. Sci. Technol. 23:1015-1020.

Berti, W.R., and S.D. Cunningham. 1997. In-place inactivation of Pb in Pb contaminated soils. Environ. Sci. Technol. 31:1359-1364.

Bertsch, P.M., D.B. Hunter, S.R. Sutton, S. Bajt, and M.L. Rivers. 1994. In-situ chemical speciation of uranium in soils and sediments by micro-X-ray absorption-spectroscopy. Environ. Sci. Technol. 28:980-984.

Bigham, J.M., U. Schwertmann, and L. Carlson. 1992. Mineralogy of precipitates formed by the biogeochemical oxidation of Fe(II) in mine drainage, p. 219-232, *In* H. C. W. Skinner and R. W. Fitzpatrick, eds. Biomineralization processes of iron and manganese: Modern and ancient environments, Vol. 21. Catena-Verlag, Cremlingen-Destedt, Germany.

Blanchar, R.W., and L.R. Hossner. 1969a. Hydrolysis and sorption reactions of orthophosphate, pyrophosphate, tripolyphosphate, and trimetaphosphate anions added to an Elliot soil. Soil Sci. Soc. Am. Proc. 33:141-144.

Blanchar, R.W., and L.R. Hossner. 1969b. Hydrolysis and sorption of ortho-, pyro-, tripoly-, and trimetaphosphate in 32 Midwestern soils. Soil Sci. Soc. Am. Proc. 33:622-625.

Borden, A. 2006. Assessment of spatial variation of radionuclide contamination in relation to soil and terrain characteristics. Savannah River Ecol. Lab., Aiken, SC.

Busman, L.M., and M.A. Tabatabai. 1985. Hydrolysis of trimetaphosphate in soils. Soil Sci. Soc. Am. J. 49:630-636.

Cao, X.D., L.Q. Ma, M. Chen, S.P. Singh, and W.G. Harris. 2002. Impacts of phosphate amendments on lead biogeochemistry at a contaminated site. Environ. Sci. Technol. 36:5296-5304.

Cao, X.D., L.Q. Ma, M. Chen, D.W. Hardison, and W.G. Harris. 2003a. Lead transformation and distribution in the soils of shooting ranges in Florida, USA. Sci. Total Environ. 307:179-189.

Cao, X.D., L.Q. Ma, M. Chen, S.P. Singh, and W.G. Harris. 2003b. Phosphate-induced metal immobilization in a contaminated site. Environ. Pollut. 122:19-28.

Cao, X.D., L.Q. Ma, S.P. Singh, M. Chen, W.G. Harris, and P. Kizza. 2003c. Field demonstration of metal immobilization in contaminated soils using phosphate amendments. 97-01-148R. FL Inst. Phosphate Res., Bartow, FL.

Celi, L., G. De Luca, and E. Barberis. 2003. Effects of interaction of organic and inorganic P with ferrihydrite and kaolinite-iron oxide systems on iron release. Soil Sci. 168:479-488.

Celi, L., S. Lamacchia, F.A. Marsan, and E. Barberis. 1999. Interaction of inositol hexaphosphate on clays: Adsorption and charging phenomena. Soil Sci. 164:574-585.

Chapman, B.M., D.R. Jones, and R.F. Jung. 1983. Processes controlling metal-ion attenuation in acid-mine drainage streams. Geochim. Cosmochim. Acta 47:1957-1973.

Chen, M., L.Q. Ma, S.P. Singh, R.X. Cao, and R. Melamed. 2003. Field demonstration of in situ immobilization of soil Pb using P amendments. Adv. Environ. Res. 8:93-102.

Clark, D.L., D.R. Janecky, and L.J. Lane. 2006. Science-based cleanup of Rocky Flats. Phys. Today 59(9):34-40.

Clark, S.B., W.H. Johnson, M.A. Malek, S.M. Serkiz, and T.G. Hinton. 1996. A comparison of sequential extraction techniques to estimate geochemical controls on the mobility of fission product, actinide, and heavy metal contaminants in soils. Radiochim. Acta 74:173-179.

Cotter-Howells, J., and S. Caporn. 1996. Remediation of contaminated land by formation of heavy metal phosphates. Appl. Geochem. 11:335-342.

Cotter-Howells, J.D., P.E. Champness, and J.M. Charnock. 1999. Mineralogy of Pb-P grains in the roots of *Agrostis capillaris* L. by ATEM and EXAFS. Mineral. Mag. 63:777-789.

Crea, F., P. Crea, A. De Robertis, and S. Sammartano. 2004. Speciation of phytate ion in aqueous solution: Characterisation of Ca-phytate sparingly soluble species. Chem. Speciation Bioavail. 16:53-59.

Davidson, C.M., A.S. Hursthouse, D.M. Tognarelli, A.M. Ure, and G.J. Urquhart. 2004. Should acid ammonium oxalate replace hydroxylammonium chloride in step 2 of the revised BCR sequential extraction protocol for soil and sediment? Anal. Chim. Acta 508:193-199.

Davis, A., J.W. Drexler, M.V. Ruby, and A. Nicholson. 1993. Micromineralogy of mine wastes in relation to lead bioavailability, Butte, Montana. Environ. Sci. Technol. 27:1415-1425.

Davis, M.L., D.H. Tomboulian, D.H. Wachter, and D.J. Bush. 1990. An abbreviated TCLP for stabilization studies, pp. 637-642, *In* J. W. Bell, (ed.) 44th Purdue Industrial Waste Conference, Purdue Univ., West Lafayette, IN. CRC Press, Boca Raton, FL.

De Groot, C.J., and H.L. Golterman. 1993. On the presence of organic phosphate in some Camargue sediments: Evidence for the importance of phytate. Hydrobiologia 252:117-126.

De Stefano, C., D. Milea, N. Porcino, and S. Sammartano. 2006. Speciation of phytate ion in aqueous solution: Cadmium(II) interactions in aqueous NaCl at different ionic strengths. Anal. Bioanal. Chem. 386:346-356.

Dermatas, D., G. Shen, M. Chrysochoou, D.G. Grubb, N. Menounou, and P. Dutko. 2006. Pb speciation versus TCLP release in army firing range soils. J. Hazard. Mater. 136:34-46.

Dick, R.P., and M.A. Tabatabai. 1986. Hydrolysis of polyphosphates in soils. Soil Sci. 142:132-140.

Dick, R.P., and M.A. Tabatabai. 1987. Factors affecting hydrolysis of polyphosphates in soils. Soil Sci. 143:97-104.

Duff, M.C., D.E. Morris, D.B. Hunter, and P.M. Bertsch. 2000. Spectroscopic characterization of uranium in evaporation basin sediments. Geochim. Cosmochim. Acta 64:1535-1550.

Duff, M.C., D.B. Hunter, I.R. Triay, P.M. Bertsch, J. Kitten, and D.T. Vaniman. 2001. Comparison of two micro-analytical methods for detecting the spatial distribution of sorbed Pu on geologic materials. J. Contam. Hydrol. 47:211-218.

EIA. 2009a. Summary production statistics of the U.S. uranium industry. Energy Inf. Admin., Washington, DC.

EIA. 2009b. Domestic uranium production report 2008. Energy Inf. Admin., Washington, DC.

Finch, W.I. 1998. Uranium, its impact on the national and global energy mix: And its history, distribution, production, nuclear fuel-cycle, future, and relation to the environment U.S. Geol. Surv., Washington, DC.

Gee, G.W., and J.W. Bauder. 1986. Particle size analysis, p. 404-408, *In* A. Klute, ed. Methods of soil analysis. Part 1. Physical and mineralogical methods, Vol. 1, 2nd ed. Soil Sci. Soc. Am., Madison, WI.

Golovan, S.P., R.G. Meidinger, A. Ajakaiye, M. Cottrill, M.Z. Wiederkehr, D.J. Barney, C. Plante, J.W. Pollard, M.Z. Fan, M.A. Hayes, J. Laursen, J.P. Hjorth, R.R. Hacker, J.R. Phillips, and C.W. Forsberg. 2001. Pigs expressing salivary phytase produce low-phosphorus manure. Nat. Biotechnol. 19:741-745.

Gomez-Ariza, J.L., I. Giraldez, D. Sanchez-Rodas, and E. Morales. 1999. Metal readsorption and redistribution during the analytical fractionation of trace elements in oxic estuarine sediments. Anal. Chim. Acta 399:295-307.

Gomez-Ariza, J.L., I. Giraldez, D. Sanchez-Rodas, and E. Morales. 2000. Selectivity assessment of a sequential extraction procedure for metal mobility characterization using model phases. Talanta 52:545-554.

Guberman, D.E. 2009. Minerals yearbook: Lead U.S. Geol. Surv., Reston, VA.

Guy, R.D., C.L. Chakrabarti, and D.C. McBain. 1978. Evaluation of extraction techniques for fractionation of copper and lead in model sediment systems. Water Res. 12:21-24.

Hammersley, A.P. 1997. FIT2D: An introduction and overview. Internal Rep. ESRF97HA02T. Eur. Synchrotron Radiation Facility, Grenoble, France.

Hammersley, A.P., S.O. Svensson, and A. Thompson. 1994. Calibration and correction of spatial distortions in 2D detector systems. Nucl. Instr. Meth. A346:312-321.

Hammersley, A.P., S.O. Svensson, M. Hanfland, A.N. Fitch, and D. Häusermann. 1996. Two-dimensional detector software: From real detector to idealized image or two-theta scan. High Pressure Res. 14:235-248.

He, Z.Q., C.W. Honeycutt, T.Q. Zhang, and P.M. Bertsch. 2006. Preparation and FT-IR characterization of metal phytate compounds. J. Environ. Qual. 35:1319-1328.

Hettiarachchi, G.M., and G.M. Pierzynski. 2004. Soil lead bioavailability and in situ remediation of lead-contaminated soils: A review. Environ. Prog. 23:78-93.

Hettiarachchi, G.M., G.M. Pierzynski, and M.D. Ransom. 2000. In situ stabilization of soil lead using phosphorus and manganese oxide. Environ. Sci. Technol. 34:4614-4619.

Hettiarachchi, G.M., G.M. Pierzynski, and M.D. Ransom. 2001. In situ stabilization of soil lead using phosphorus. J. Environ. Qual. 30:1214-1221.

Hochella, M.F., J.N. Moore, U. Golla, and A. Putnis. 1999. A TEM study of samples from acid mine drainage systems: Metal-mineral association with implications for transport. Geochim. Cosmochim. Acta 63:3395-3406.

Holmgren, G.G.S., M.W. Meyer, R.L. Chaney, and R.B. Daniels. 1993. Cadmium, lead, zinc, copper, and nickel in agricultural soils of the United States of America. J. Environ. Qual. 22:335-348.

Hossner, L.R., C.L. Trostle, and H. Shahandeh. 2004. Hydrolysis of cyclotri- and cyclotetraphosphate in soil. Soil Sci. Soc. Am. J. 68:74-81.

Hughes, J.M., and J. Rakovan. 2002. The crystal structure of apatite, $Ca_5(PO_4)_3(F,OH,Cl)$, p. 1-12, *In* M. J. Kohn, et al., eds. Phosphates: Geochemical, geobiological, and materials importance, Vol. 48. Mineral. Soc. Am., Washington, DC.

Hunter, D.B., and P.M. Bertsch. 1998. In situ examination of uranium contaminated soil particles by micro-X-ray absorption and micro-fluorescence spectroscopies. J. Radioanal. Nucl. Chem. 234:237-242.

Jackman, R.H., and C.A. Black. 1951a. Solubility of iron, aluminum, calcium, and magnesium inositol phosphates at different pH values. Soil Sci. 72:179-186.

Jackman, R.H., and C.A. Black. 1951b. Hydrolysis of iron, aluminum, calcium, and magnesium inositol phosphates by phytase at different pH values. Soil Sci. 72:261-266.

Jackson, B.P., J.F. Ranville, P.M. Bertsch, and A.G. Sowder. 2005. Characterization of colloidal and humic-bound Ni and U in the 'dissolved' fraction of contaminated sediment extracts. Environ. Sci. Technol. 39:2478-2485.

Jackson, M.L. 1958. Soil chemical analysis Prentice-Hall, Englewood Cliffs, NJ.

Jambor, J.L. 1999. Nomenclature of the alunite supergroup. Can. Mineral. 37:1323-1341.

Jensen, M.P., K.L. Nash, L.R. Morss, E.H. Appelman, and M.A. Schmidt. 1996. Immobilization of actinides in geomedia by phosphate precipitation, p. 272-285, *In* J. S. Gaffney, et al., eds. Humic and fulvic acids: Isolation, structure and environmental role, Vol. 651. Am. Chem. Soc., Washington, DC.

Kaplan, D.I., and A.S. Knox. 2004. Enhanced contaminant desorption induced by phosphate mineral additions to sediment. Environ. Sci. Technol. 38:3153-3160.

Karapanagiotis, N.K., R.M. Sterritt, and J.N. Lester. 1991. Heavy metal complexation in sludge amended soil: The role of organic matter in metal retention. Environ. Technol. 12:1107-1116.

Kashkay, C.M., Y.B. Borovskaya, and M.A. Babazade. 1975. Determination of $\Delta G^{\circ}_{f,\,298}$ of synthetic jarosite and its sulfate analogues. Geochem. Int. 12:115–121.

Kingston, H.M., P.J. Walter, S. Chalk, E. Lorentzen, and D. Link. 1997. Environmental microwave sample preparation: Fundamentals, methods, and applications, p. 223–349, *In* H. M. Kingston and S. J. Haswell, eds. Microwave-enhanced chemistry:

Fundamentals, sample preparation and application. Am. Chem. Soc., Washington, DC.

Knox, A.S., D.I. Kaplan, D.C. Adriano, T.G. Hinton, and M.D. Wilson. 2003. Apatite and phillipsite as sequestering agents for metals and radionuclides. J. Environ. Qual. 32:515-525.

Langmuir, D. 1997a. Actinides and their daughter and fission products, p. 486-557, *In* D. Langmuir, ed. Aqueous environmental geochemistry. Prentice Hall, Upper Saddle River, NJ.

Langmuir, D. 1997b. Aqueous environmental geochemistry Prentice Hall, Upper Saddle River, NJ.

Langmuir, D. 1997c. Adsorption-desorption reactions, p. 343-402, *In* D. Langmuir, ed. Aqueous environmental geochemistry. Prentice Hall, Upper Saddle River, NJ.

Lanson, B., M.A. Marcus, S. Fakra, F. Panfili, N. Geoffroy, and A. Manceau. 2008. Formation of Zn-Ca phyllomanganate nanoparticles in grass roots. Geochim. Cosmochim. Acta 72:2478-2490.

Lenhart, J.J., S.E. Cabaniss, P. MacCarthy, and B.D. Honeyman. 2000. Uranium(VI) complexation with citric, humic and fulvic acids. Radiochim. Acta 88:345-353.

Lin, Z.X., B. Comet, U. Qvarfort, and R. Herbert. 1995. The chemical and mineralogical behavior of Pb in shooting range soils from central Sweden. Environ. Pollut. 89:303-309.

Lind, O.C., B. Salbu, L. Skipperud, K. Janssens, J. Jaroszewicz, and W. De Nolf. 2009. Solid state speciation and potential bioavailability of depleted uranium particles from Kosovo and Kuwait. J. Environ. Radioact. 100:301-307.

Lindsay, W.L. 1979. Chemical equilibria in soils Wiley, New York, NY.

Linsalata, P. 1994. Uranium and thorium decay series radionuclides in human and animal food chains: A review. J. Environ. Qual. 23:633-642.

Ma, Q.Y., S.J. Traina, T.J. Logan, and J.A. Ryan. 1993. In-situ lead immobilization by apatite. Environ. Sci. Technol. 27:1803-1810.

Ma, Q.Y., T.J. Logan, S.J. Traina, and J.A. Ryan. 1994a. Effects of NO_3^-, Cl^-, F^-, SO_4^{2-}, and CO_3^{2-} on Pb^{2+} immobilization by hydroxyapatite. Environ. Sci. Technol. 28:408-418.

Ma, Q.Y., S.J. Traina, T.J. Logan, and J.A. Ryan. 1994b. Effects of aqueous Al, Cd, Cu, Fe(II), Ni, and Zn on Pb immobilization by hydroxyapatite. Environ. Sci. Technol. 28:1219-1228.

Manahan, S.E. 1990. Environmental chemistry. 4th ed. Lewis Publishers, Boston, MA.

Manceau, A., N. Tamura, M.A. Marcus, A.A. MacDowell, R.S. Celestre, R.E. Sublett, G. Sposito, and H.A. Padmore. 2002. Deciphering Ni sequestration in soil ferromanganese nodules by combining X-ray fluorescence, absorption, and diffraction at micrometer scales of resolution. Am. Mineral. 87:1494-1499.

Martinez, C.E., A.R. Jacobson, and M.B. McBride. 2004. Lead phosphate minerals: Solubility and dissolution by model and natural ligands. Environ. Sci. Technol. 38:5584-5590.

Mason, C.F.V., W. Turney, B.M. Thomson, N. Lu, P.A. Longmire, and C.J. Chisholm-Brause. 1997. Carbonate leaching of uranium from contaminated soils. Environ. Sci. Technol. 31:2707-2711.

Match! 2003. Phase identification from powder diffraction Crystal Impact GbR, Bonn, Germany.

McBride, M.B. 1994. Environmental chemistry of soils. 1 ed. Oxford Univ. Press, New York, NY.

McClain, D.E., A.C. Miller, and J.F. Kalinich. 2005. Status of health concerns about military use of depleted uranium and surrogate metals in armor-penetrating munitions Human Factors and Medicine (HFM) panel Research Task Group (RTG) 099 meeting: Radiation bioeffects and countermeasures. North Atlantic Treaty Organ., Bethesda, MD.

McKenzie, R.M. 1989. Manganese oxides and hydroxides, p. 439-466, *In* J. B. Dixon and S. B. Weed, eds. Minerals in soil environments, Vol. 1, 2nd ed. Soil Sci. Soc. Am., Madison, WI.

McLean, E.O. 1982. Soil pH and lime requirement, p. 208-209, *In* A. L. Page, ed. Methods of soil analysis. Part 2. Chemical and microbiological properties, Vol. 1, 2nd ed. Soil Sci. Soc. Am., Madison, WI.

Meers, E., G. Du Laing, F.M.G. Tack, and M.G. Verloo. 2009. Heavy metal displacement by exchangeable bases (Ca, Mg, K, Na) in soils and sediments. Soil Sci. 174:202-209.

Melamed, R., X.D. Cao, M. Chen, and L.Q. Ma. 2003. Field assessment of lead immobilization in a contaminated soil after phosphate application. Sci. Total Environ. 305:117-127.

Miller, W.P., D.C. Martens, and L.W. Zelazny. 1986. Effect of sequence in extraction of trace metals from soils. Soil Sci. Soc. Am. J. 50:598-601.

Morris, D.E., P.G. Allen, J.M. Berg, C.J. Chisholm-Brause, S.D. Conradson, R.J. Donohoe, N.J. Hess, J.A. Musgrave, and C.D. Tait. 1996. Speciation of uranium in Fernald soils by molecular spectroscopic methods: Characterization of untreated soils. Environ. Sci. Technol. 30:2322-2331.

Mudd, G.M. 2001a. Critical review of acid in situ leach uranium mining: 2. Soviet Block and Asia. Environ. Geol. 41:404-416.

Mudd, G.M. 2001b. Critical review of acid in situ leach uranium mining: 1. USA and Australia. Environ. Geol. 41:390-403.

Nash, K.L., M.P. Jensen, and M.A. Schmidt. 1998. Actinide immobilization in the subsurface environment by in-situ treatment with a hydrolytically unstable organophosphorus complexant: Uranyl uptake by calcium phytate. J. Alloys Compounds 271:257-261.

NCEH. 2009. Children's blood lead levels in the United States [Online]. Available by Cent. Disease Control Prevention www.cdc.gov/nceh (posted 13 March 2009; verified 11 June).

Nelson, D.W., and L.E. Sommers. 1982. Total carbon, organic carbon, and organic matter, p. 570-571, *In* A. L. Page, ed. Methods of soil analysis. Part 2. Chemical and microbiological properties, Vol. 1, 2nd ed. Soil Sci. Soc. Am., Madison, WI.

NIST. 1989. X-ray powder diffraction intensity set SRM 674a. U.S. Dep. Commerce, Gaithersburg, MD.

NIST. 2000. Buffalo River sediment RM 8704. U.S. Dep. Commerce, Gaithersburg, MD.

NIST. 2003. San Joaquin soil: Baseline trace element concentrations SRM 2709. U.S. Dep. Commerce, Gaithersburg, MD.

Nriagu, J.O. 1973. Lead orthophosphates: 2. Stability of chloropyromorphite at 25 degrees C. Geochim. Cosmochim. Acta 37:367-377.

Nriagu, J.O. 1984. Formation and stability of base metal phosphates in soils and sediments, p. 318-329, *In* J. O. Nriagu and P. B. Moore, eds. Phosphate minerals, 1 ed. Springer-Verlag, Berlin.

Ostergren, J.D., G.E. Brown, G.A. Parks, and T.N. Tingle. 1999. Quantitative speciation of lead in selected mine tailings from Leadville, CO. Environ. Sci. Technol. 33:1627-1636.

Paar, W.H., K. Mereiter, R.S.W. Braithwaite, P. Keller, and P.J. Dunn. 1986. Chenite, $Pb_4Cu(SO_4)_2(OH)_6$, a new mineral, from Leadhills, Scotland. Mineral. Mag. 50:129-135.

Panfili, F.R., A. Manceau, G. Sarret, L. Spadini, T. Kirpichtchikova, V. Bert, A. Laboudigue, M.A. Marcus, N. Ahamdach, and M.F. Libert. 2005. The effect of phytostabilization on Zn speciation in a dredged contaminated sediment using scanning electron microscopy, X-ray fluorescence, EXAFS spectroscopy, and principal components analysis. Geochim. Cosmochim. Acta 69:2265-2284.

Papp, C.S.E., L.H. Filipek, and K.S. Smith. 1991. Selectivity and effectiveness of extractants used to release metals associated with organic-matter. Appl. Geochem. 6:349-353.

PDF-2. 2003. Powder diffraction files. Int. Cent. Diffraction Data, Newtown Square, PA.

Pettersen, J., and E.G. Hertwich. 2008. Critical review: Life-cycle inventory procedures for long-term release of metals. Environ. Sci. Technol. 42:4639-4647.

Punshon, T., K.F. Gaines, and R.A. Jenkins. 2003a. Bioavailability and trophic transfer of sediment-bound Ni and U in a southeastern wetland system. Arch. Environ. Contam. Toxicol. 44:30-35.

Punshon, T., K.F. Gaines, P.M. Bertsch, and J. Burger. 2003b. Bioavailability of uranium and nickel to vegetation in a contaminated riparian ecosystem. Environ. Toxicol. Chem. 22:1146-1154.

Punshon, T., P.M. Bertsch, A. Lanzirotti, K. McLeod, and J. Burger. 2003c. Geochemical signature of contaminated sediment remobilization revealed by spatially resolved X-ray microanalysis of annual rings of *Salix nigra*. Environ. Sci. Technol. 37:1766-1774.

Punshon, T., B.P. Jackson, P.M. Bertsch, and J. Burger. 2004. Mass loading of nickel and uranium on plant surfaces: Application of laser ablation-ICP-MS. J. Environ. Monit. 6:153-159.

Quevauviller, P. 2002. Operationally-defined extraction procedures for soil and sediment analysis: Part 3. New CRMs for trace-element extractable contents. Trac-Trends Anal. Chem. 21:774-785.

Quevauviller, P., G. Rauret, H. Muntau, A.M. Ure, R. Rubio, J.F. Lopez-Sanchez, H.D. Fiedler, and B. Griepink. 1994. Evaluation of a sequential extraction procedure for the determination of extractable trace-metal contents in sediments. Fresenius J. Anal. Chem. 349:808-814.

Raksasataya, M., A.G. Langdon, and N.D. Kim. 1996. Assessment of the extent of lead redistribution during sequential extraction by two different methods. Anal. Chim. Acta 332:1-14.

Rauret, G., J.F. Lopez-Sanchez, A. Sahuquillo, R. Rubio, C. Davidson, A. Ure, and P. Quevauviller. 1999. Improvement of the BCR three step sequential extraction procedure prior to the certification of new sediment and soil reference materials. J. Environ. Monit. 1:57-61.

Reed, S.J.B. 1996. Electron microprobe analysis and scanning electron microscopy in geology. 1st ed. Cambridge Univ. Press, New York, NY.

Reilly, T.J., N.S. Fishman, and A.L. Baehr. 2009. Effect of grain-coating mineralogy on nitrate and sulfate storage in the unsaturated zone. Vadose Zone J. 8:75-85.

Ryan, J.A., and R.L. Chaney. 1992. Heavy metals and toxic organic pollutants in MSW-composts: Research results on phytoavailability, bioavailability, fate, etc., pp. 451-506 Science and engineering of composting: Design, environmental, microbiological and utilization aspects, Columbus, OH. Natl. Tech. Inf. Serv., U.S. Dep. Commerce, Springfield, VA.

Ryan, J.A., K.G. Scheckel, W.R. Berti, S.L. Brown, S.W. Casteel, R.L. Chaney, J. Hallfrisch, M. Doolan, P. Grevatt, M. Maddaloni, and D. Mosby. 2004. Reducing children's risk from lead in soil. Environ. Sci. Technol. 38:18A-24A.

Scheckel, K.G., C.A. Impellitteri, J.A. Ryan, and T. McEvoy. 2003. Assessment of a sequential extraction procedure for perturbed lead-contaminated samples with and without phosphorus amendments. Environ. Sci. Technol. 37:1892-1898.

Scheckel, K.G., J.A. Ryan, D. Allen, and N.V. Lescano. 2005. Determining speciation of Pb in phosphate-amended soils: Method limitations. Sci. Total Environ. 350:261-272.

Schroeder, P.A., N.D. Melear, L.T. West, and D.A. Hamilton. 2000. Meta-gabbro weathering in the Georgia Piedmont, USA: Implications for global silicate weathering rates. Chem. Geol. 163:235-245.

Seaman, J.C., T. Meehan, and P.M. Bertsch. 2001a. Immobilization of cesium 137 and uranium in contaminated sediments using soil amendments. J. Environ. Qual. 30:1206-1213.

Seaman, J.C., J.S. Arey, and P.M. Bertsch. 2001b. Immobilization of nickel and other metals in contaminated sediments by hydroxyapatite addition. J. Environ. Qual. 30:460-469.

Seaman, J.C., J.M. Hutchison, B.P. Jackson, and V.M. Vulava. 2003. In-situ treatment of metals in contaminated soils with phytate. J. Environ. Qual. 32:153-161.

Seaman, J.C., V.M. Vulava, A.G. Sowder, B.P. Jackson, S.A. Aburime, and P.M. Bertsch. 2005. Metal extractability from contaminated SRS sediments: Comparison of column and batch results Environ. Geosci. 12:235-242.

Shan, X.Q., and C. Bin. 1993. Evaluation of sequential extraction for speciation of trace-metals in model soil containing natural minerals and humic acid. Anal. Chem. 65:802-807.

Shang, C., and L.W. Zelazny. 2008. Selective dissolution techniques for mineral analysis of soils and sediments, p. 33-80, *In* A. L. Ulery and L. R. Drees, eds. Methods of soil analysis. Part 5. Mineralogical methods, Vol. 1. Soil Sci. Soc. Am., Madison, WI.

Sharpley, A., and B. Moyer. 2000. Phosphorus forms in manure and compost and their release during simulated rainfall. J. Environ. Qual. 29:1462-1469.

Shober, A.L., D.L. Hesterberg, J.T. Sims, and S. Gardner. 2006. Characterization of phosphorus species in biosolids and manures using XANES spectroscopy. J. Environ. Qual. 35:1983-1993.

Smith, G.R. 2004. Lead recycling in the United States in 1998, p. 73-85, *In* S. F. Sibley, ed. Flow studies for recycling metal commodities in the United States. U.S. Geol. Surv., Reston, VA.

Sowder, A.G., P.M. Bertsch, and P.J. Morris. 2003. Partitioning and availability of uranium and nickel in contaminated riparian sediments. J. Environ. Qual. 32:885-898.

Sparks, D.L. 2003. Environmental soil chemistry. 2nd ed. Academic Press, San Diego, CA.

Strucken, E.F., T.S. Floyd, and D.P. Manchester. 1988. Remote operation of microwave systems for solids content analysis and chemical dissolution in highly radioactive environments, p. 187-202, *In* H. M. Kingston and L. B. Jassie, eds. Introduction to microwave sample preparation: Theory and practice. Am. Chem. Soc., Washington, DC.

Szymanski, W.N. 1994. Uranium in-situ leach mining in the United States, p. ix-xxx, *In* EIA, ed. Uranium industry annual 1993. Energy Inf. Admin., Washington, DC.

Tessier, A., and P.G.C. Campbell. 1988. Comments on the testing of the accuracy of an extraction procedure for determining the partitioning of trace-metals in sediments. Anal. Chem. 60:1475-1476.

Tessier, A., and P.G.C. Campbell. 1991. Pitfalls of sequential extractions: Comment. Water Res. 25:115-117.

Tessier, A., P.G.C. Campbell, and M. Bisson. 1979. Sequential extraction procedure for the speciation of particulate trace metals. Anal. Chem. 51:844-851.

Tipping, E., N.B. Hetherington, J. Hilton, D.W. Thompson, E. Bowles, and J. Hamilton-Taylor. 1985. Artifacts in the use of selective chemical-extraction to determine distributions of metals between oxides of manganese and iron. Anal. Chem. 57:1944-1946.

Tokunaga, T.K., J.M. Wan, Y.M. Kim, S.R. Sutton, M. Newville, A. Lanzirotti, and W. Rao. 2008. Real-time X-ray absorption spectroscopy of uranium, iron, and manganese in contaminated sediments during bioreduction. Environ. Sci. Technol. 42:2839-2844.

Tokunaga, T.K., J.M. Wan, J. Pena, E.L. Brodie, M.K. Firestone, T.C. Hazen, S.R. Sutton, A. Lanzirotti, and M. Newville. 2005. Uranium reduction in sediments under diffusion-limited transport of organic carbon. Environ. Sci. Technol. 39:7077-7083.

Tsao, G.T., Y.Z. Zheng, J. Lu, and C.S. Gong. 1997. Adsorption of heavy metal ions by immobilized phytic acid. Appl. Biochem. Biotechnol. 63-65:731-741.

Turner, B.L., M.J. Paphazy, P.M. Haygarth, and I.D. McKelvie. 2002. Inositol phosphates in the environment. Philos. Trans. R. Soc. Lond. Ser. B-Biol. Sci. 357:449-469.

Ure, A.M., P. Quevauviller, H. Muntau, and B. Griepink. 1993. Speciation of heavy-metals in soils and sediments - an account of the improvement and harmonization of extraction techniques undertaken under the auspices of the BCR of the

Commission-of-the-European-Communities. Int. J. Environ. Anal. Chem. 51:135-151.

USDOE. 1996. Closing the circle on the splitting of the atom: The environmental legacy of nuclear weapons production in the United States and what the Department of Energy is doing about it. 0-16-048448-0. Office Environ. Manage., Washington, DC.

USEPA. 1976. RCRA subtitle C: Hazardous waste. U.S. Environ. Prot. Agency, Washington, DC.

USEPA. 1992. Method 1311: Toxicity Characteristic Leaching Procedure. U.S. Environ. Prot. Agency, Washington, DC.

USEPA. 1996. Method 3052: Microwave assisted acid digestion of siliceous and organically based matrices. U.S. Environ. Prot. Agency, Washington, DC.

Vantelon, D., A. Lanzirotti, A.C. Scheinost, and R. Kretzschmar. 2005. Spatial distribution and speciation of lead around corroding bullets in a shooting range soil studied by micro-X-ray fluorescence and absorption spectroscopy. Environ. Sci. Technol. 39:4808-4815.

Wright, C.W., and H.M. Meyer. 1933. Lead, p. 53-66, *In* O. E. Kiessling, ed. Minerals yearbook 1932-33. U.S. Gov. Printing Office, Washington, DC.

Xu, Y.P., and F.W. Schwartz. 1994. Lead immobilization by hydroxyapatite in aqueous-solutions. J. Contam. Hydrol. 15:187-206.

Xu, Y.P., F.W. Schwartz, and S.J. Traina. 1994. Sorption of Zn^{2+} and Cd^{2+} on hydroxyapatite surface. Environ. Sci. Technol. 28:1472-1480.

Yoon, J.K., X.D. Cao, and L.Q. Ma. 2007. Application methods affect phosphorus-induced lead immobilization from a contaminated soil. J. Environ. Qual. 36:373-378.

Zabinski, C.A. 2006. The effect of chemical speciation on the uptake and bioavailability of uranium and nickel on the earthworm *Eisenia fetida*. Savannah River Ecol. Lab., Aiken, SC.

APPENDICES

A. Detail Calculation of pH-Dependent Solubility of Common Lead Minerals

Hypothetical scenario under which pyromorphite [$Pb_5(PO_4)_3Cl$] controls Pb solubility in hydroxyapatite [$Ca_5(PO_4)_3OH$] amended soil that contains some calcium and where soil iron hydroxide [$Fe(OH)_3$] controls iron solubility. Three sets of equations represent phosphate availability in distinct regions of soil pH. First set of equations corresponds to acidic pH range where it is dissolution of strengite ($FePO_4 \cdot 2H_2O$), as controlled by soluble levels of soil iron, and not dissolution of the apatite that controls phosphate level, because strengite is much less soluble than the amendment. As pH progresses to mildly acidic and higher pH, phosphate level becomes controlled directly by apatite dissolution. Second set of equations corresponds to region between this transition pH and neutral pH, where solution concentration of calcium controls the apatite solubility. At even higher pH, above neutral pH, dissolved levels of carbon dioxide [$CO_2(g)$] and presence of calcite ($CaCO_3$) implicitly determine phosphate level as described by the third and the last set of equations. This concept together with the equilibrium constants was adapted from (Lindsay, 1979).

1.

$$Pb_5(PO_4)_3Cl + 6H^+ \leftrightarrow 5Pb^{2+} + 3H_2PO_4^- + Cl^- \qquad -25.05$$

$$3Fe^{3+} + 3H_2PO_4^- + 6H_2O \leftrightarrow 3FePO_4 \bullet 2H_2O + 6H^+ \qquad +3\times 6.85$$

$$3Fe(OH)_3 + 9H^+ \leftrightarrow 3Fe^{3+} + 9H_2O \qquad \underline{+3\times 2.70}$$

$$3.60$$

$$Pb_5(PO_4)_3Cl + 3Fe(OH)_3 + 9H^+ \leftrightarrow 5Pb^{2+} + Cl^- + 3FePO_4 \bullet 2H_2O + 3H_2O$$

$$K = \frac{(Pb^{2+})^5(Cl^-)}{(H^+)^9}$$

$$\log_{10} K = 5\log_{10}(Pb^{2+}) + \log_{10}(Cl^-) - 9\log_{10}(H^+) \quad \log_{10} K = 3.60$$

$$\log_{10}(Pb^{2+}) = 0.72 - 0.2\log_{10}(Cl^-) - 1.8pH$$

2.

$$Pb_5(PO_4)_3Cl + 6H^+ \leftrightarrow 5Pb^{2+} + 3H_2PO_4^- + Cl^- \qquad -25.05$$

$$5Ca^{2+} + 3H_2PO_4^- + H_2O \leftrightarrow Ca_5(PO_4)_3OH + 7H^+ \qquad \underline{+(-14.46)}$$

$$-39.51$$

$$Pb_5(PO_4)_3Cl + 5Ca^{2+} + H_2O \leftrightarrow 5Pb^{2+} + Cl^- + Ca_5(PO_4)_3OH + H^+$$

$$K = \frac{(Pb^{2+})^5(Cl^-)(H^+)}{(Ca^{2+})^5}$$

$$\log_{10} K = 5\log_{10}(Pb^{2+}) + \log_{10}(Cl^-) + \log_{10}(H^+) - 5\log_{10}(Ca^{2+}) \quad \log_{10} K = (-39.51)$$

$$\log_{10}(Pb^{2+}) = (-7.902) - 0.2\log_{10}(Cl^-) + 0.2pH + \log_{10}(Ca^{2+})$$

3.

$$Pb_5(PO_4)_3Cl + 6H^+ \leftrightarrow 5Pb^{2+} + 3H_2PO_4^- + Cl^- \qquad -25.05$$

$$5Ca^{2+} + 3H_2PO_4^- + H_2O \leftrightarrow Ca_5(PO_4)_3OH + 7H^+ \qquad +(-14.46)$$

$$5CaCO_3 + 10H^+ \leftrightarrow 5Ca^{2+} + 5CO_2(g) + 5H_2O \qquad \underline{+5\times 9.74}$$

$$9.19$$

$$Pb_5(PO_4)_3Cl + 5CaCO_3 + 9H^+ \leftrightarrow 5Pb^{2+} + Cl^- + 5CO_2(g) + Ca_5(PO_4)_3OH + 5H_2O$$

$$K = \frac{(Pb^{2+})^5(Cl^-)(CO_2(g))^5}{(H^+)^9}$$

$$\log_{10} K = 5\log_{10}(Pb^{2+}) + \log_{10}(Cl^-) + 5\log_{10}(CO_2(g)) - 9\log_{10}(H^+) \quad \log_{10} K = 9.19$$

$$\log_{10}(Pb^{2+}) = 1.84 - 0.2\log_{10}(Cl^-) - \log_{10}(CO_2(g)) - 1.8pH + \log_{10}(Ca^{2+})$$

B. Soil Particle Selection for Synchrotron Analysis

Soil particles show as a dark spots on visible wavelength image of the Pb contaminated soil from a decommissioned lead-acid battery recycling facility in Jacksonville, FL. The image was obtained in normal incidence by an optical microscope with TV attachment. Viewed particles were randomly surveyed for Pb content and those with detected Pb Lα fluorescence radiation were mapped for elemental content by a Radiant Vortex-EX silicon drift detector, which was situated at 45° to the sample stage and 90° to the incident micro-beam. Pixels with the highest count for the selected chemical element were selected for diffraction analysis.

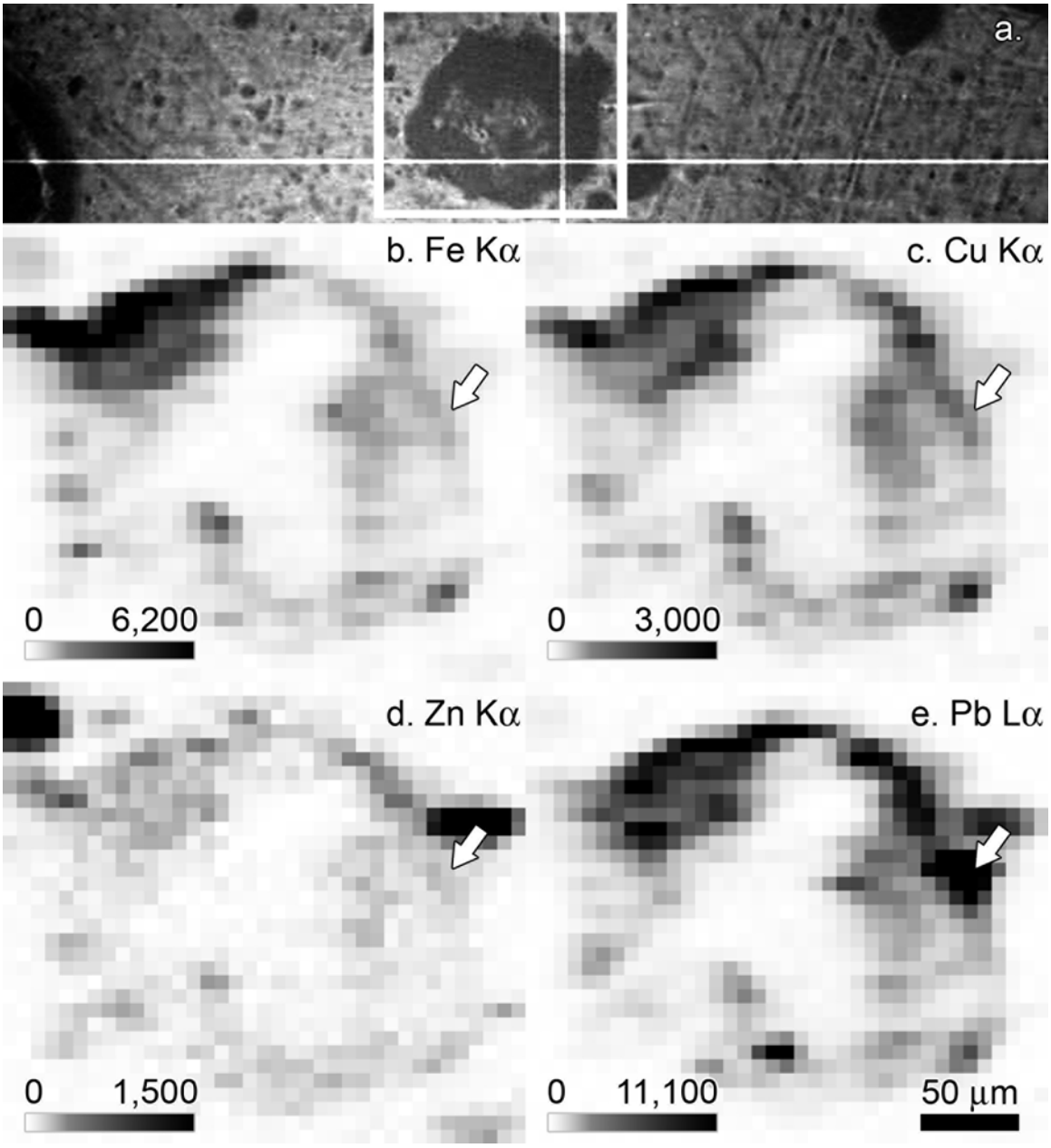

Figure 34. Image of sample slide for untreated, lead contaminated soil (Jacksonville, FL) sealed between Kapton films (*a*), selected particle is bound in a box. The other images capture selected particle in a series of element synchrotron micro-X-ray fluorescence maps, Fe Kα (*b*), Cu Kα (*c*), Zn Kα (*d*), and Pb Lα (*e*). Spot with the highest Pb count that was selected for µ-X-ray diffraction (pattern IX in Table 5 and Fig. 16) is marked by an arrow. Scale bar units are counts per second.

C. Metal Trends in Batch Equilibration of the Uranium and Nickel Contaminated Sediment

The supernatants from the equilibration study of Ni and U contaminated sediment amended with four phosphate amendments to immobilize contaminants that were equilibrated in 0.001 *M* $CaCl_2$ for a period of 170 hours were in addition to Ni and U analyzed for solution concentrations of Mg, Ca, Al, Fe, and Mn. The drop in concentration of metals in solution at the highest Na-IP6 treatment level (Figs. 35 through 39) matched similar trend in U and P in solution (Figs. 25 and 29). As speculated in the results section the drop might be a result of overcoming certain critical level of the dissolved, dispersed and complexed metals and dissolved IP6, at which phytate precipitates free ions and colloidal forms of these polyvalent cations.

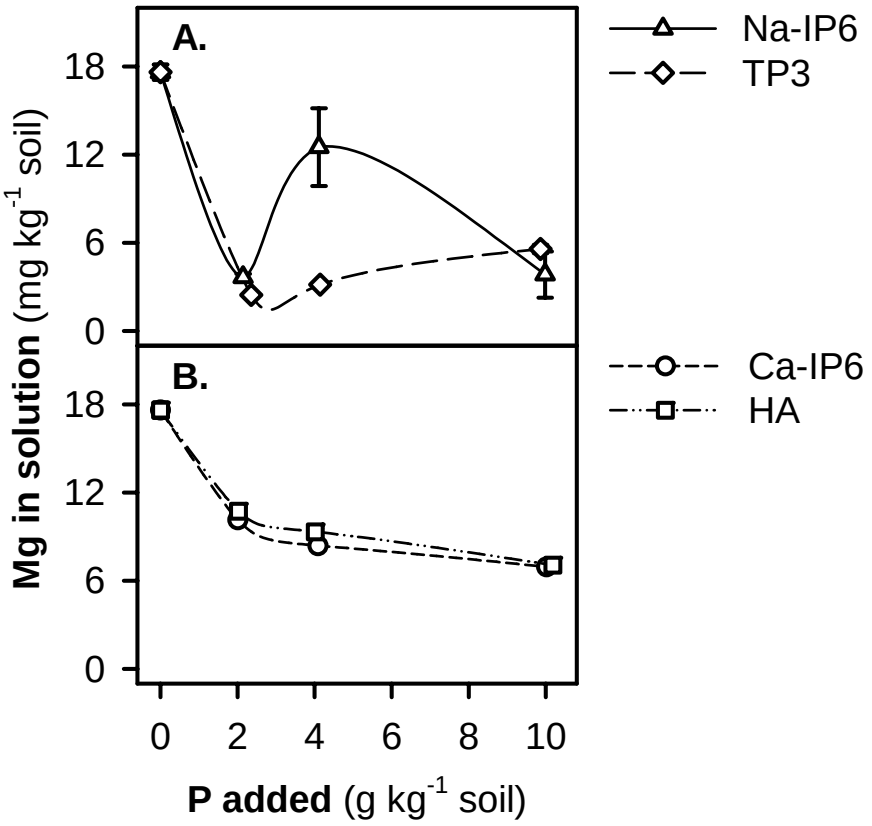

Figure 35. Effect of addition of calcium phytate (Ca-IP6), hydroxyapatite (HA), sodium phytate (Na-IP6), and trisodium trimetaphosphate (TP3) to the Tims Branch sediment on soluble manganese (*A* and *B*) after equilibration for 170 hours in 0.001 *M* $CaCl_2$ on a reciprocal shaker. Error bars represent one standard deviation of the treatment level means. Splines were included to improve data readability and do not represent exact trends.

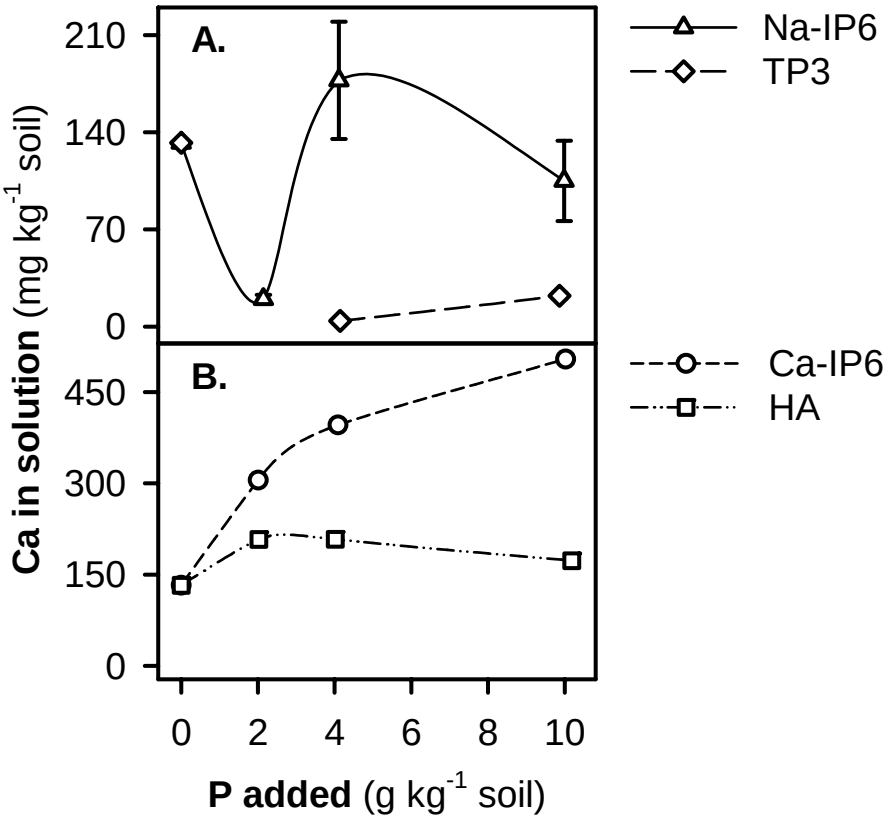

Figure 36. Effect of addition of calcium phytate (Ca-IP6), hydroxyapatite (HA), sodium phytate (Na-IP6), and trisodium trimetaphosphate (TP3) to the Tims Branch sediment on soluble calcium (*A* and *B*) after equilibration for 170 hours in 0.001 *M* $CaCl_2$ on a reciprocal shaker. Error bars represent one standard deviation of the treatment level means. Splines were included to improve data readability and do not represent exact trends.

Figure 37. Effect of addition of calcium phytate (Ca-IP6), hydroxyapatite (HA), sodium phytate (Na-IP6), and trisodium trimetaphosphate (TP3) to the Tims Branch sediment on soluble aluminum (*A* through *C*) after equilibration for 170 hours in 0.001 *M* $CaCl_2$ on a reciprocal shaker. Error bars represent one standard deviation of the treatment level means. Splines were included to improve data readability and do not represent exact trends.

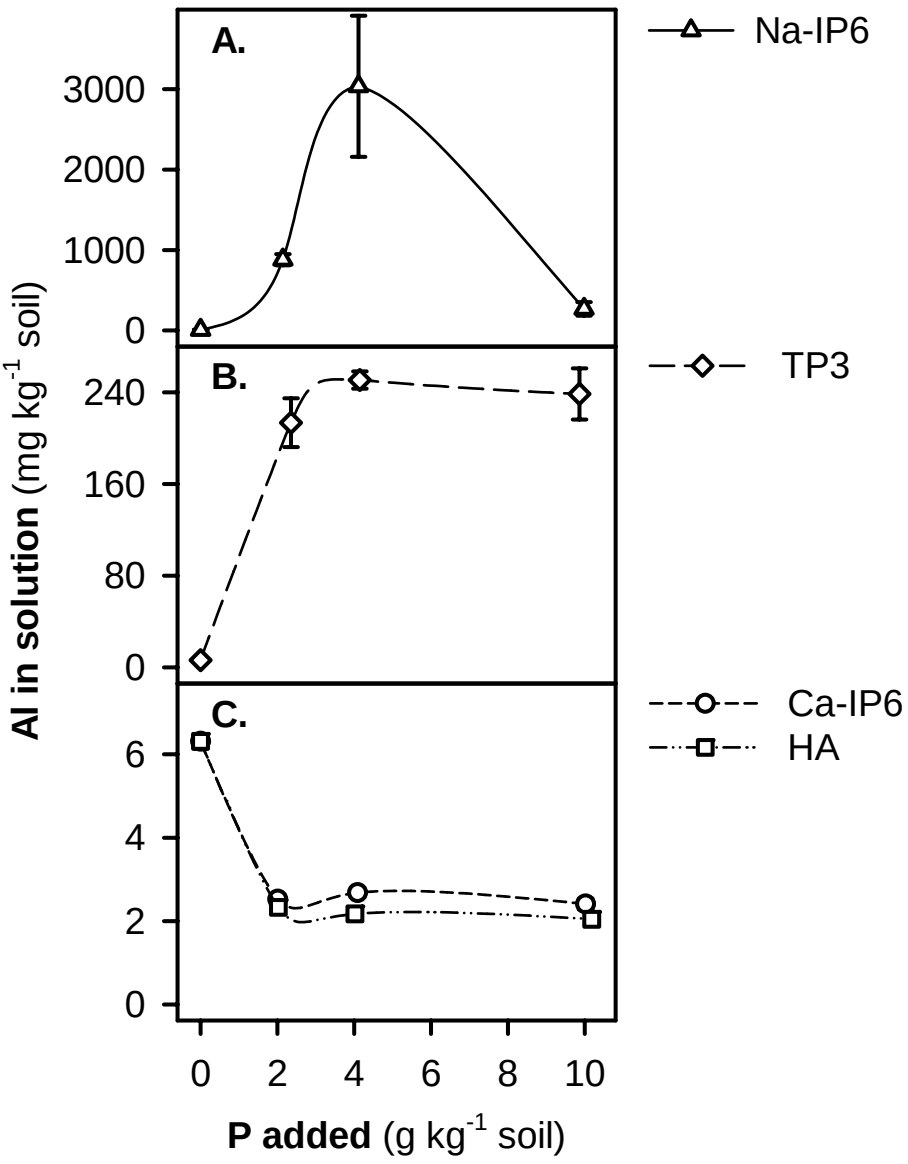
A.
B.
C.
3000
2000
1000
0
240
160
80
0
6
4
2
0
0
2
4
6
8
10
Al in solution (mg kg-1 soil)
P added (g kg-1 soil)
Na-IP6
TP3
Ca-IP6
HA

Figure 38. Effect of addition of calcium phytate (Ca-IP6), hydroxyapatite (HA), sodium phytate (Na-IP6), and trisodium trimetaphosphate (TP3) to the Tims Branch sediment on soluble iron (*A* through *C*) after equilibration for 170 hours in 0.001 *M* $CaCl_2$ on a reciprocal shaker. Error bars represent one standard deviation of the treatment level means. Splines were included to improve data readability and do not represent exact trends.

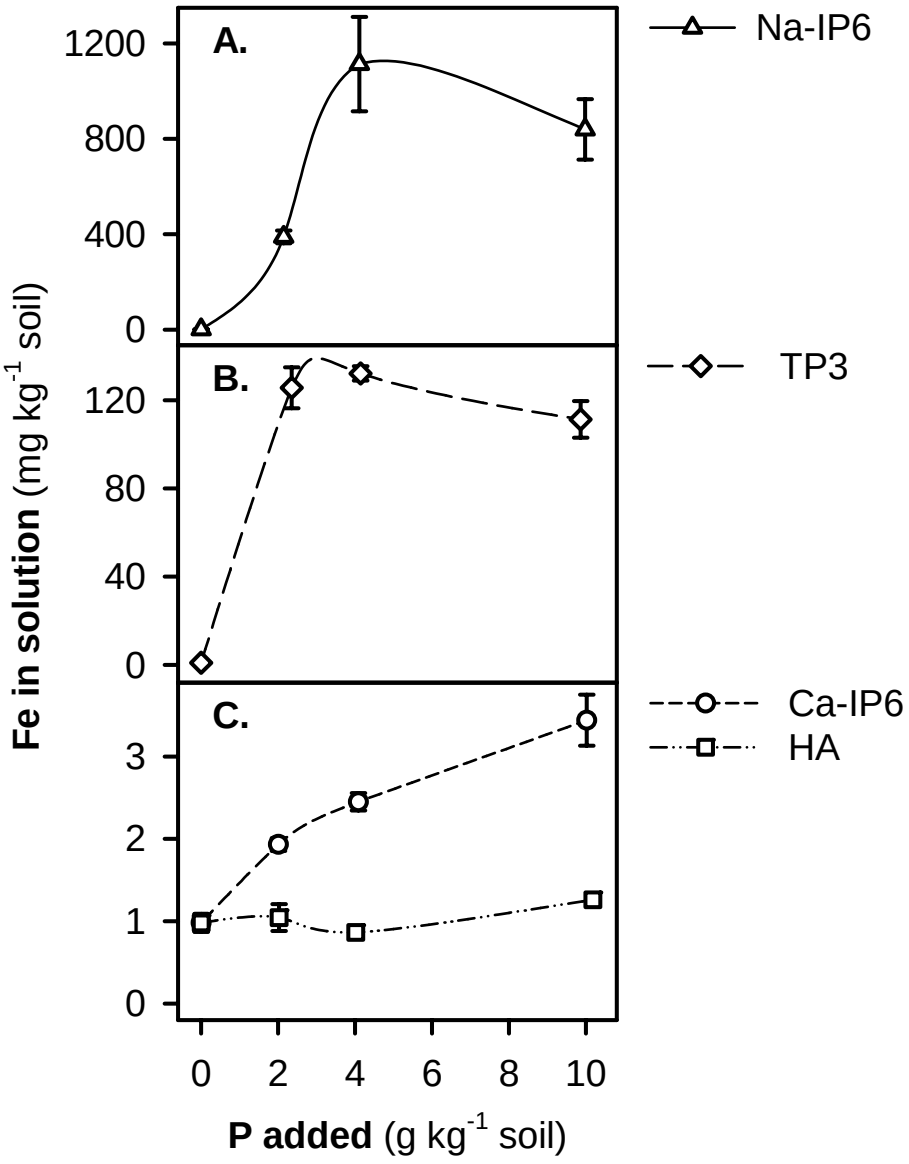
A.
B.
C.
1200
800
400
0
120
80
40
0
3
2
1
0
0
2
4
6
8
10
Fe in solution (mg kg-1 soil)
P added (g kg-1 soil)
Na-IP6
TP3
Ca-IP6
HA

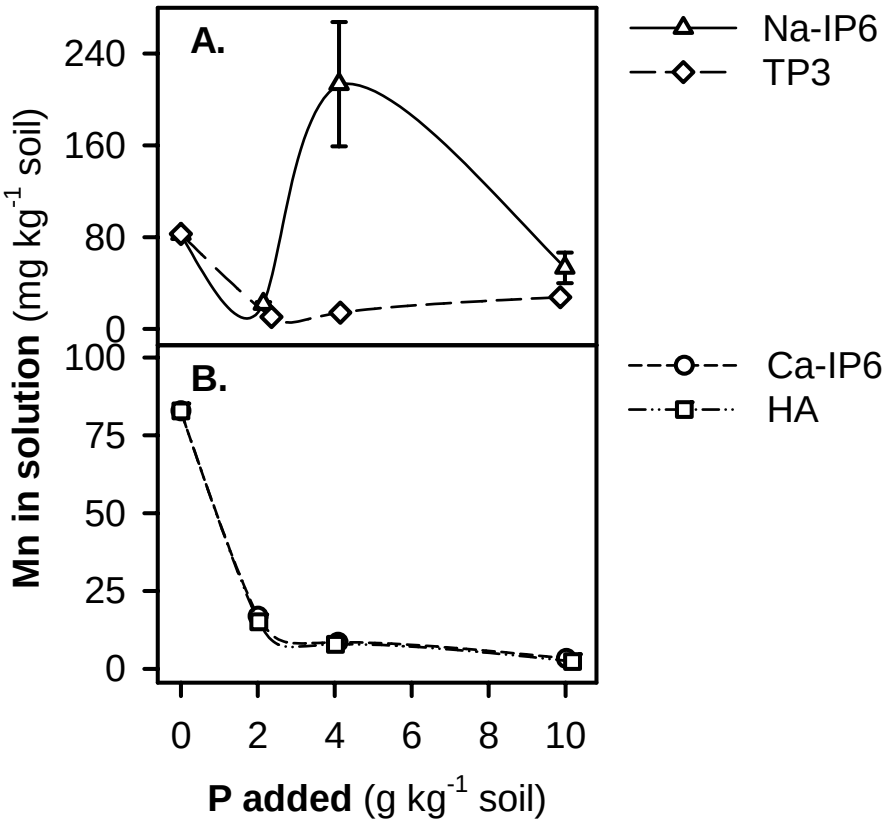

Figure 39. Effect of addition of calcium phytate (Ca-IP6), hydroxyapatite (HA), sodium phytate (Na-IP6), and trisodium trimetaphosphate (TP3) to the Tims Branch sediment on soluble manganese (*A* and *B*) after equilibration for 170 hours in 0.001 *M* $CaCl_2$ on a reciprocal shaker. Error bars represent one standard deviation of the treatment level means. Splines were included to improve data readability and do not represent exact trends.